Numerical Modelling of Extreme Hydrodynamic Loading on Coastal Structures

Samieh Sarjamee

Submitted under the supervision of

Professor Ioan Nistor

Professor Majid Mohammadian

Thesis submitted to the

Faculty of Graduate and Postdoctoral Studies

In partial fulfillment of the requirements for the

Master of Applied Science Environmental Engineering

Under the auspices of the Ottawa-Carleton Institute for Environmental Engineering

University of Ottawa

Acknowledgment

I would like to express my sincere gratitude to my advisors professors Ioan Nistor and Majid Mohammadian. I feel fortunate and honored to have them as my supervisors. Their pure enthusiasm, vast knowledge, and dynamic illustrations, intensified my eagerness to be an environmental engineer. My personal commitment to being the best student I can possibly be is, in large part, due to the enthusiasm that my advisors brought to the field.

My advisors have been a wonderful driving force behind my success here at uOttawa. They were so helpful and so well connected. They always had an open office door as well as an open mind for conversation. I had spent many hours discussing a wide variety of subjects with my advisors. They genuinely care about me as individual and serve as a life mentor as well as an academic mentor.

Their unwavering enthusiasm is apparent in their warm welcomes and instantly assure me that I am capable of achieving all my ambitions. That feeling is sometimes hard to come by at such a large university like uOtttawa and specifically as an international student. My advisors are more than just a professor is; they are a teacher, a mentor, an inspiration, and a friend. It has been a rewarding experience to have my advisors guidance throughout my graduate education.

Beside my advisors, I would like to thank my husband Afshin and my son Hooman for supporting me spiritually throughout writing this thesis.

Abstract

Natural disasters usually occur without any warning. They can leave trail of destruction and cause much tragedy. We are at a time when we witness fast technological advances; hence, we need to apply the force of scientific advancements to decrease economic losses and the number of human deaths. Tsunami is one of the extreme environmental events that leaves nothing but a path of death and destruction, and as a result, it is essential to understand this phenomenon and identify the mitigation strategies. Several mitigation strategies have been proposed so far; however, more investigations are still required to achieve an acceptable solution. Researchers around the world are studying different aspects of this phenomenon. One of the proposed solutions that has received much attention is designing tsunami-resistant structures which can withstand the force of a tsunami bore. Various studies have been done so far to understand the base shear force of tsunami bore on structures. The focus of this thesis is to improve and better understand the characteristics of the tsunami base shear forces on structures. Hence, in this thesis, two numerical studies were proposed and performed with the main goal of estimating the total tsunami forces on structure under two different conditions. Those include structures with various cross sections, as well as positioning a mitigation wall at an appropriate location relative to the structure. The first study focused on developing a numerical model to study the relationship between tsunami forces and the geometry of the structure. The main goal of this study was to define a numerical model capable of simulating this case precisely. To ensure the accuracy of the model, a comparison was carried out between the results of the numerical model and experimental test performed at the NRC-CHC (National Research Council- Canadian Hydraulics Center) laboratory in Ottawa, Canada and Université Catholique de Louvain (UCL), Belgium, which revealed a very good agreement between the results of the experimental test and numerical model. Further, the validated model was applied to investigate the tsunami force on structures with various cross sections. The second study focus was on developing a numerical model for understanding the role of mitigation wall (a novel idea proposed as a mitigation strategy by the second author of technical paper 2) on reducing the exerted force of tsunami on structures. After developing various models and applying several turbulence models, a valuable result was obtained which demonstrated that a Large Eddy Simulation (LES) model seems to be an excellent approach for predicting the tsunami forces on the structure with a mitigation wall in the direction of the flow.

The results of this study will be used to better estimate the tsunami forces exerted on coastal structures which will light the path to the main goal of designing tsunami resistant-structures.

Table of Contents

List of Figures

List of symbols

Latin characters

x	*x-component of position vector*	*m*
y	*y-component of position vector*	*m*
z	*z-component of position vector*	*m*
g	*acceleration due to gravity*	m/s^2
C_α	*Compression coefficient*	-
C_O	*Courant number*	-
U	*velocity vector*	*m*
U_C	*Compression velocity vector*	*m/s*
d	*distance*	*m*
F	*mass fluid flux*	*kg/s*
h_u	*Upstream depth*	*m*
k	*turbulent kinetic energy*	m^2/s^2
n	*unit normal vector*	-
p	*pressure*	*pa*
t	*time*	*seconds*
V	*Volume*	m^3

Greek Characters

α	*phase fraction*	-
ε	*turbulent dissipation*	m^2/s^3
μ_t	*turbulent dynamic viscosity*	Ns/m^2
μ	*dynamic viscosity*	Ns/m^2
τ	*stress tensor*	*pa*
ω	*specific turbulent dissipation*	m^2/s^3

k	*curvature*	*1/m*
λ	*Damping coefficient*	*-*
ρ	*density*	kg/m^3
$\emptyset$	*Generalized conservative physical quantity*	*-*
σ	*surface tension coefficient*	*N/m*

Mathematical Operators

Δ	*change of quantity*
∇	*gradient*
$\nabla.$	*divergence*
δ	*delta*
$\lvert\ \rvert$	*absolute value*

Abbreviation

FEMA	*Federal Emergency Management Agency*
CFD	*Computational Fluid dynamics*
VOF	*Volume Of Fluid*
FV	*Finite Volume*
OpenFOAM	*Open Field Operation And Manipulation*
LHS	*Left Hand Side*
RHS	*Right Hand Side*
SPH	*Smoothed Particle Hydrodynamics*
WG	*Wave Gauge*

Chapter 1

Introduction

1.1. Background

Tsunamis or seismic ocean waves are a progression of huge waves made by a submerged disturbance such as quakes, landslides or volcanic eruptions. It can move several kilometers in every hour in the untamed sea and crush very high waves into area. From the original location of seismic waves, waves travel in all headings. Upon arrival of the tsunami wave to the shore, it grows and develops in stature that is significantly dependent on the parameters such as the topography of the coastline and seabed. Because these parameters alter in different locations, the height of the tsunami waves may be in the range from 30cm to 30m. Generally, there is a high possibility of multiple waves and the following one might be bigger than the one preceding.

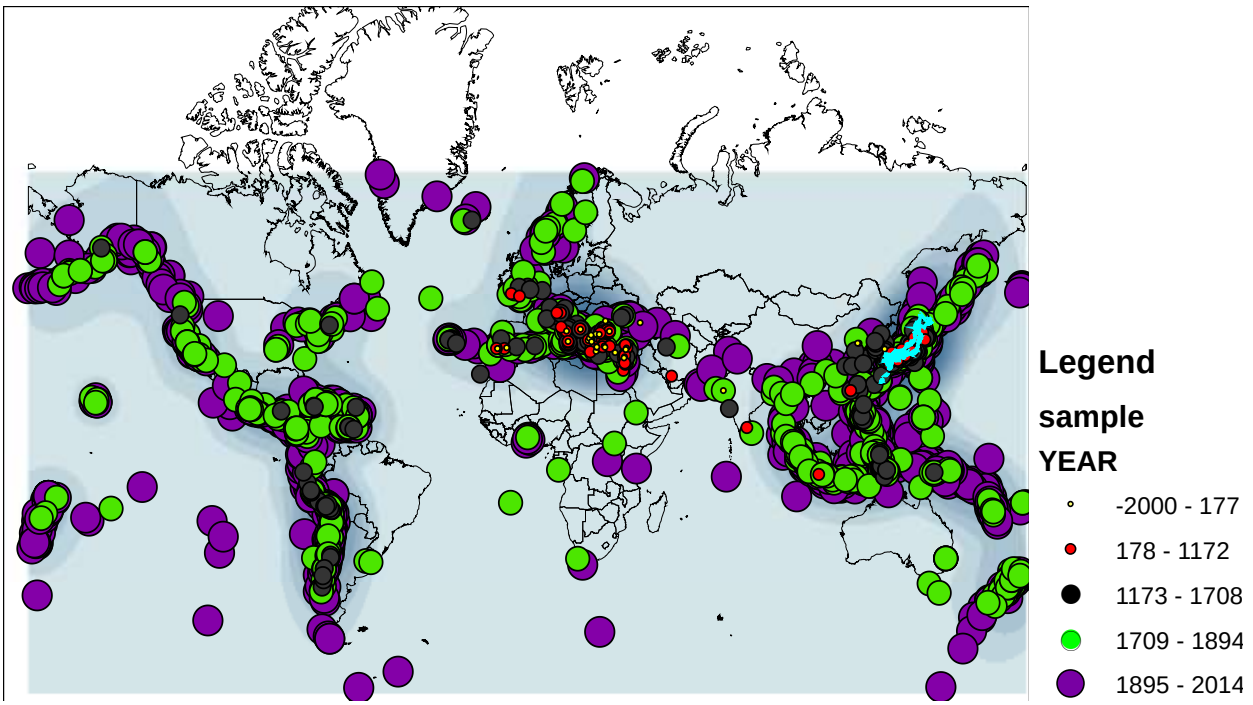

Figure 1:This map is created by Sarjamee based on the database gained from 'NOAA /WDS Global Historical Tsunami Database at NGDC'v.

Based on "FEMA646a" tsunamis fall into three different categories including a far-source, a mid-source and near source generated tsunami, based on the time that it takes the wave to get to a coastline and the

Travel distance. The latter is one in which furious tsunami waves can reach the site less than thirty minutes. In this case, the alarm mitigation strategy may become impractical. "The 1993 tsunami that hit Japan reached the shoreline within 5 minutes after the earthquake"(FEMAp646a) which was a real surprise for the community and caused a lot of death.

Figure 2:Damage caused by 1993 Okushiri Tsunami, Japan (FEMAp646a) Damage caused by 1993 Okushiri Tsunami, Japan (FEMAp646a)

Tsunamis are a risk to people's lives and potentially hazardous regions. One of the primary mitigation implication plans is horizontal evacuation to uphill or inland locations, which requires significant warning time to execute effectively. It motivated the researchers to focus on the need for improving tsunami-warning systems, which are designed to increase awareness of an impending tsunami danger and help evacuate the tsunami hazard areas in time. However, in many cases, tsunami warning systems failed to address properly the near-source tsunami events. Furthermore, in case where the affected coastal regions are low-lying, horizontal evacuation does not lessen the huge social, economic, environmental, and political losses. In this case, vertical evacuation using tsunami-resistant structures can be an ideal mitigation strategy and, hence, studies are required to fully understand tsunami loading and to determine the optimal structure capable of withstanding the tsunami impact and loading.

1.2. Objectives of the Study

The ultimate objective of the present study is to understand and quantify the extreme hydrodynamic impacts of tsunami bores on structural elements, and propose rules and guidelines for structures situated in coastal regions. This study aims to advance the development of tsunami resistance coastal communities along the vulnerable coastal regions. Furthermore, it posits the challenge of assessing bore-structural approaches in the context of numerical methods. This can be attributed to the fact that the present built environment is not ready to withstand the power of compelling tsunami wave actuated by the overland movement of expansive waves. The results of the numerical study presented herein strive to maintain a reasonable understanding of the characteristics of a tsunami bore with the purpose of assisting the engineers to better understand the involved factors that may contribute in the estimation of tsunami forces.

It is clear that scientific investigations are still at the beginning of an ongoing process to provide coastal communities with required tools to understand the nature of tsunami as well as addressing the issue of tsunami via designing tsunami resistant structures.

The foremost topic of this study is associated with computational analysis of the characteristics of a flow that occurs in the locale of the interaction of the bore and structure. This study is divided into two major sections as follows:

- **Interaction of bores with structures of various cross sections**
  - Evaluate the capabilities of the OpenFOAM solver, namely interFoam, to reproduce a series of tests that are available in literature.
  - Assess the influence of structure geometry on the tsunami forces.
- **Bore-structure interaction with considering the influence of mitigation walls of various cross sections**
  - Evaluate the influence that low-height wall can have on the seismic wave forces on the structures in addition to the above objectives.
  - Examine the capabilities of RANS (Raynold Averaged Navier Stoke) turbulence model and Large Eddy Simulation (LES) model in simulating the turbulence.

1.3. Scope of the Study

The performance of the numerical model and its capability of finding the solution for the related equations is assessed via comparing the outcomes of the physical tests and numerical analysis. Net force of tsunami wave is considered as an item for this comparison. For the technical paper 1, first the model was validated through the performed comparisons between the obtained numerical results and available data. Then, the

validated model was applied in order to study the influence of tsunami bores on structures. We considered not only circular and square cross section columns which are typical in most physical tests, but also on columns with triangular, T-shaped and frontally curved cross sections.

For the case of technical paper2, the scope was evaluation of the performance of different simulation models including RANS and LES.

1.4. Novelty

There have been several studies investigating the force exerted on structural elements such as vertical walls. However, the efficiency and effectivity of mitigation walls in reducing the force generated by the impact of a tsunami bore on near-shore structures has received little research effort. While there are a number of studies engaged in the science of tsunamis such as inundation, modelling and propagation, only few studies have focused mainly on tsunami hazard mitigation aspects. To the best knowledge of the authors, LES modeling of tsunami bores using an equation for subgrid scale kinetic energy has not been performed prior to this study. Furthermore, numerical simulation of the effect of low-height mitigation walls on force reduction for tsunami bores has not been conducted before as well.

1.5. Thesis Outline

This thesis has been divided into 6 chapters. Chapter 1 is a brief introduction of the topic and highlights some of the objectives as well as the novelty of the present study.

Chapter 2 provides literature review and is focused on the previous numerical and physical studies that investigated the characteristics of tsunami bores and its associated impact on the on the structure.

Chapter 3, titled mathematical and numerical models, describes the necessity of numerical mode development as a prominent tool corresponding to investigate the bore-structure interaction phenomenon.

Chapters 4 and 5 are the core of this thesis. The main investigation of this thesis is presented in the format of two technical papers.

The last chapter contains the conclusion of this work along with some suggestions for improving this numerical study.

Chapter 2

Literature Review

The study of fluid dynamics is composed of two different categories, including physical experiments and numerical models. The development of the latter is highly dependent on the outcomes of the first one for the validation process. Experimental study results are often considered as a fundamental basis for scientific investigation. There are pros and cons with each of these methods; however, the numerical model can provide the users with most of the required variables throughout the domain. It is also possible to focus on the role of one parameter and study its effect without the interference of the other parameters.

In this chapter, the dam-break wave generation technique is studied, followed by reviewing some related previous experimental and numerical studies focusing on the relationship between the bore and the structure.

2.1 Physical modeling of tsunami like bore applying dam-break approach

Various techniques have been developed over the past years to generate a series of waves containing the characteristics of real tsunami waves such as solitary-wave, volume-driven wave generation and dam-break waves. In this part, only the last one is explained because the physical experiment that is applied in this thesis employed the dam-break approach for tsunami wave generation for the purpose of model validation.

Cross (1967) was one of the first users of this method. This method has received a lot of attention because the user can have control over the inundation in terms of length scale and time via changing the geometry of the domain. Hence, it has become very popular among the other methods. In 2006, Chanson demonstrated that the tsunami like wave that is generated by applying this method has characteristics very similar to a naturally generated tsunami wave. The data for his study originated from a video analysis that was captured from the Indian 2004 tsunami. Chanson (2009) defined an analytical solution for dam-break wave assuming dry bed condition and turbulent characteristic for the flow. He also had the Ritter (1892) analytical solution underhand, which was developed with the purpose of defining the water surface profile. Chanson's analytical solution consists of three different parts for defining various regions of the dam-break wave. The first region represents the reservoir locale. The intermediate region is the locale of ideal fluid, which acts as a link between the first and the last region and finally last region representing the bore front locale, considering friction between the bore tip and bed.

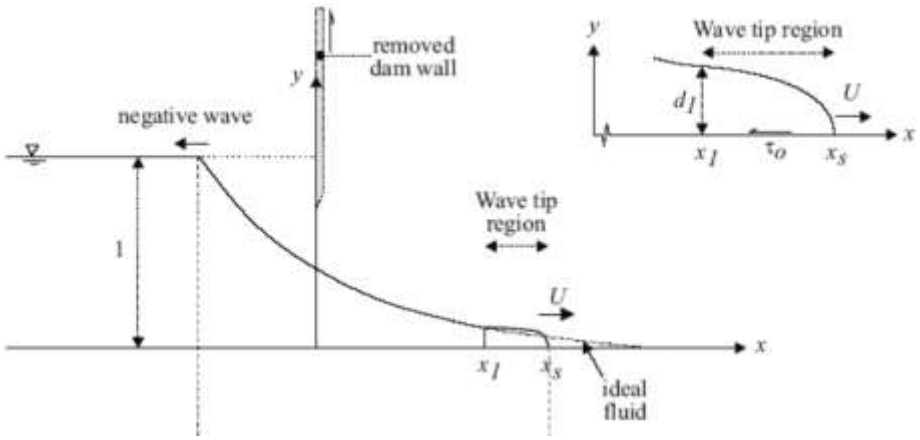

Figure 3:Schematization of a dam-break wave in a horizontal flume assuming dry bed condition (Chanson, 2009).

The main feature of dam-break wave is a certain volume of water that is at rest in the upstream reservoir. The abrupt opening of the gate directs water through the channel, resulting in a wave that is very similar to the natural case. The initial condition can be observed in the following figure.

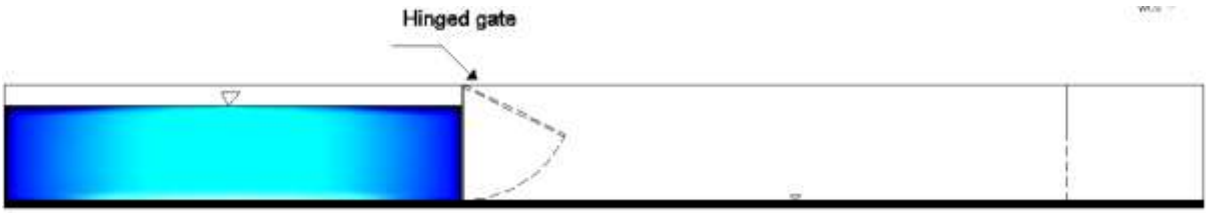

Figure 4:Schematization of the initial condition of a dam-break event

2.2 Physical modeling of bore-structure interaction

In this section, the structure-bore interaction in terms of the exerted net force on the structure is studied under three different conditions, including physical experiment considering 2D and 3D models and numerical investigation. The focus is on the exerted force of tsunami, which is the main subject of the present thesis.

2.2.1 Two-dimensional studies

The path of physical investigation was started by Stoker (1957), who studied the effect of tsunami loading on a wall that was placed in a laboratory channel vertically. Ramsden and Raichlen (1990) examined the hydrodynamic interaction between a vertical wall and a bore. Their findings revealed that the maximum force exerted on a vertical wall occurs immediately after the maximum run-up and that its magnitude exceeds that of the hydrostatic force. Ramsden (1996) performed a similar experiment as Stoker, but

considered two different bed conditions, including dry and wet, and finally made a comparison between the obtained results under the two different conditions. The experiment was conducted in a rectangular prism shaped flume and the wave generation technique was the dam-break approach. In this experiment, he set the impoundment depth of dry bed condition equal to the difference of the impoundment depth and wet bed depth aiming to keep the same celerity for both cases. He observed that the bore tip is steeper when considering the bed being wet and the bore depth was lower at any point through the channel. However, the reverse was true for the other case. Further, a comparison was made under the two mentioned conditions in terms of studying the characteristics of the bore and surge in water profile format. In case of wet bed, the initial run-up was recorded higher than dry bed which was attributed to higher mass of water of the bore tip. Comparing the pressure time history, it can be said that the recorded value for pressure due to the initial impact was higher for the bore. In this empirical experiment, the stream-wise force acting on a vertically erected wall, as a result of the reflection of various waveforms on a dry bed, was also estimated. This revealed that the maximum force increased in the transition of a wave from an undular to a turbulent bore. It should be noted that the scale of his prototype was small rather than large, which may increase the level of inaccuracy of the experiment.

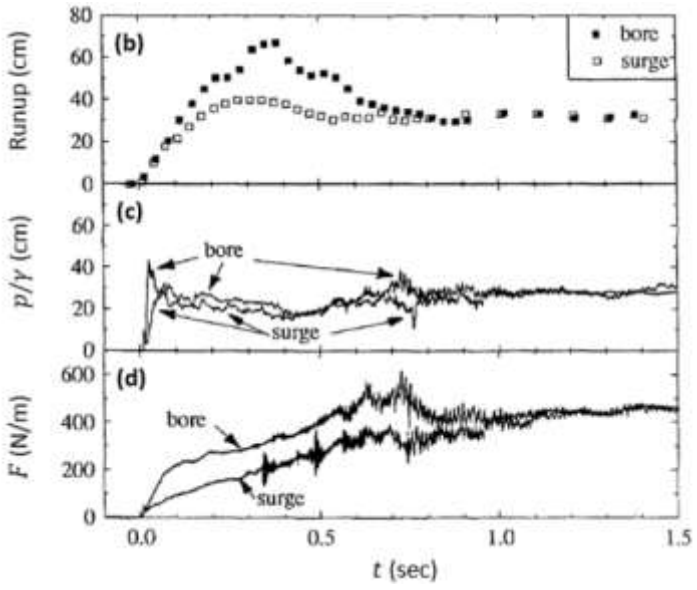

Figure 5:Run-up, pressure and force estimated on a vertical wall caused by a turbulent bore moving over a dry and wet bed conditions (Ramsden, 1993).

Arikawa (2008) studied the interaction of a bore and a wall constructed of concrete and wood. It was a large-scale experiment to understand the behavior of the initial splash of tsunami wave and the resulted loading mechanism on the wall. His focus was on the concrete wall because he tested eight concrete walls versus only one wood wall. He demonstrated that the wall fails due to the impact force of a tsunami 2.5 meters in

height. Oshnack (2010) performed a similar experiment with aluminum walls. He also placed the structure in different positions about the direction of the tsunami and repeated the experiment. Linton (2013) performed a large-scale experiment to evaluate the force of tsunami on walls constructed of wood, which is typical in coastal construction in the United States. His experiment was repeated several times considering various frame configurations and tsunami heights. Both of the forces, including the peak force that was resulted from the initial impact of the bore and the force that was resulted from the reflection of bore into the coming flow, were observed in each test that was performed with considering a different tsunami height. The impulsive force was not observed in those tests.

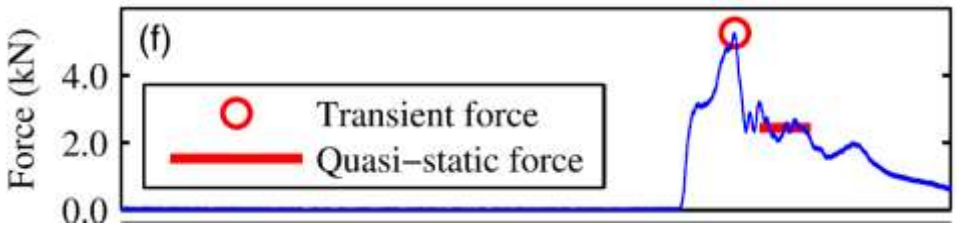

Figure 6:Exerted force of tsunami on wood frame wall (Linton, 2013).

2.2.2 Three-Dimensional studies

A series of experiments was performed by Árnason (2005) to study the interaction of a propagating single bore, by applying the dam break approach, with vertically erected columns of different types: square, round, and rhomboidal cross-sections and considering a dry bed condition. Using a load cell, the force exerted on the vertical columns was estimated for the impact of various bore heights. A tank 16m long x 0.61m wide x 0.45m deep was used to simulate a tsunami-induced bore. Árnason (2005) found that the estimated force exerted on a 0.12m square column facing the flow is larger than the tsunami wave force exerted on a circular column. In the case of square column, he observed a higher initial force than the hydrodynamic force considering the condition of the impoundment depth equal to or smaller than 0.175m. The impulsive force was more distinguishable as the impoundment depth increased from 0.1m to 0.3m. In the following figures, it can be observed that hydrodynamic force values are higher in comparison to the force that occurred due to the collapse of rise bore into the coming bore. Comparing this result with that of Linton et al. (2013), a higher difference between the magnitude of collapse force and the hydrodynamic force can be observed. In addition, such a difference in the recorded magnitudes is more distinguishable in Árnason's(2005) experiment. The reason of this difference can be attributed to the dimension of the tests being 2D for the test performed in 2013 and 3D for the one conducted in 2005. Three-dimensional objects allow a larger volume of water to pass along the structure. However, the wall tends to prevent the water from propagating

through the channel and reflects a larger portion of water, resulting in a larger peak force and larger difference between the peak and hydrodynamic force.

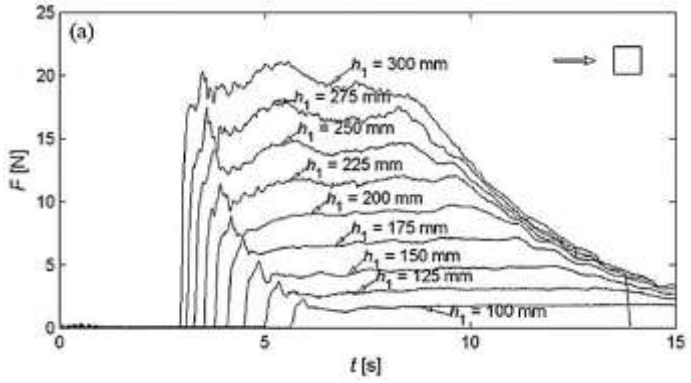

Figure 7:The force on a column of square shape considering different values of water depth in the reservoir, Árnason, 2005, reprinted with permission.

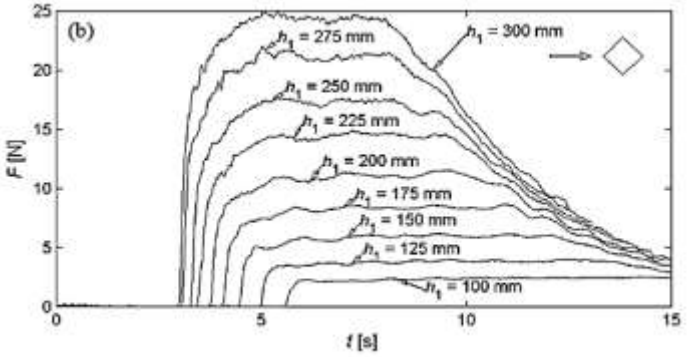

Figure 8: The force on a square considering different values of water depth in the reservoir, Árnason, 2005, reprinted with permission.

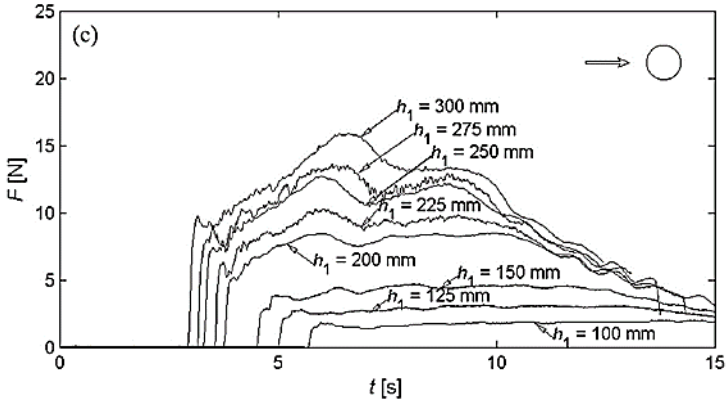

Figure 9: The force on a circular column considering different values of water depth in the reservoir, Árnason, 2005, reprinted with permission.

Matsumi (1991) performed a large-scale experiment to study the impact of tsunami waves on a three-dimensional structure. The purpose was to provide more accurate results because of the larger dimension of the test, and in turn, a closer resemblance to reality. The milestone work of Matsutomi (1991) was investigating the characteristics of tsunami wave force on a land-based coastal structure. Thusyanthan and Madabhushi (2008) proposed a novel design for a typical coastal house located in the USA, and demonstrated its tsunami-resistant features by comparing its resistance factor under tsunami loading to that of an existing, regular house. The idea behind their design was that tsunami waves could pass through the openings of the building and that the hydrostatic loading could thus be controlled. Lukkunaprasit1 et al. (2009) investigated the load caused by tsunami on buildings containing openings, and demonstrated that the openings can lead to a significant reduction of the tsunami load on a structure. Another goal of their research was to prove that the proposed drag coefficient by FEMA P646 (2012) was in a sufficiently good agreement with the value that was measured from the physical test. However, the estimated impulsive load of the drag force equation was inaccurate. Another important finding was the role of scaling effects assigned to a small prototype and showing that a smaller value for force coefficient is needed in case of a smaller model. The experiment of Nouri's et al. (2010) clearly demonstrated the influence of reservoir geometry on hydrodynamic forces generated by the bores on the model structures. Upon gate opening, the presence of a sharp 180^0 bend in the reservoir of the laboratory flume was found to cause brief flow acceleration, accompanied by a premature reduction in the flow intensity. The reduction in the flow intensity resulted in a higher but less sustained run-up force. The results of laboratory studies described in the literature and the numerical simulations performed in their research clearly showed that the bed condition (i.e. wet vs. dry) had a significant influence on the propagation characteristics of a hydraulic bore. A wet bed caused a bore front to have a sharper interface with the thin layer of water that was expanded on the bed. The bore tip velocity was observed to be even higher than the case that a bore propagated over a dry bed. When the bed is slightly wet (i.e. a downstream depth of just a few millimeters), the changes in the bore front profile might not be significant. However, it is suspected that due to turbulence associated with the momentum transfer, considerable air entrainment occurs. It is well known from many related past studies that ensnared air pockets can essentially suppress impulsive shock pressure at introductory contact of the structure and a bore resulting in a damping effect on the estimated force. They also found that a bore, which was generated by the typical dam-break scenario, was generally two-dimensional; the force at initial impact with a slender structure was theoretically not affected by the width of the test channel. To investigate the influence of reservoir size on both wave dynamics and resulting hydrodynamic forces, the length of a straight reservoir was varied numerically. Consistent with analytical and empirical relationships, the model simulation showed that as time advances, the depth and velocity of the flow at any location downstream of the gate tends to *(4/9)hu* and, (2/3) $\sqrt{g}$ *hu* respectively for a long reservoir. The recent experimental work of Al-

Faesly et al. (2012) is most closely related to this study. The authors of this comprehensive experimental program investigated the impact of a tsunami bore on two different column configurations, including circular and square cross sections. They also studied the effectiveness of a low-height wall positioned at an appropriate place close to the structure at the direction of the flow. This work was inspired by observations of undamaged structures located behind the natural dunes during several recent tsunami events, with the purpose of improving the understanding of the complex mechanism of a structure and a tsunami bore protected by a low-height wall. In this research the influence of column shape on hydrodynamic loading and water level profile evolution were studied as well as the influence of mitigation walls with various shapes on hydrodynamic loading. In addition, the characteristics of the flow around the columns and mitigation walls were analyzed. Frame by frame video analysis was used to examine the hydrodynamic loading generated because of a tsunami bore impact on column as well as the structure blockage. Based on their findings, the impoundment depth and hence, the magnitude of the dam-break, noticeably affected the force exerted on the square structure. In addition, the force of tsunami bore was less for the case of circular column, which indicated that the more hydrodynamically shaped structures allowed the bore to be deflected along the sides of the structure, thus reducing the maximum base shear force exerted on it. Another important part of their research was investigating the process of wave impingement columns applying different configurations of mitigation walls to find the best distance that would have a damping effect on the force.

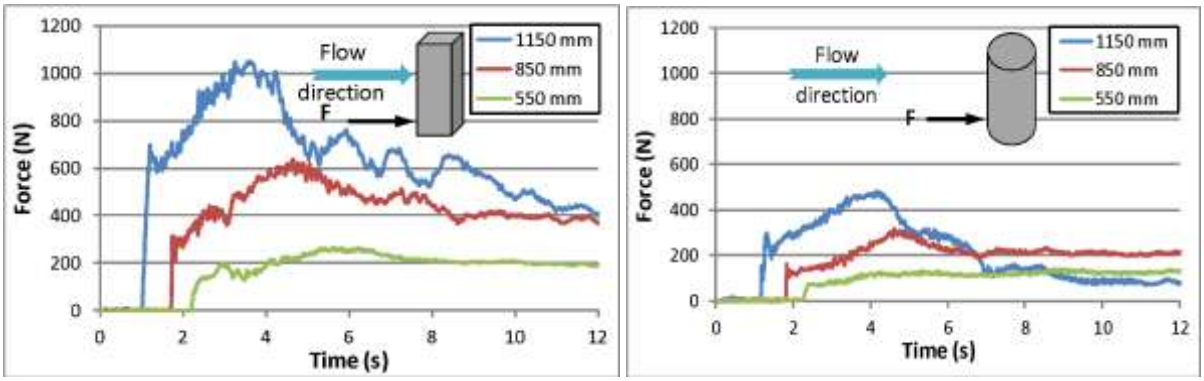

Figure 10:The force profile exerted on square and circular columns as time advances (Al-Faesly et al., 2012.

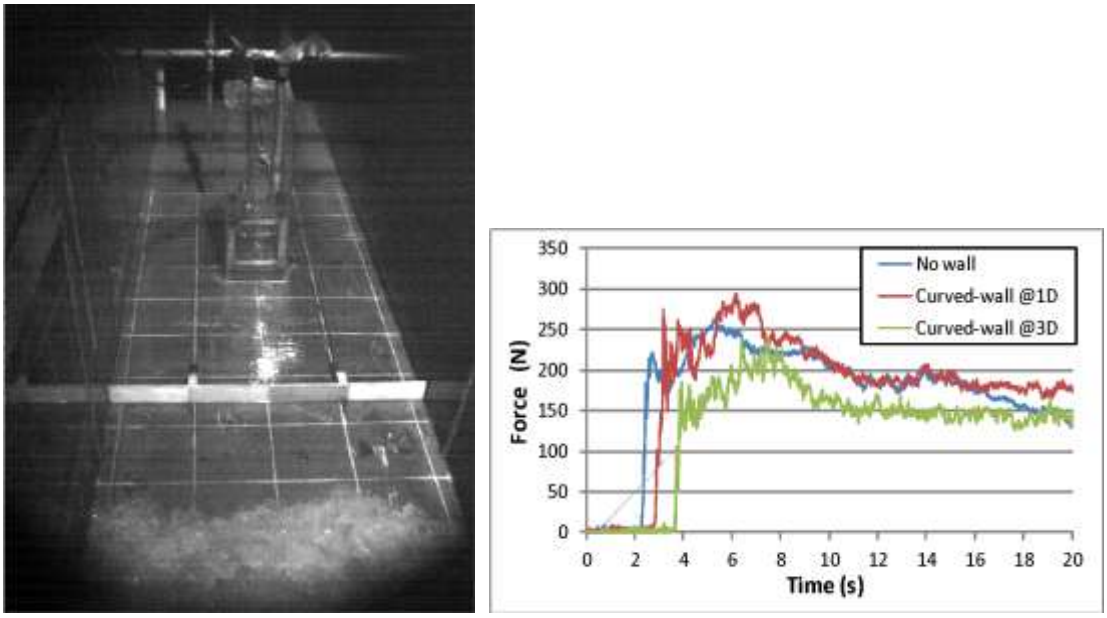

(a) **(b)**

Figure 11: (a) Tsunami force exerted on square model subjected to a tsunami simulated bore generated by the impoundment depth of 550 mm. (b) Total hydrodynamic force for dry bed condition with curved mitigation wall and an initial impoundment water depth of 55 cm.

2.3 Numerical modeling of the tsunami bore on 3D structure

Nouri's et al., (2010) developed a numerical model of the physical test performed by himself initially prior to his numerical study by applying a single-phase 3D weakly compressible smoothed particle hydrodynamics (WCSPH) numerical model. It was a large-scale test which was set up to investigate the characteristics of the bore at impact point with a square column. Numerical time histories of the water profile and hydrodynamic loading withstanding by the column were compared with the results of physical test. The experiments were performed in a 12.87-m-long x 2.7-m-wide x 1.4-m-deep high-discharge flume. Based on the quantitative comparison of numerical results with physical results and extensive analysis of numerical results, their research demonstrated the suitability of the relatively new numerical methods for reproducing such violent and nonlinear water impacts. In St-Germain et al. (2012), the simulation of the impact with columns of tsunami waves rapidly flowing on wet and dry beds was performed using a three-dimensional numerical model based on the Smoothed Particle Hydrodynamics (SPH) method. The resulting pressure versus time and force versus time on a structure (a slender column with square cross section and a vertical wall with a width corresponding to the width of the test flume) and wall positioned vertically due to the bores impact were compared quantitatively. In that research, initially the experimental results of the

time history of pressures and net total base horizontal force acting on a square column were successfully reproduced using the numerical model. While significant air entrainment was observed during the physical tests (the air phase was not considered in the numerical model), this feature was deemed to be mainly responsible for the observed discrepancies in the quantitative comparison of the experimental and numerical results. Their research showed that the hydrodynamic forces on structures that resulted from tsunami-bore propagation were highly dependent on whether the bed on which the waves are propagating was dry or wet. As an alternative in the literature, to overcome the present drawbacks of model validation by comparing the numerical results and experimental results, Altomare et al, (2014), proposed a new method of validation where the technique is validated against physical model results of wave propagation and run-up over sandy beaches. Their method employed a coupling between two different numerical models, characterized by different computational cost and different capabilities, which may help to get holistic representation of phenomenon of wave propagation, transformation and interaction with coastal structures.

2.4 Discussion

From the literature review described here, it is clear that there are still many challenges that need to be addressed prior to developing acceptable and practical tsunami resistant structures. The first important challenge is that the proposed techniques of laboratory tsunami generation still need improvement even though they appear very similar to real tsunami waves. The initial errors that are generated at this stage put the toll on all the other factors involved in the bore-structure interaction phenomena.

Numerical modeling is becoming an essential alternative and complementary tool to laboratory experiments for the assessment of wave transformation and wave-structure interaction phenomena. Although the developed numerical models to date have performed pretty well, there still seems to be a long way until a practical model becomes available. For example, grid-based models are not able to represent violent phenomena characterized by large deformations, where mesh-free models are still computationally too expensive or require scientific development. For instance, SPH is a grid-less Lagrangian numerical method, which indicates potential for investigating the phenomena involved with extreme deformation. On a basic level, the technique ought to have the capacity to overcome both dissemination issues associated with Eularian techniques and the grid deformation associated with Lagrangian technique. Reviewing the related papers, it was found that SPH could be well suited for transmission of tsunami bore loads to coastal structures upon finding a solution for some problematic parts. However, it is clear that at present, SPH is not able to simulate the initially impulsive pressure at impact point of the structure and a tsunami bore as well as the impulsive forces that occur later due to the air entrainment and gravity acceleration. The capacity to simulate these late-time phenomena accurately will necessitate broad technique advancement and calibration of numerical models. In addition, it will be computationally a concern since achieving such late

times with an explicit dynamic calculation is time consuming and requires considering a lot of time for running the simulation which makes it become very expensive. OpenFOAM is another technique that is recently widely used and it is proven to be more capable of simulating tsunami phenomena. However, most of the inaccuracies observed in the results are attributed to the approximation of eddy viscosity and the fact that OpenFOAM appears not being able to simulate the trapped air perfectly because it treats the air as being incompressible for simplification. Reviewing similar studies in the literature investigating the impact of seismic waves on coastal structures, reveals that air pockets in the flow can remarkably decrease the value of impulsive shock pressure at the procedure of water structure interaction. Boussinesq or nonlinear shallow water models have limitations due to the approximation of the governing equations: Navier-Stokes-based methods can model the physics of fluid hydrodynamics but still require huge computational capacities.

The lessons learned from this review are: (1) The need to develop a tsunami generator wave technique with a high resemblance to the real world. (2) The need to introduce a technique for generating multiples bores not a single bore and study the loading effects on the impacted structures. (3) The need to consider the influence that bed condition can have on the magnitude of the impulsive forces caused after the initial strong impact of the invasive bore and the structure. (4) The need to advance sophisticated numerical models capable of simulating a tsunami wave where an extreme hydrodynamic loading affects a structure. (5) The necessity to improve the performance of numerical models by defining true properties of the invasive tsunami waves which are a combination of water, soil and air.

As an alternative, to overcome these drawbacks, a coupling between two different numerical models, characterized by different computational cost and different capabilities, is proposed which may help to get holistic representation of phenomenon of wave propagation, transformation and interaction with coastal structures. Overall, it is clear that further research should be undertaken with a view of reducing the inaccuracies in the present methods.

Chapter 3

Mathematical and numerical models

There are various sophisticated solvers available in OpenFOAM software that can be employed in order to solve these equations. One of these solvers, named interFoam, is capable of solving the Navier-Stokes equations in 3D format for two incompressible fluids.

For the purpose of this thesis, the interFoam solver is employed in the numerical investigations for both involved fluids (air and water). It is possible to consider a constant density for an element of fluid moving with the flow velocity or consider a value with the magnitude of zero for the divergence of the fluid velocity. The conservative equations can be expressed as:

1-The continuity and momentum equations

The continuity equation defines mass conservation principle. It is based on the principle that the mass of fluid needs to be conserved which means that the amount of fluid particles that move in and out of a fluid region needs to be equal. In addition, the equation derivation is based on considering a control volume in the form of a cube and equal the net flow to zero to meet the requirement of the mass conservation law.

Reynolds-averaged continuity equation

The differential form of the continuity equation for a three-dimensional system is written as (Rodi, 1993).

$$\frac{\partial \underline{u}}{\partial x} + \frac{\partial \underline{v}}{\partial y} + \frac{\partial \underline{w}}{\partial z} = 0 \qquad (1)$$

where $\underline{u}$, $\underline{v}$, and $\underline{w}$ are the mean velocity components in the x, y, and z directions, respectively, defined as

$$u(t) = \underline{u} + \acute{u} \qquad v(t) = \underline{v} + \acute{v} \qquad w(t) = \underline{w} + \acute{w} \qquad p(t) = \underline{p} + \acute{p} \qquad (2)$$

Reynolds-averaged momentum equation

The differential form of the momentum equation for a three-dimensional system can be written as (Chamani, 2013).

$$\underline{u}\frac{\partial \underline{u}}{\partial x} + \underline{v}\frac{\partial \underline{u}}{\partial y} + \underline{w}\frac{\partial \underline{u}}{\partial z} = -\frac{1}{\rho}\frac{\partial \underline{p}}{\partial x} + g_x + \nu\left(\frac{\partial^2 \underline{u}}{\partial x^2} + \frac{\partial^2 \underline{u}}{\partial y^2} + \frac{\partial^2 \underline{u}}{\partial z^2}\right) - \left(\frac{\partial \underline{u'^2}}{\partial x} + \frac{\partial \underline{\acute{u}\acute{v}}}{\partial y} + \frac{\partial \underline{\acute{u}\acute{w}}}{\partial z}\right) \qquad (3)$$

$$\underline{u}\frac{\partial \underline{v}}{\partial x}+\underline{v}\frac{\partial \underline{v}}{\partial y}+\underline{w}\frac{\partial \underline{v}}{\partial z}=-\frac{1}{\rho}\frac{\partial \underline{p}}{\partial y}+g_x+\nu\left(\frac{\partial^2 \underline{v}}{\partial x^2}+\frac{\partial^2 \underline{v}}{\partial y^2}+\frac{\partial^2 \underline{v}}{\partial z^2}\right)-\left(\frac{\partial \underline{\underline{v'^2}}}{\partial y}+\frac{\partial \underline{\underline{u'v'}}}{\partial x}+\frac{\partial \underline{\underline{u'w'}}}{\partial z}\right) \quad (4)$$

$$\underline{u}\frac{\partial \underline{w}}{\partial x}+\underline{v}\frac{\partial \underline{w}}{\partial y}+\underline{w}\frac{\partial \underline{w}}{\partial z}=-\frac{1}{\rho}\frac{\partial \underline{p}}{\partial z}+g_x+\nu\left(\frac{\partial^2 \underline{w}}{\partial x^2}+\frac{\partial^2 \underline{w}}{\partial y^2}+\frac{\partial^2 \underline{w}}{\partial z^2}\right)-\left(\frac{\partial \underline{\underline{w'^2}}}{\partial z}+\frac{\partial \underline{\underline{w'v'}}}{\partial y}+\frac{\partial \underline{\underline{u'w'}}}{\partial x}\right) \quad (5)$$

where t is the time, p is the fluid pressure, ρ is the fluid density, and g is the gravitational acceleration

As mentioned above, the algorithm in interFoam is based on the VOF method. This method's performance is based on solving two equations including one momentum and one continuity equation respectively for the gas and liquid phases. The physical variables of each phases are computed as a weighted average taking into account the volume of the two fluids in one cell (Hemida, 2008).

InterFoam solves the continuity equation:

$$\nabla . U = 0 \quad (6)$$

The momentum equation takes the following form:

$$\frac{\partial \rho u}{\partial t}+\nabla .(\rho uu)=-\nabla\rho+\nabla .(\mu\nabla u+\nabla^T u)+\rho g+F_s \quad (7)$$

F_s , which is the surface tension can be estimated as: $F_s = \sigma k(x) n$, where n is a vector perpendicular to the normal and can be estimated as:

$$n=\frac{\nabla\alpha}{|\nabla\alpha|} \quad (8)$$

K, which captures the curvature of the interfaces, is the form of:

$$k(x) = \nabla . n. \quad (9)$$

The VOF in a cell is calculated as $V_{fluid} = \alpha * V_{cell}$, where the V_{cell} is the volume of a computational cell in a domain and α is a scalar function which can be a value between zero and one depending on the fraction of two phases: air and liquid. The α parameter can be estimated from the following indicator function:

$$\frac{\partial \alpha}{\partial t}+\nabla .(\alpha u)=0 \quad (10)$$

An extra compression term may be needed to apply for estimating the surface compression using the following equation:

$$\frac{\partial \alpha}{\partial t}+\nabla .(\alpha u)=-\nabla .[\alpha(1-\alpha)v] \quad (11)$$

Where $0 <= \alpha =< 1$ is the volume fraction (a sharp function). v is a velocity field appropriate for compressing the interface. For calculation of the density at any location of the domain, the following equation can be used: (Hemid, 2008)

$$\rho = \alpha\rho + (1 - \alpha)\rho. \quad (12)$$

In reality, for the concept of the indicator function to be applied, the behavioral tendencies will be like that of a step function with intermittent jumps from zero to one, which crosses through the boundaries between the two phases. Nevertheless, a vital issue with reproducing the convection of such a function is by maintaining the transport of a sharp interface while taking into account the preservation of the boundedness and conservation of the phase fraction (Berbeovic, 2010). Various techniques have been employed to combat this challenge. The implementation of the current techniques in the VOF solvers available in OpenFOAM v2.4.0 use the approach acquired by Weller (2008), the creator and chief developer of OpenFOAM. In this procedure, the numerical diffusion of steep gradients of the phase fraction is represented by the introduction of a synthetic compression term (third term on the RHS of the following equation) into the transport equation, taking on the shape of:

$$\frac{\partial \alpha}{\partial t} + \nabla.(U\alpha) + \nabla.(U_c\alpha(1 - \alpha)) = 0 \quad (13)$$

Where the U_c term can be defined as the compression velocity. It should be noted the mentioned indicator function accompanying a new term to its RHS is only active for the case that the transitional locale of the interface is narrow. Otherwise, for locations away from the interface, the original indicator function should be employed for estimation.

Another role of this additional term is bounding the phase fraction current to a direction that is perpendicular to the interface (Berberovic, 2010). Hence, in this case, this term will be only active as a vector in the reverse side of the interface. As a result of that, the creator of OpenFOAM came up with the following equation capable of estimating U_c generally:

$$U_c = \min[C_\alpha|U|, \max(|U|)]\frac{\nabla\alpha}{|\nabla\alpha|} \quad (14)$$

2-Turbulence modelling

It is clear that there are no unique and universal turbulence models. A turbulence model is a computational procedure to close the system of mean flow equations, which is dependent on the progress of the CFD field and is intensely subject to the improvement of PC related technologies and the improvement of our comprehension and solving ordinary and partial differential equations. The nonlinear, time-dependent, three-dimensional PDE characteristic of the Navier-Stoke equations are responsible largely in setting-up a turbulence model, which make it strongly complex.

The Navier-Stoke equations can be written as

$$\frac{\partial \rho}{\sigma t} + \frac{\partial \rho u}{\partial x} + \frac{\partial \rho v}{\partial y} + \frac{\partial \rho w}{\partial z} = 0 \quad (15)$$

$$\frac{\partial U_i}{\partial t} + U_j \frac{\partial U_i}{\partial x_j} = -\frac{\partial P}{\partial x_i} + v \frac{\partial^2 U_i}{\partial x_i \partial x_j} - \frac{\partial \underline{u_i' u_j'}}{\partial x_j} \quad (16)$$

When the flow is turbulent, the variable velocity may be decomposed into a time-averaged velocity and instantaneous velocity fluctuation:

$$u(t) = u^- + u'(t) \quad u = u^- + u' \quad v = v^- + v' \quad w = w^- + w' \quad p = p^- + p'$$

So the Reynolds form of Navier-Stoke's equation can be rewritten as below where $\partial \underline{\acute{u}_i \acute{u}_j}$ is the Reynolds stress tensor, which is unknown. Because of the present inability in solving the Navier-Stokes equations for flows with turbulent characteristics, it is required to model turbulent gradients by applying either RANS (Reynolds Averaged Navier-Stokes) or LES (Large Eddy Simulation) models.

3- Classification of turbulent models

There is a wide variety of turbulence models that have been developed so far. Determining which one to choose depends on the nature of the problem. The turbulent flow parameters can be obtained by directly applying Direct Navier-Stokes equations (DNS) or it can be obtained in temporally averaged form by applying Reynolds-Averaged Navier-Stokes equations (RANS) or by using the spatially filtered form (LES) model. In this thesis, RANS and LES are applied as turbulence models and their capability in terms of simulating the turbulence accurately is compared. RANS and LES models are explained in the papers by introducing the related equations.

Turbulence models can be classified into the following groups (Sodja, 2007):

- **Eddy Viscosity Models (zero equation models)**

Boussinesq's approximation is one of the most popular ways of estimating Reynolds stress. Based on this assumption, eddy viscosity can be applied in order to model the momentum that is generated by turbulence eddies. The positive amount of eddy viscosity can be estimated from a mixing length, which is independent of the analyzed flow. Boussinesq eddy viscosity states that the Reynolds stress tensor corresponds to the trace-less mean strain rate tensor and can be written as follows:

$$\rho \underline{u_i u_j} = -(\mu_t)(\underline{u_{i,j}} + \underline{u_{j,i}}) + \frac{2}{3} \delta_{i,j} \rho_k \quad (17)$$

In order to define the turbulent viscosity, a dimensional analysis can be applied. The dimension of the velocity is meter squared over second, so the same dimension can be gained by multiplying two variables, including a turbulent velocity U and length scale L so it can be written as:

$$v_t \propto UL \tag{18}$$

where L is a mixing length and U is the flow velocity. This model is not generally accurate because the mixing length should be determined.

- **One-equation models**

One-equation turbulence models operate through solving one turbulent transport equation, which is in most cases the turbulent kinetic energy. Algebraic expression should be applied in order to find the unknown turbulent length scale, which is proportional to the thickness of the boundary layer. This model is not practical due to the unattainable general expression for an algebraic length scale.

- **Two-equation models**

Two-equation models are amongst the most well-known turbulence models. There are main two-equation models offered for turbulent flow: k-e and k-omega turbulence models, which have become industry standard models and are regularly utilized for many sorts of engineering problems.

4-Finite volume method (FVM)

A very common and appropriate discretization method in the engineering field that is capable of simulating a broad range of fluid mechanic problems and arises from conservation of principle laws is the finite volume method. It can be applied to different geometries and domains, using unstructured or structured grid points. One of the most attractive features of this method, which makes it practical for fluid mechanics, is the fact that numerical flux can be conserved from one cell to its neighbor cell.

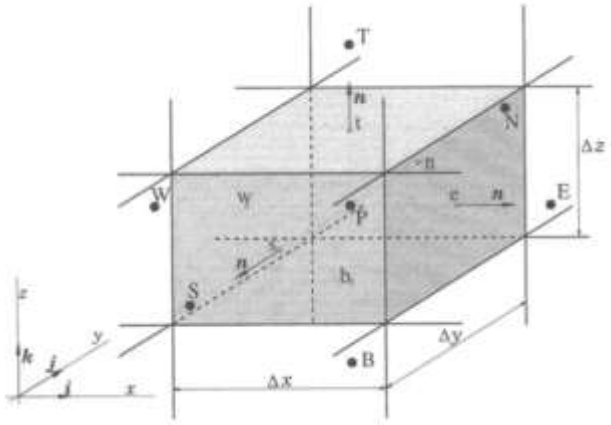

Figure 12:A typical CV and the notation used for a Cartesian 3D grid (Ferzieger, 2002)

Chapter 4

Technical paper 1:

Numerical Investigation of the Influence of Extreme Hydrodynamic Forces on the Geometry of Structures using OpenFOAM

Samieh Sarjamee, Ioan Nistor, Abdolmajid Mohammadian

Abstract

The main focus of the present study is to numerically examine the effects of tsunami –like induced hydrodynamic loading applied to freestanding structures with various architectural geometries. To accomplish these goals, the authors employed a multi-phase numerical model utilizing the Volume of Fluid (VoF) method in the three dimensional space. The second objective of the present study is to improve the understanding of hydrodynamic loads on structural components in order to develop practical guidelines for the engineering design of structures located in areas with a high risk of tsunami hazards. In order to evaluate the performance of the numerical model, the results of the simulation are compared with various available experimental data and physical modeling studies. The tsunami-like wave was reproduced via a sudden release of water located in an impounding reservoir located at the upstream part of a flume (dambreak wave). The shear force exerted by the hydrodynamic force on the square and round structures in the downstream area are estimated to obtain the value of tsunami loading. Finally, the validated numerical model is employed to examine the influence of the structure's geometry on the hydrodynamic loads exerted on it.

Keywords: hydrodynamic loading, tsunami, extreme hydrodynamic forces, OpenFOAM, force time histories

1. Introduction

Natural disasters occur all over the world and they are often devastating for communities and the environment. On March 11, 2011, one of the largest earthquakes to have ever occurred in the world led to a catastrophic tsunami, measuring of 9.0 moment magnitude unleashed a deluge of water onto Japan's northeastern coastal area of Tohoku. The extreme hydrodynamic force of the coastal inundation generated by the extreme tsunami waves flooded cities and rural areas alike, swept kilometers inland, and left a trail of death and devastation in its wake. This natural disaster led to huge social, economic, environmental, and

political losses. A large number of people lost their lives and a huge amount of economic losses was reported as the tsunami lashed across the coasts of over 13 Pacific Rim nations. The damaging and extensive tsunami waves struck not only the coasts of Japan but also Hawaii and California.

An extensive review on the current design standard (Nistor et al., 2009; Chock et al. 2012) and the results of numerous surveys done by reconnaissance teams regarding the effects of earthquakes and tsunamis (the Tohoku Earthquake Tsunami joint survey Group, 2011) outlined flaws in the current tsunami force-estimation methods and revealed that the tremendous forces and impacts generated by tsunamis had not been properly taken into account when considering loads used to design buildings and coastal structures. Estimating the interaction of bores with obstacles is critical and needs to be considered as one of the key questions when designing structures capable of withstanding the impact of tsunami inundation.

When a tsunami-induced turbulent coastal flood moves inland, they can cause massive structural failures. Because of the existing analogies in the literature between tsunami-induced coastal flooding and dam-break waves (Chanson, 2006), in this numerical investigation, a dambreak wave approach is used to numerically generate a broken tsunami wave using a Computational Fluid Dynamics (CFD) model, namely OpenFOAM, which allows for simulation of complex physical problems.

Although there have been several studies investigating the total base force exerted on various structural models, in most cases the focus has been on rectangular and circular shape structures. Hence, there are still many open questions on the interactive aspects between a tsunami bore or surge and the structure's characteristics, including, for instance, more complex geometries. Additional numerical studies are needed to fill the gap in the understanding of the relationship between hydraulic forces and different geometric structures.

In this paper, the results of various numerical experiments are presented. These are conducted to study the characteristics of the forces due to a hydrodynamic bore which is exerted on free-standing structures with different geometries (including square, triangular, front curve, and T-shape cross-sections) in order to study the interaction between structure's geometry and the tsunami-induced forces. The goal of this ongoing research is to trigger a review of existing structural codes which, to date, have not explicitly considered structure's geometry in the design of coastal structures that are at risk for tsunamis.

In this paper, computational simulations of the laboratory experiments by Al-Faesly et al. (2012) and Soares-Frazao (2002) has been conducted. Results of these physical tests are used to validate the proposed numerical model. Following validation, the model is then applied to provide engineering guidance in terms of the force exerted on some composite structures, with sufficient confidence.

The paper is structured as follows: first, the capabilities of the applied model in predicting forces have been evaluated by comparing it with the available experimental data in the literature; then by employing the validated model, the net base shear forces acting on structures with varying geometry are calculated. Some concluding remarks complete the study.

2. Literature Review

There are extensive studies reported in the literature which investigated tsunami-induced loading on structures. Therefore, only selected works directly related to this study are mentioned in this brief review. The present work focuses on investigating the relationship between the magnitude of the exerted force and the geometric shape of a structure. Estimating tsunami loading on structures has been experimentally and numerically conducted in recent years. The path of investigation started by the preliminary experimental investigation of tsunami loading on vertical walls performed by Stoker (1957), who introduced a novel solution to analytically obtain the force on a vertical wall. Applying a dry bed condition, Fukui et al. (1963) suggested that the surge-tip velocity is proportional to the impulsive pressure. They also argued that the magnitude of the hydrodynamic pressure caused by the tsunami wave becomes larger in comparison to that of the gravity wave. An investigation of the surge propagation was performed by Cross (1967), who also proposed a theory to estimate the force generated by a bore that was exerted onto a vertical wall. Ramsden and Raichlen (1990) examined the hydrodynamic interaction between a vertical wall and a bore. Their findings revealed that the maximum force exerted on a vertical wall occurs immediately after the maximum run-up and that its magnitude exceeds that of the hydrostatic force. Examinations of the impact of tsunami waves on a three-dimensional structure were examined in the milestone work of Matsutomi (1991), who examined the characteristics of tsunami wave force on a land-based coastal structure. In Ramsden's (1993) empirical experiment (Fig.13), the stream-wise force acting on a vertically erected wall as a result of the reflection of various waveforms on a dry bed was estimated: this revealed that the maximum force increased in the transition of a wave from an undular to a turbulent bore.

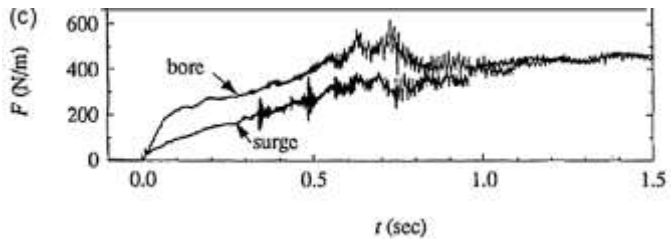

Figure 13:Force estimated on a vertical wall caused by a turbulent bore moving over a dry bed condition (Ramsden, 1993, reprinted with permission)

Árnason (2005) conducted a laboratory experiment to study the interaction of a propagating single bore, by applying the dam break approach with vertically erected columns of different types: square, round, and

rhomboidal cross-sections and considering a dry bed condition. Using a load cell, the force exerted on the vertical columns was estimated for the impact of various bore heights. A tank with the dimensions 16m long x 0.61 wide x 0.45m deep was used to simulate a tsunami-induced bore. Árnason found that the estimated force exerted on a square column with an edge facing the flow (Fig.14) is larger than the tsunami wave force exerted on a circular column (Figs.15 and Fig.16).

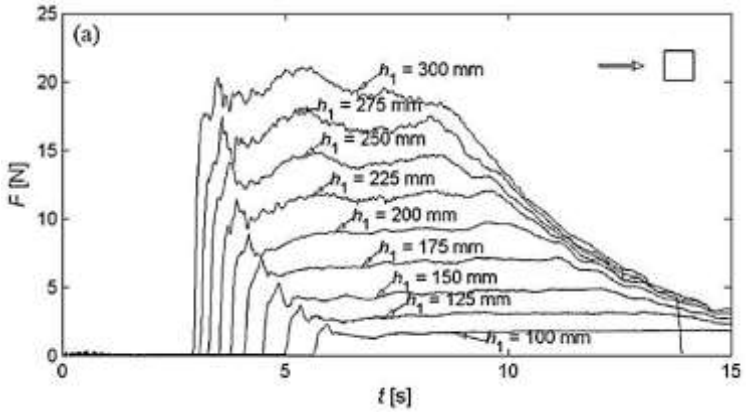

Figure 14:The force on a column of square shape with considering different values of water depth in the reservoir, Árnason, 2005, reprinted with permission.

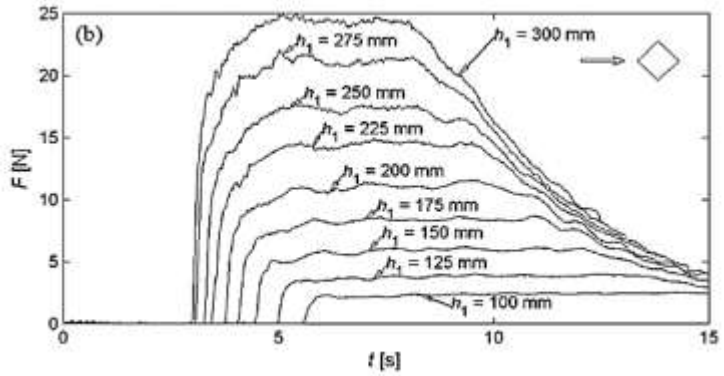

Figure 15 :The force on a square considering different values of water depth in the reservoir, Árnason, 2005, reprinted with permission.

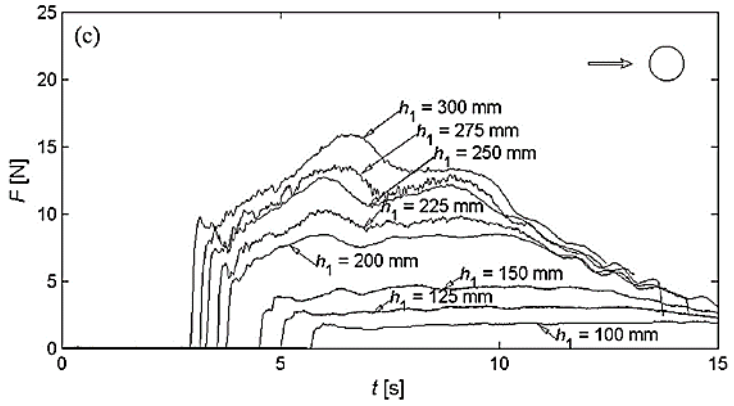

Figure 16:The force on a circular column considering different values of water depth in the reservoir, Árnason, 2005, reprinted with permission.

Thusyanthan and Madabhushi (2008) proposed a novel design for a typical coastal house located in the USA, and demonstrated its tsunami-resistant features by comparing its resistance factor under tsunami loading to that of a local, regular house. The idea behind their design was that the tsunami waves could pass though the openings of the building and that the hydrostatic loading could thus be controlled. Lukkunaprasit1 et al. (2009) investigated the load caused by a tsunami on buildings containing openings, and demonstrated that the openings can lead to a significant reduction of the tsunami load on a structure. In Nouri's et al. (2010) laboratory experiment (Fig.17), a dam-break approach was employed to generate a tsunami bore by applying 4 different impoundment depths:0.5, 0.75, 0.85 and 1 meter and the resulting dam-break wave force exerted on square and circular columns was evaluated. The recorded force time-history for the cylindrical structure showed that for the first 3 mentioned depth values, the force resulting from the first interaction of the coming flow and column was smaller than hydrodynamic force. However, the calculated force overestimated the hydrodynamic force for the case of the 1 m impoundment depth. Chinnarasri et al. (2013) examined experimentally the effect of tsunami waves on buildings, by subjecting a structural model with 1:100 scale to a bore-like broken wave. Based on their results, the estimated total shear force exerted during the run-up process for a square building was equal to that which was recorded in the case of a square configuration, while being percent less than the value reported for an octagonal building. Moreover, the open layout of the front panel resulted in a considerable reduction of wave force (Chinnarasri et al., 2013).

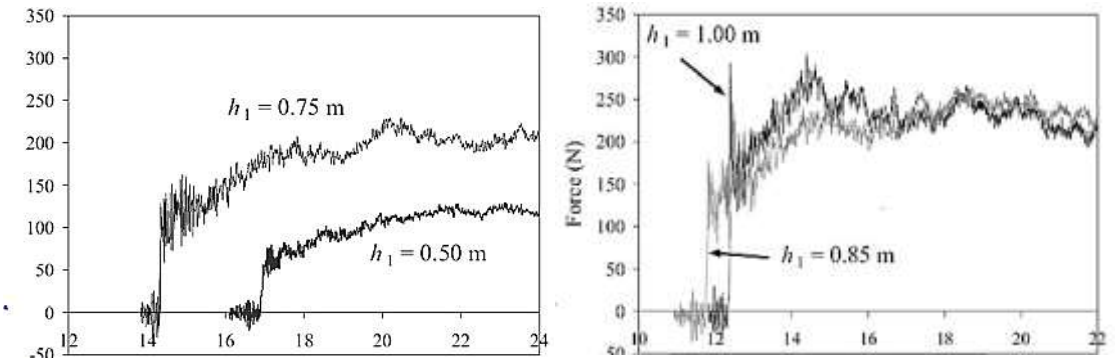

(a) **(b)**

Figure 17:Total force time-histories exerted on a circular column for initial water depth of: (a) 0.5 and 0.75 m (b) 0.85 and 1 m (reprinted with permission from Nouri, 2010)

Al-Faesly et al. (2012) performed comprehensive laboratory experiments by applying hydrodynamic forces generated by a dambreak wave with 3 different impoundment depths to a square and a circular free-standing column (Fig.18). They also examined the effect of mitigation walls with various shapes on the forces exerted on the two column types. Based on their findings, the impoundment depth and, hence, the magnitude of the dambreak, noticeably affected the force exerted on the square structure: the maximum force magnitude recorded for the 1.0m, 0.85m and 0.55m impoundment depths decreased from 1,000 N for the 1m depth to 600 N and 230 N for the other two depths, respectively (Al-Faesly et al., 2012). St-Germain et al. (2012) simulated numerically the experiments of Al-Faesly et al.'s (2012) and estimated the exerted force on the two free-standing square and circular cross-section columns by applying an SPH model. They concluded that the experimental and numerical results showed good comparison and that the most noticeable discrepancy was the fact that the computed initial impact force was significantly larger than the experimentally-recorded one. It was speculated that trapped air during the initial impact was responsible to a great extent for this. Douglas and Nistor (2015) investigated the bed condition as a significant parameter that affects the hydrodynamic loads on structures. They also validated their model using Al-Faesly et al.'s (2012) experimental data.

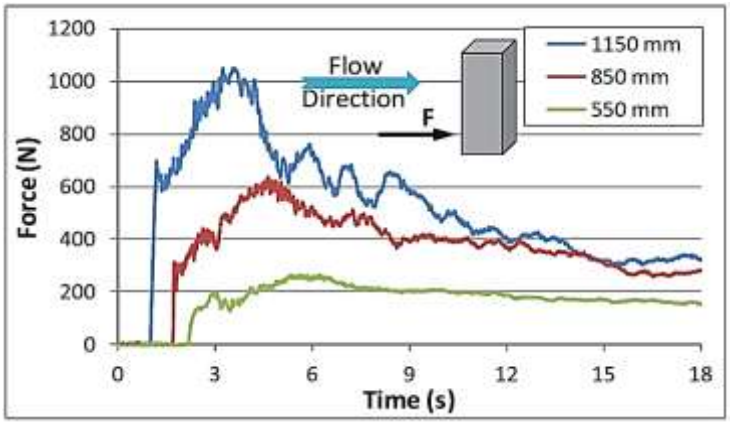

Figure 18:Force-time histories for three impoundment depths onto a square column in the direction of flow (reprinted with permission from Al-Faesly et al., 2012).

3. Experimental test description

In this section, the physical tests used for the verification of the numerical model are briefly described. Following physical tests description in part 3.1 and 3.2, part 3.3 describes the geometry of the flume that was applied later in the numerical investigation in order to examine the influence of structure's shape on the total base shear force exerted on the structures by employing the validated numerical model.

3.1 NRC-CHC Experimental Program (Al-Faesly et al., 2012)

The laboratory tests employed a rectangular high-discharge flume located at the NRC-CHC (National Research Council- Canadian Hydraulics Center) laboratory in Ottawa, Canada. The length, width, and height of the flume are 13.17m, 2.7m and 1.4m, respectively. In order to customize the flume's geometry to the desired dimensions of the test program, a sheet of metal was installed exactly along the middle of the flume, extending in length-wise direction in such a way that 2.32m of the channeled width remained open at the reservoir side, doubling thus the volume of water and therefore extending the time of water flow from the reservoir. The experimental plan is shown in Fig.19. The tsunami wave was reproduced by suddenly releasing the water impounded by means of a rapidly opening gate, with the water exiting through a rectangular-shaped drain located at the downstream part of the flume. The structural models considered for the tests were a 1m high and their cross-sections were a 0.305m-diameter circle and a 0.305x0.305 m square, respectively.

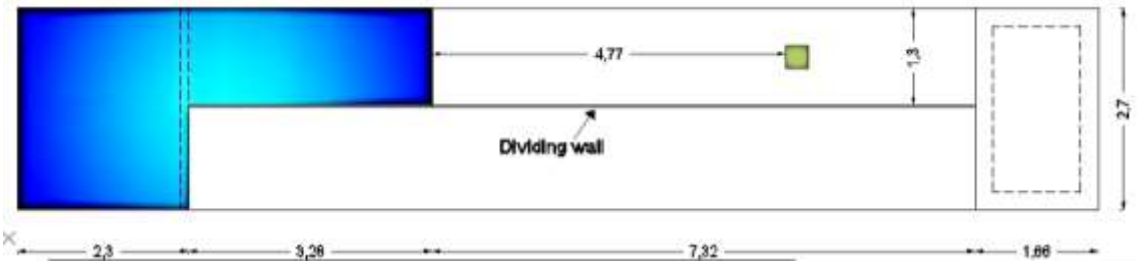

(a)

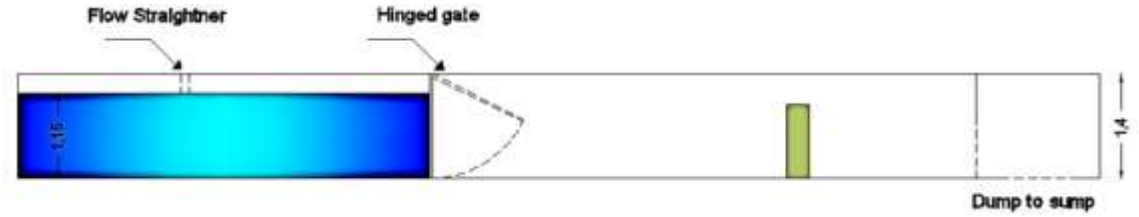

(b)

Figure 19:Floor plan (a) and side view (b) of the OCRE-NRC Canada, laboratory flume (dimensions in meters)

3.2 Experimental Tests at Université Catholique de Louvain (UCL), Belgium

The experimental tests conducted at UCL (Soarez-Frazao, 2002) are considered here. The physical domain (Fig. 20) is a rectangular prismatic structure 5.6m long, 0.5m wide, constructed of glass. The 2.39m long upstream reservoir holds a prescribed volume of water with an impoundment depth of 0.111m. A 0.025m high reservoir is located at the downstream end and a 0.065m-high symmetrical obstacle with a bed slope of 0.014 is placed upstream of this reservoir. The sudden opening of the gate releases the water initially impounded from the upstream reservoir into the channel. The closed system of the physical domain does not allow for the water to go out of the channel, and hence the water returns after hitting the downstream end wall of the flume and continues to flow freely between the two reservoirs.

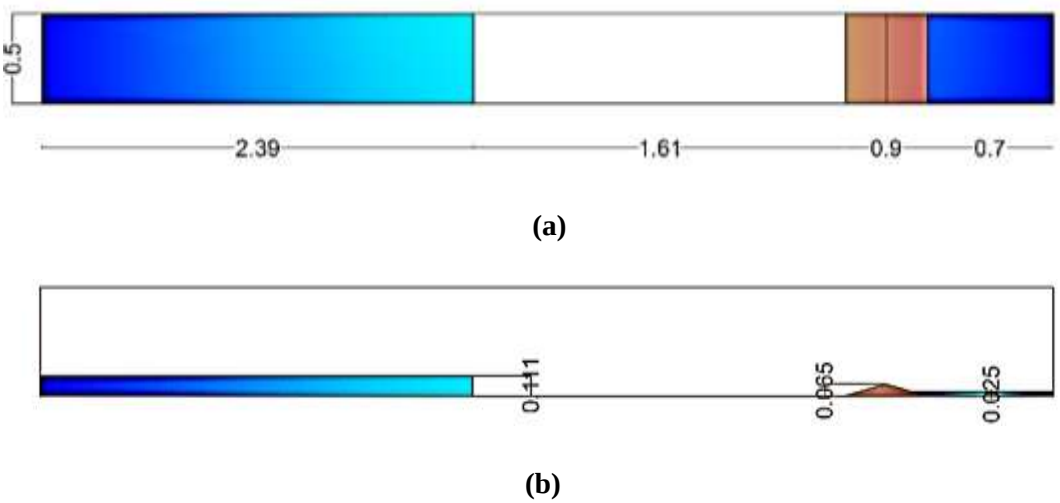

Figure 20:Floor plan (a) and side view (b) of the flume at UCL (dimensions in meters)

3.3 Numerical test conducted at the Hydraulic Lab at the University of Ottawa

For the purpose of model validation, a numerical reproduction of two physical tests explained in parts 3.1 and 3.2 is developed in this paper to compare the experimental data with numerical model results. Then, the validated numerical model was applied to estimate the tsunami base shear force on structures with various geometries based on the flume at the Hydraulic Laboratory at the University of Ottawa. The University of Ottawa physical domain (Fig. 21) is a rectangular prismatic structure 30 m long, 1.5 m wide, 1 m height, constructed of concrete. The 10 m long upstream reservoir holds a prescribed volume of water with an impoundment depth of 0.95 m. The sudden opening of the gate releases the water initially impounded from the upstream reservoir into the channel**.**

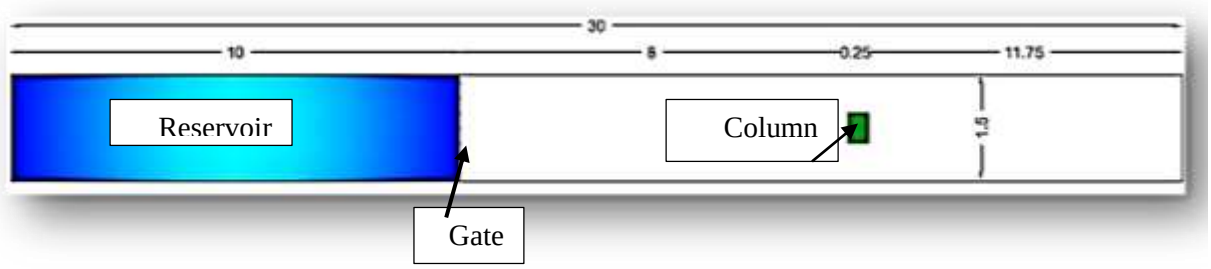

Figure 21:Floor plan view of the University of Ottawa flume (dimensions in meters)

4. Development of the Numerical model

The open-source software employed to develop the proposed computational model is OpenFOAM v2.3.0, which runs on Linux. The OpenFOAM (Open Field Operation and Manipulation) code is a numerical

simulation package which offers customized numerical solvers written in C++ language and is provided by Open CFD Ltd. The open-source aspect of OpenFOAM enables users to customize and extend its existing functionality and make it more efficient based on their own projects. For example, the extensibility aspect enables users to create typical modeling components such as boundary conditions or turbulence models or boundary and initial conditions without the need to change the existing source code. The most attractive feature of this software is its object-oriented library for CFD, which is an alternative for programmers to cope with the problem of the complexity of traditional programs. A wide range of engineering problems can be simulated using this software via solving the form of partial differential equations. The model uses Finite Volume Method (FVM) with polyhedral grid and it can also be used for massively parallel computing (Jasak et al., 2007). The main advantage of OpenFOAM is that its source code is publicly available, so, if needed, users can assess and modify it. If the model requires additional functionality, this can be added by the user. One of the notable aspects of OpenFOAM is equation representation, which provides close resemblance to the equations being solved and enables model users to develop various custom solvers (OpenFOAM 2014).

InterFoam is an OpenFOAM solver capable to handle the free-surface problem where a sharp boundary divides two fluids. InterFoam predicts the flow by applying a finite volume method for the discretization process that captures the interface. Turbulence is modeled using an incompressible RANS model. Structured meshes are employed for the simulation domain (OpenFOAM 2014).

4.1. Governing equations

Navier-Stokes equations can describe the motion of fluid - they are derived from the conservation laws and govern the movement of all types of flows regardless of their type. The Reynolds-Averaged Navier-Stokes (RANS) equations represent therefore a mathematical model of the motion of a fluid which is applied in this study and which are also available in OpenFOAM.

4.1.1. Reynolds-averaged continuity equation

The differential form of the continuity equation for a three-dimensional system is written as (Rodi, 1993).

$$\frac{\partial \bar{u}}{\partial x} + \frac{\partial \bar{v}}{\partial y} + \frac{\partial \bar{w}}{\partial z} = 0 \tag{1}$$

where $\bar{u}$, $\bar{v}$, and $\bar{w}$ are the mean velocity components in the *x*, *y*, and *z* directions, respectively, defined as

$$u(t) = \bar{u} + \acute{u} \qquad v(t) = \bar{v} + \acute{v} \qquad w(t) = \bar{w} + \acute{w} \qquad p(t) = \bar{p} + \acute{p} \tag{2}$$

4.1.2. Reynolds-averaged momentum equation

The differential form of the momentum equation for a three-dimensional system can be written as (Chamani, 2013).

$$\bar{u}\frac{\partial \bar{u}}{\partial x}+\bar{v}\frac{\partial \bar{u}}{\partial y}+\bar{w}\frac{\partial \bar{u}}{\partial z}=-\frac{1}{\rho}\frac{\partial \bar{p}}{\partial x}+g_x+v\left(\frac{\partial^2 \bar{u}}{\partial x^2}+\frac{\partial^2 \bar{u}}{\partial y^2}+\frac{\partial^2 \bar{u}}{\partial z^2}\right)-\left(\overline{\frac{\partial \acute{u}^2}{\partial x}}+\overline{\frac{\partial \acute{u}\acute{v}}{\partial y}}+\overline{\frac{\partial \acute{u}\acute{w}}{\partial z}}\right) \quad (3)$$

$$\bar{u}\frac{\partial \bar{v}}{\partial x}+\bar{v}\frac{\partial \bar{v}}{\partial y}+\bar{w}\frac{\partial \bar{v}}{\partial z}=-\frac{1}{\rho}\frac{\partial \bar{p}}{\partial y}+g_y+v\left(\frac{\partial^2 \bar{v}}{\partial x^2}+\frac{\partial^2 \bar{v}}{\partial y^2}+\frac{\partial^2 \bar{v}}{\partial z^2}\right)-\left(\overline{\frac{\partial \acute{v}^2}{\partial y}}+\overline{\frac{\partial \acute{u}\acute{v}}{\partial x}}+\overline{\frac{\partial \acute{u}\acute{w}}{\partial z}}\right) \quad (4)$$

$$\bar{u}\frac{\partial \bar{w}}{\partial x}+\bar{v}\frac{\partial \bar{w}}{\partial y}+\bar{w}\frac{\partial \bar{w}}{\partial z}=-\frac{1}{\rho}\frac{\partial \bar{p}}{\partial z}+g_z+v\left(\frac{\partial^2 \bar{w}}{\partial x^2}+\frac{\partial^2 \bar{w}}{\partial y^2}+\frac{\partial^2 \bar{w}}{\partial z^2}\right)-\left(\overline{\frac{\partial \acute{w}^2}{\partial z}}+\overline{\frac{\partial \acute{w}\acute{v}}{\partial y}}+\overline{\frac{\partial \acute{u}\acute{w}}{\partial x}}\right) \quad (5)$$

where t is the time, p is the fluid pressure, ρ is the fluid density, and g is the gravitational acceleration

4.1.3. The k − ε turbulence model

Solving the continuity and momentum equations analytically is impossible, except for a few simplified cases. In 1877, Boussinesq developed a novel idea of the turbulent viscosity and defined the Reynolds stress numerically by time-averaging the flow equations, which led to

$$-\rho\overline{u_i' u_j'}=\mu_t\left(\frac{\partial \bar{u}_i}{\partial x_j}+\frac{\partial \bar{u}_j}{\partial x_i}\right)-\frac{2}{3}\rho\delta_{ij}k \quad (6)$$

As observed in Eq. (6), there is another unknown parameter introduced with the new equation (μ_t) and a suitable turbulence model had to be employed to estimate it and close the solution system. Choosing an appropriate turbulence model is thus important to obtain accurate and realistic results.

There is no unique and universally-valid turbulence model. Also, the progress of the CFD (Computational Fluid Dynamics) field heavily depends on the advancement of computing tools and on the development in the numerical methods for partial differential equations, as well as of the flow characteristics. Solving CFD problems involves four steps, which are: defining the geometry and generating the numerical grid; creating a numerical model of the problem and solving and analyzing the obtained data. It is important to note that setting up a physical model for turbulent flow is not necessarily an accurate approach, so it is essential to fully figure out the essence of the relevant physics for each case. The nonlinear, time-dependent, three-dimensional characteristics of the Navier-Stokes equations can be used in developing turbulence models.

The two-equation turbulence models are some of the most common turbulence models. There are various two-equation models offered for turbulent flow, among which the k-ϵ and k-ω models have become industry standards and are commonly used for most types of engineering problems. For instance it was applied for simulating ship flows (Xing et al., 2007), for cases associated with heat conduction in porous

media (Fourie and Plessis 2003), aerodynamic flows (Menter, 1993) and etc. Because the $k-\varepsilon$ model has been applied in this experiment, it is briefly reviewed herein.

The two-equation turbulence models appeared following the milestone work of Kolmogorov (1942), while 26 years later, the $k-\varepsilon$ model for turbulence was introduced through the endeavors of Harlow and Nakayama (1968).

$$\mu_t = \rho C_\mu \frac{k^2}{\epsilon} \tag{9}$$

where k refers to turbulent kinetic energy, ε refers to the dissipation rate of the turbulent kinetic energy and μ_t is the eddy viscosity. Two transport equations are employed in the standard k- ε model to calculate the values of turbulent kinetic energy and its dissipation rate as (Rodi, 1993).

$$\frac{\partial(\rho k)}{\partial t} + \frac{\partial(\rho \bar{u}_j k)}{\partial x_j} = \frac{\partial}{\partial x_j}\left(\mu + \frac{\mu_t}{\sigma_k}\right)\frac{\partial k}{\partial x_j} + P_k - \rho\epsilon \tag{10}$$

$$\frac{\partial(\rho \epsilon)}{\partial t} + \frac{\partial(\rho \bar{u}_j \epsilon)}{\partial x_j} = C_{\epsilon 1} P_k \frac{\epsilon}{k} - \rho C_{\epsilon 2} \frac{\epsilon^2}{k} + \frac{\partial}{\partial x_j}\left(\frac{\mu_t}{\sigma_\epsilon}\right)\frac{\partial \epsilon}{\partial x_j} \tag{11}$$

where the turbulent kinetic energy production rate (P_k) is calculated as:

$$P_k = \mu_t \left(\frac{\partial \bar{u}_i}{\partial x_j} + \frac{\partial \bar{u}_j}{\partial x_i}\right)\frac{\partial \bar{u}_i}{\partial x_j} \tag{12}$$

$C_{\epsilon 1}$ = 1.44, $C_{\epsilon 2}$ = 1.92, C_μ = 0.09, σ_k = 1.0, σ_ϵ = 1.3.

4.1.4 Free surface tracking

The Volume of Fluid (VOF) technique is a method to track the free surface of a flow. This interface-capturing method estimates the flow occurring in two fluids (water and air) and assumes them as a single fluid with physical properties changing through the interface which separates them. Physical variables such as $\rho \; and \; \mu$ can be obtained by considering the value of the volume fraction, c (Andrillon, 2004), where the variable c equals to 0 or 1 for the gas (air) and liquid (water), respectively. The advection term defines the behavior of the free surface, which can be assumed as a treatment for the sensitivity of the VOF to the grid dimensions.

$$\rho = c\rho_1 + (1-c)\rho_2 \tag{13}$$

The two-phase algorithm of the solver InterFoam, which is based on the VOF technique, estimates the volume of the fluid in every computational cell by employing a transport equation. The physical variables

should be computed because their weighted averages depend on this phase fraction c. Using the VOF technique, the surface can be approximately obtained based on the volume fraction field. In the case where the volume of computational cell is 100% water, the value of the phase fraction is 1; however if the volume of water of the cell 0%, then this value is equal to 0. This value can be any amount between 0 and 1 if the cell is not completely full or empty. The corresponding transport equation is written as follows (Heyns et al., 2013),

$$\frac{\partial c}{\partial t} + \vec{\nabla}.(c\overrightarrow{u_c}) = 0 \tag{14}$$

Where $\overrightarrow{u_c}$ is the estimated relative velocity between air (gas phase) and water (liquid).

4.1.5 Computational domain, initial conditions and boundary conditions

In these numerical tests, a specified volume of water impounded behind a rapidly-opening gate represents the initial domain. Therefore, at time=0, most of the variables within the domain boundaries have the value of 0, including the initial pressure, velocity, and phase fractions for all of the computational cells other than those in the reservoir cells, which have a value of 1. Then the gate is instantaneously removed in the model and the initially-impounded water flows through the channel. The released water further impacts in one test a free standing vertical solid structure (Fig. 22a) and a triangular obstacle in the second one (Fig. 22b). The test is also repeated using structures with different geometries based on the flume at the Hydraulic Lab at the University of Ottawa (Fig. 22c).

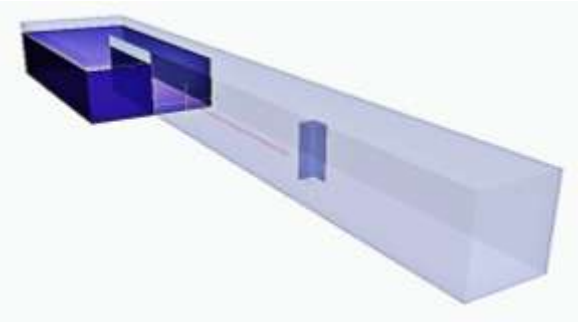

(a)

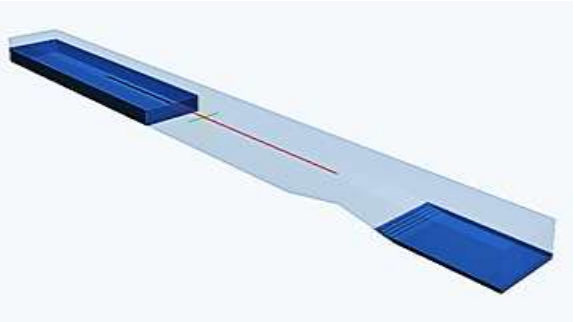

(b)

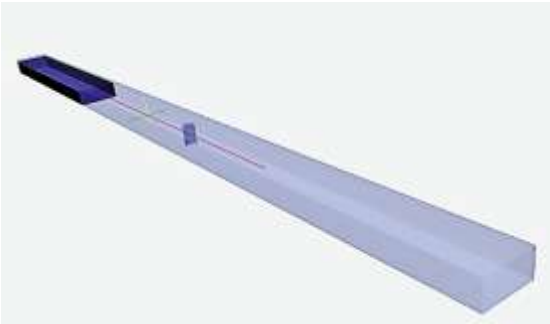

(c)

Figure 22:Initial conditions for the computational domain reproducing the tests performed at the (a) OCRE-NRC, Canada, (b) UCL and (c) UOttawa-Canada flumes at time=0

The flumes have been modeled computational domains formed by vertical (side) and horizontal (bottom) faces joined along their edges. All boundaries are specified as of "wall-type" in OpenFOAM, except for the outlet, which has been introduced as a zero gradient condition to properly account for its role as an outlet located at the downstream end of the flume. The value of the pressure variable is set to zero for the computational cells that form the walls, and, in terms of the velocity, it satisfies the no-slip condition.

The geometries of the flumes employed to simulate the composite structures are different from those utilized for model validation purposes. First, the domain was modeled using exactly the same dimensions as the flumes at the NRC-Canada and UCL, which enabled model validation and an exact comparison of the numerical model results with those obtained from the physical tests. Then, the dimensions of the flume at the University of Ottawa were employed to perform the numerical tests on composite structures which enabled the comparison with experimental tests. To set up a numerical model for all cases investigated, a mesh of uniformly-spaced virtual boxes with dimensions of 2x2x2cm was generated. The selection of the mesh size was based on the results of a sensitivity analysis investigation. In order to reduce the computational cost, a customized grid was generated for each impoundment depth used in the tests. For each composite structure, a corresponding mesh was generated. It should be mentioned that the existence of a grid layer located on top of the reservoir was essential in order to avoid any overflow of water from the flume.

4.1.6 Courant number and the time step

There is a trade-off that cannot be overlooked between applying a shorter time step to obtain a precise answer and applying a longer time step to obtain simulation results at higher speed. Deciding on the time step control is a challenging procedure and, to avoid convergence issues, a self-adapting technique for the

time step size is considered. This should be set at the start of the temporal simulation, and it depends on the Courant number, Co, as defined below (Berberović, 2010):

$$Co = \frac{|U|}{d}\Delta t \tag{15}$$

where the vector d is the distance between the interfaces of two computational cells and Δt is the time step. Thus, the maximum local Courant number, Co_{max}, can be employed to calculate the time step size uing the following equation:

$$\Delta \mathrm{t} = \min\left\{min\left[min\left(\frac{Co_{max}}{Co_0}\Delta t_0, \left(1+\lambda_1\frac{Co_{max}}{Co_0}\right)\Delta t_0\right), \lambda_2\Delta t_0\right], \Delta t_{max}\right\} \tag{16}$$

To reduce numerical oscillations, two variables, $\lambda_1\ and\ \lambda_2$, were proposed to control the rise in the time step.

5. Model validation

The accuracy of the numerical model was further evaluated by comparing the simulation results with the ones recoded during the experiments.

5.1. Test Case1 – Experimental data - total base shear force exerted on a square column induced by a dam break propagating over dry bed

5.1.1 Sensitivity of the mesh density on the magnitude of the total base shear force exerted on a square column

In an attempt to achieve sufficiently accurate results independent of the mesh resolution, an appropriate grid was determined by running trial simulations starting from an initially coarse mesh of 5x5x5cm cells. The numerical results were compared with the experimental data of Al-Faesly et al. (2012). The comparison shows that the numerical model can reproduce the laboratory data with good accuracy and indicates also that reducing the dimensions of cubic control volumes to values smaller than 2x2x2cm does not significantly improve the accuracy; hence, it was not worth increasing computational cost by further reducing the size of the computational grid, and, as a result, this computational grid of 2x2x2cm was employed to model various cases (Fig.23). The total base shear force exerted on the column was estimated by integrating in space and time the pressures exerted on the column.

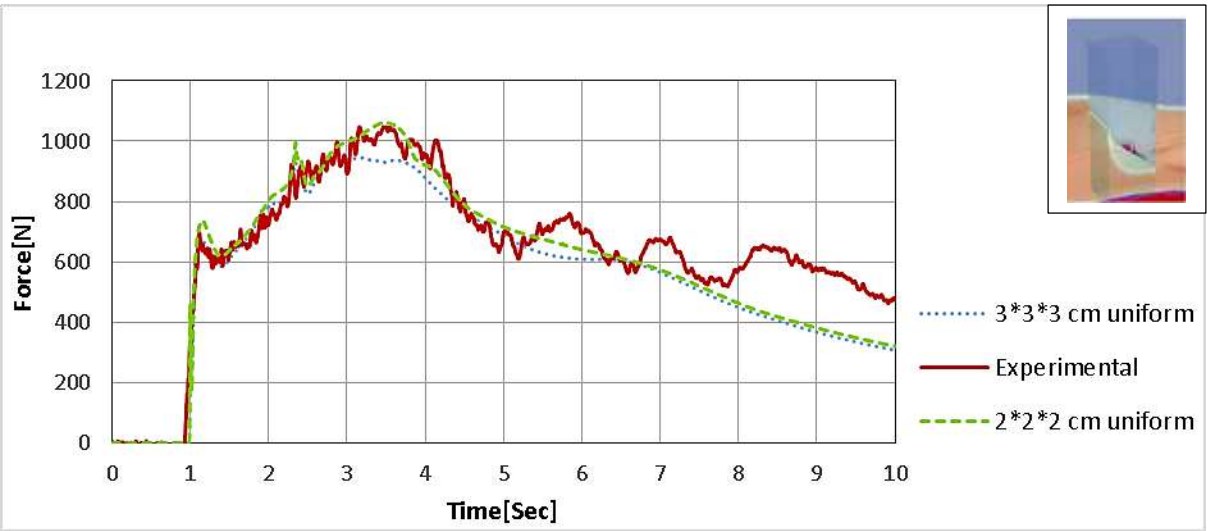

Figure 23:Effect of mesh density on the time-history of the base shear-force for a 1.15m impoundment depth exerted on a square column with dimensions 0.305x0.305x1m

5.1.2. Comparison of the force exerted by a hydrodynamic bore on structures

Fig.23 shows comparison of the numerical results with the data obtained from the laboratory experiments and shows that the first peak force is due to the initial impact of the dambreak wave on the upstream side of the structure: this is in perfect agreement with the numerical simulation results. Then, the force increase reduces because flow velocity reduces to zero and a resulting reduction in the base shear force value is recorded. This is due to the fact that some water reaches the lateral sides of the column and passes by it. After the first impact, the impacting flow of water collapses onto the incoming flow and impacts the water surface beneath, leading to the occurrence of a second peak recorded at time=1.5 sec. This sudden change in the total base shear force has also been documented in other experiments such as those of Nouri et al. (2010), Arnason (2005), or in numerical results of Douglas and Nistor (2014). Another noticeable discrepancy occurs after t=5 s, when large fluctuations are observed in the experimental data, which are most probably the result of air entrainment and turbulence; however, it appears that OpenFOAM can reasonably predict the total base shear force exerted on the column.

Figure 24 reveals the comparison of the numerical and experimental results of the time history of pressure estimated at the upstream side of the structure located at the elevation of 2 cm from the bed. A fairly perfect agreement is observed, however the significant discrepancy can be observed at the first interaction of the coming wave and column, while the estimated force time histories of the same experiment does not reveal this phenomenon at the initial interaction of the bore and column. The reason can be attributed to the fact that this phenomenon occurs for only a moment (one tenth of a second) as a result its influence is negligible by integrating the pressure over the column surfaces.

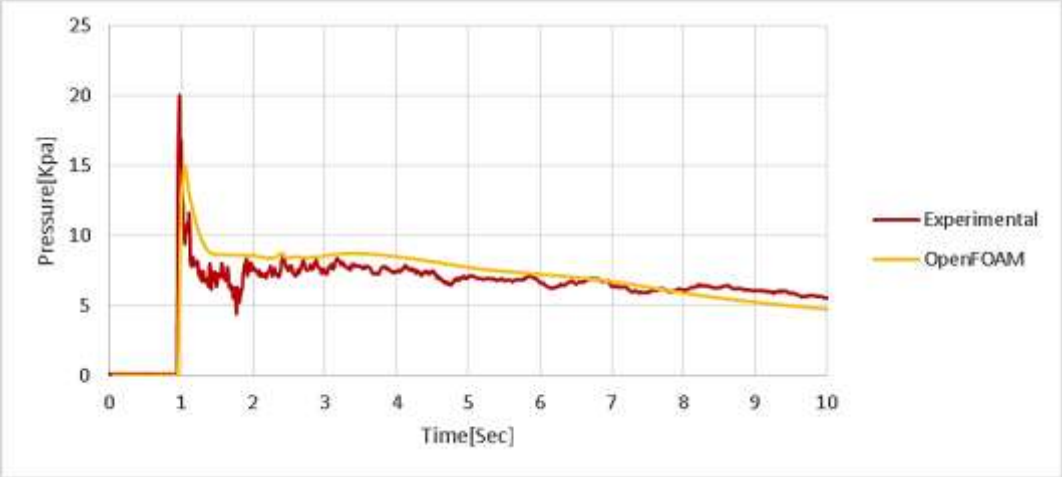

Figure 24:Total pressure for dry bed conditions. Initial impoundment water depth of 115 cm.

5.2. Test Case 2 - Comparison between the recorded and estimated total force obtained from laboratory tests and numerical simulations induced by a dambreak wave over a dry bed.

5.2.1. The effect of mesh density on the force exerted on the cylindrical column

A similar procedure was performed for this case as well: data plotted in Fig.25 confirm that the refined mesh leads to a better agreement with the experimental data.

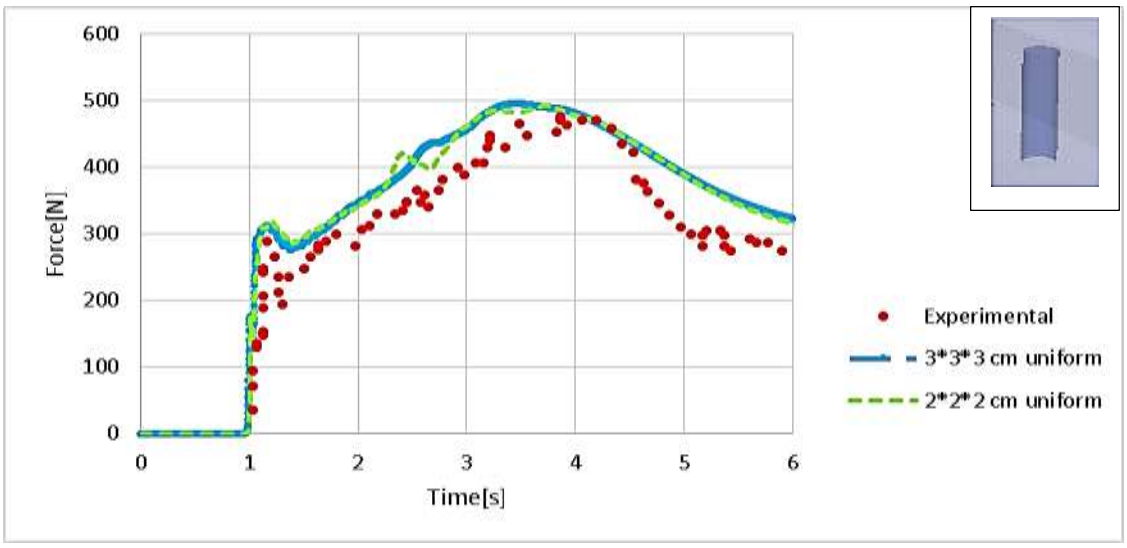

Figure 25:Effect of mesh density on the time history of the base shear force for a 1.15m impoundment depth exerted on a circular column with dimensions 0.305x0.305x1m

5.2.2. Comparison of the hydrodynamic force of a bore on a structure

Figure 25 compares the simulated force exerted onto a vertical column of circular cross-section with the experimental results. The numerically-simulated force time-history revealed that the numerical model results reproduce with reasonable accuracy the data from laboratory experiments. The initial peak (Fig.25), which occurs at initial impact, differs slightly from that of the experimental data.

Some distinction is observed after t=4.5s from the initial bore impact when the experimental and numerical test results diverge significantly especially in the wake area of the column. It may be concluded that the model acts better in simulating the local force exerted on the circular column comparing to the results of St-Germain et al. (2012), which were calculated for a circular column with an impoundment depth of 0.85m using a smooth particle hydrodynamic (SPH) model. The results of the force time history of St-Germain et al. (2012) indicated significant discrepancy and the authors concluded that this was because of the inadequate estimation of the time-history of the water surface.

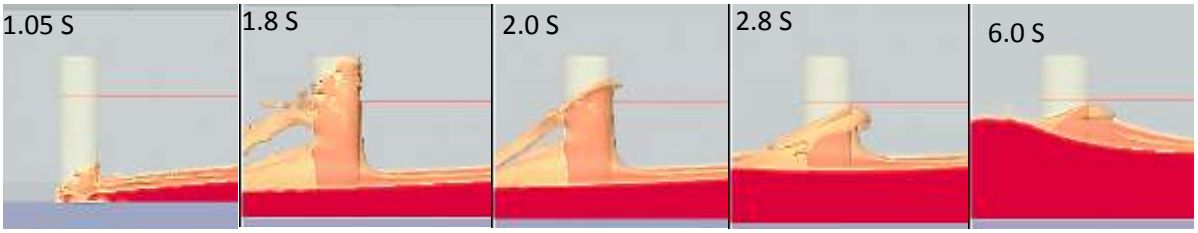

Figure 26:(a) Time-history of the interaction between the dambreak wave and the circular column (b) Moment of occurrence of the initial peak of the base shear force (c) Start of the collapse of the runup flow onto the column due to gravity (d) The return flow impacts the incoming flow surface (e) Instant of the occurrence of the maximum force

Figure 26 provides detailed behavior of the interaction between the bore and the circular column. Figure 26(b) reveals the instant of maximum initial impact force. Figure 26 (e) projects the instant of the occurrence of the Maximum hydrodynamic force.

5.3 Test Case 3 - Numerical modeling of the time-history of the water surface elevation at different times along a channel with a triangular obstacle

In the process of validating the proposed numerical model, a comparison is performed for the time-history of the water surface obtained from the numerical model with the results of the experimental data of Soarez-Frazao (2002) conducted at UCL, as well as with the numerical results obtained by Biscarini et al. (2010) who also used an OpenFoam numerical model. The proposed model used the k-ω turbulence model. Figure 27 shows the side view of the flume at UCL conducted by Soarez-Frazao (2002). The comparative results of these experimental tests and numerical simulations are shown in Figures 29 to 32.

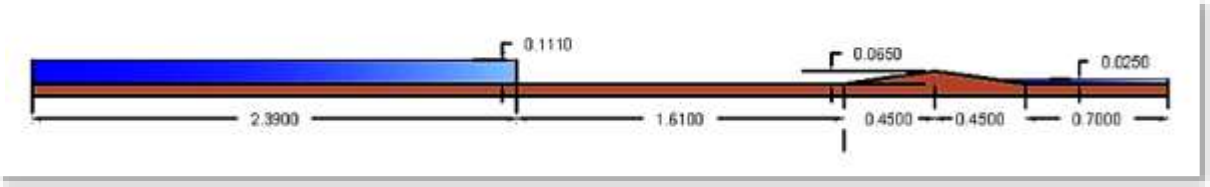

Figure 27:Computational domain for the (UCL) experiment for time=0

At time t=1.8 s (Fig. 28) from the opening of the gate, the dam break wave has overtopped the triangular obstacle and reached the middle of the downstream slope (Fig.29) and further splashed on the end wall surface of the small reservoir. Overall, the results of the numerical simulation results agree well with the physical model ones and with the numerical results of Biscarini et al. (2010). However, the modelled data of the time-history of the water levels over the downstream slope do not agree well with the physical test results. This may be due to the fact that the splashing water causes the entrainment of air bubbles in the pool of water formed over the downstream slope - the present numerical model is not capable of simulating air entrainment.

Figure 28:Visual of the water surface elevation at time=1.8 s from gate opening

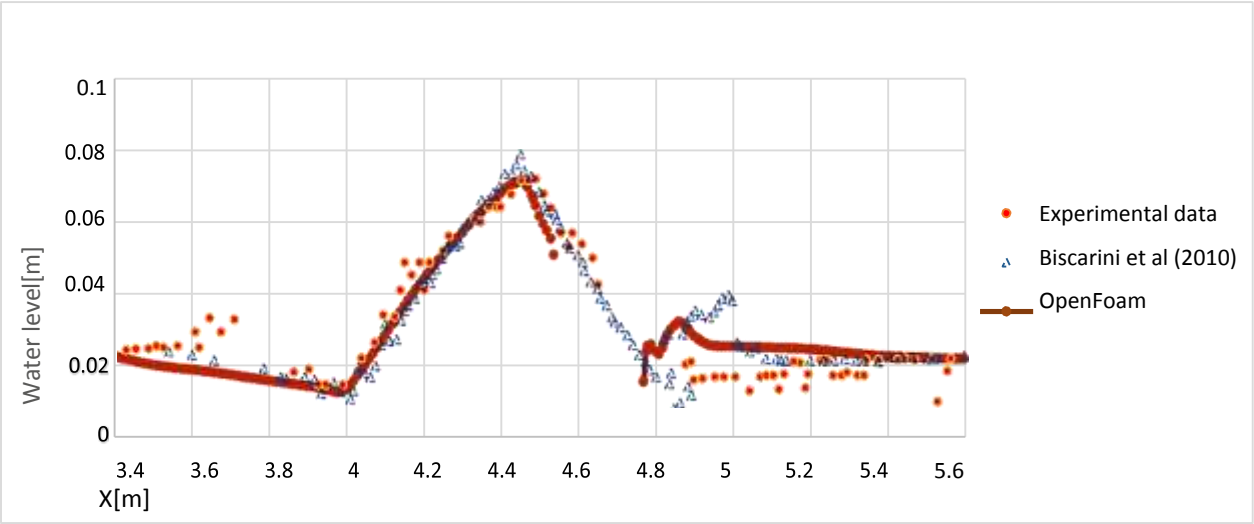

Figure 29:Comparison of the maximum water surface elevation for the experimental data and the numerical data of Biscarini et al. (2010) and the present model at time 1.8 s from gate opening

At time t=3 s (Fig.30 and Fig.31), a similar trend is observed between the simulated and experimental data, but the largest discrepancies in the water surface are observed in the pool of water formed over the downstream slope. A similar comparison of the numerically calculated water surface at location X=4.2 m to 4.4 m from gate opening shows less accuracy comparing to the water surface recorded in the experimental tests.

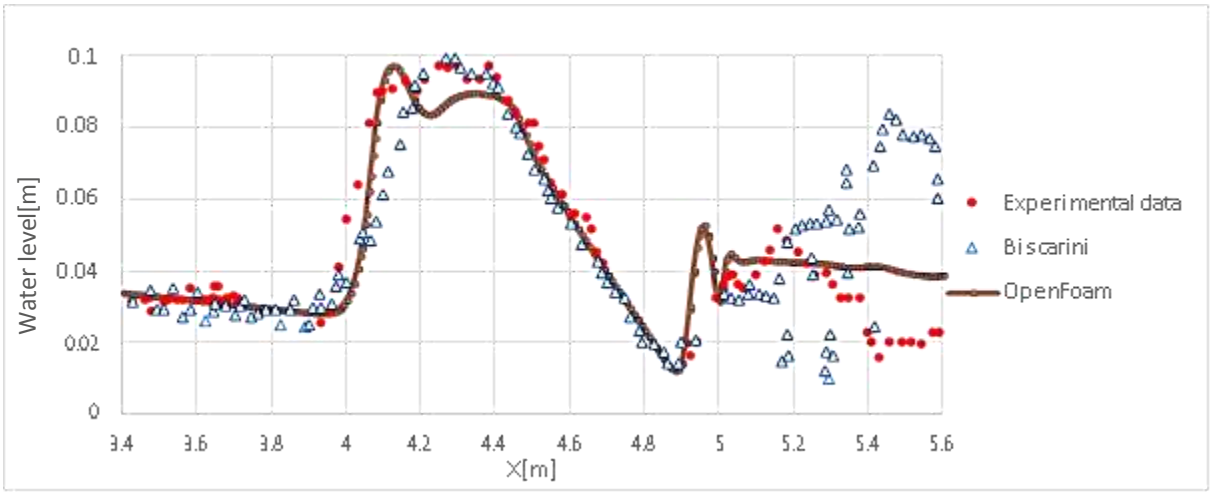

Figure 30:Comparison of the maximum water surface elevation for the experimental data and the numerical data of Biscarini et al. (2010) and the present model at time 3.0 s from gate opening.

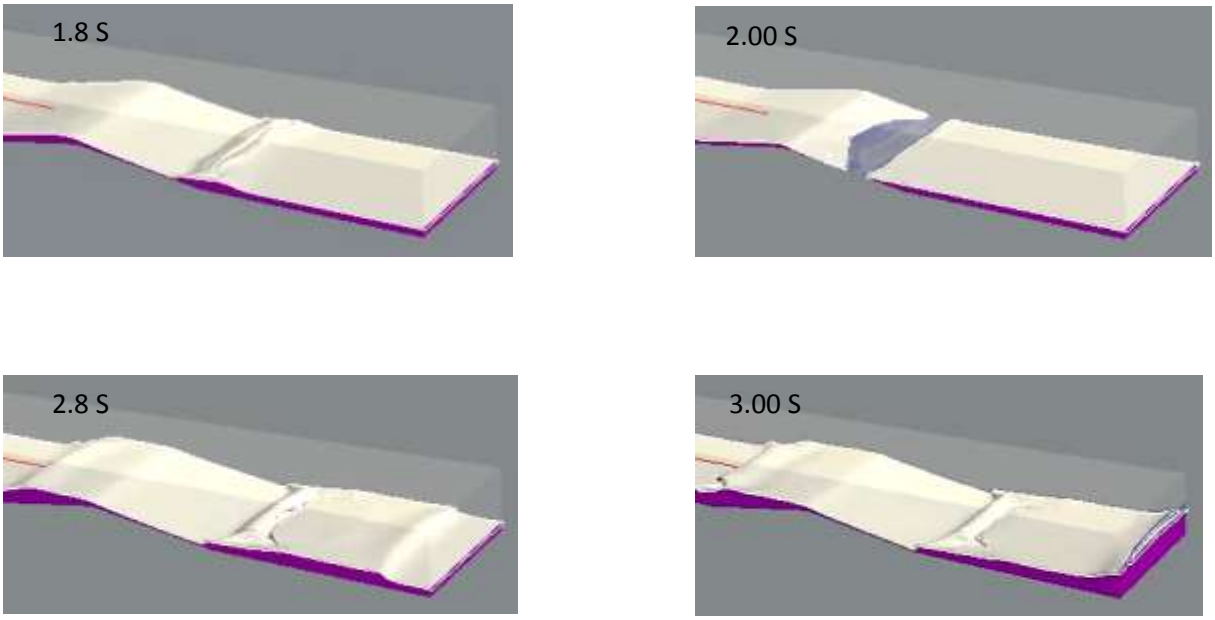

Figure 31:Visual of water surface profile flowing over a triangular obstacle between time 1.8 s and 3s.

At time t=3.7s (Fig.32 and Fig.33) water started flowing in the opposite direction to the initial flow (that is, in upstream direction) as a result of it being reflected by the downstream wall. Generally, good agreement is observed, but the profile of the water surface over the triangular obstacle slope facing the upper reservoir is not in good agreement with the laboratory data.

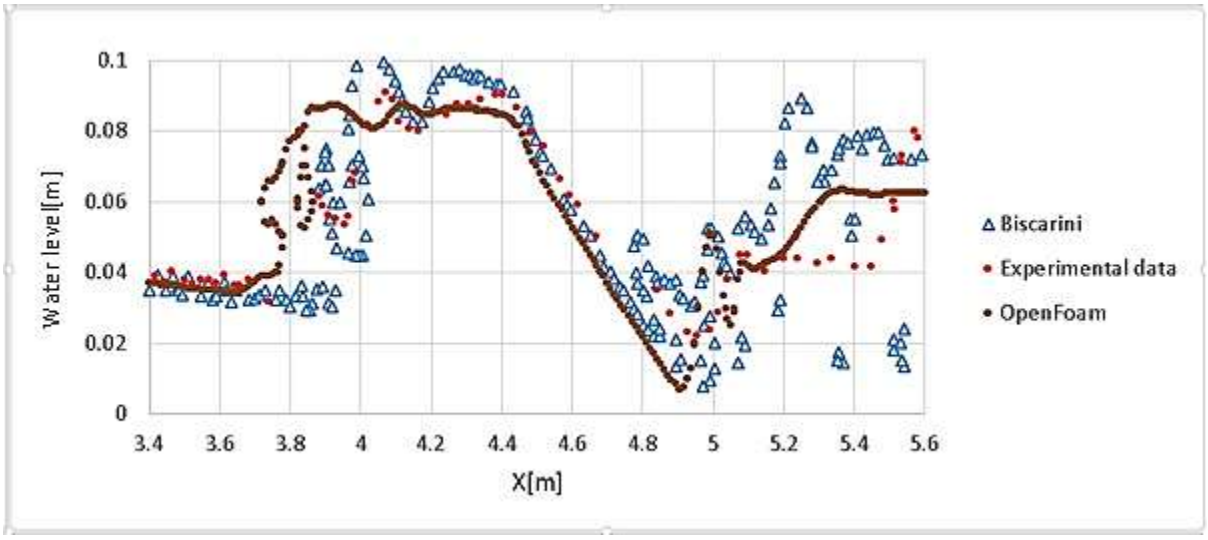

Figure 32:Comparison of the maximum water surface elevation for the experimental data and the numerical data of Biscarini et al. (2010) and the present model at time 3.7 s from gate opening.

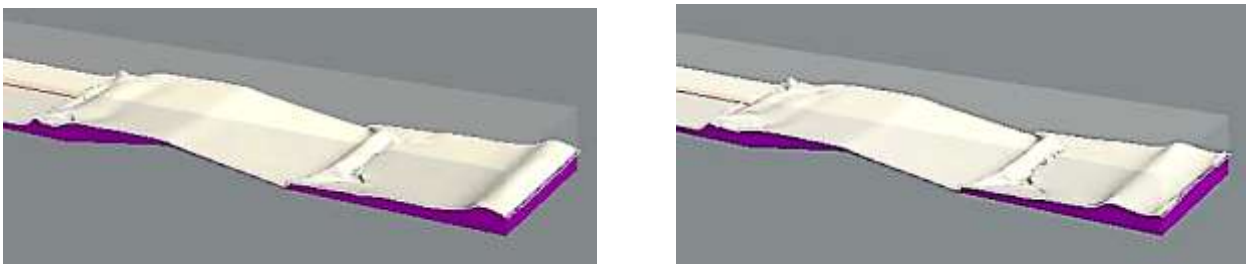

Figure 33:The dambreak wave impacts the end wall of the flume and flows back over the triangular structure.

It can be concluded that the refined grid yields a sufficiently accurate result and that the numerical model is able to simulate the experimental data: hence, this grid was further used in subsequent simulations to study the application of the model to investigate the relationship between the tsunami-induced force and structure's shape.

6. Application of the proposed numerical model to study the impact of structure's shape on the total base shear force

Base shear force on various structural cross-sections

Studying the relationship between the geometry of a structure and the hydrodynamic loading exerted by coastal flooding due to tsunami is important when designing near shore structures as their shape can considerably affect their stability and capacity to withstand the impact of these extreme forces. As a result, the numerical model that was validated in the last section, is now employed to study the effect of structural shape of a building (Fig. 34). The bore characteristics were set identical for all cases investigated. In Fig. 35, the time-history of the total base shear force exerted by the bore on the structure is shown.

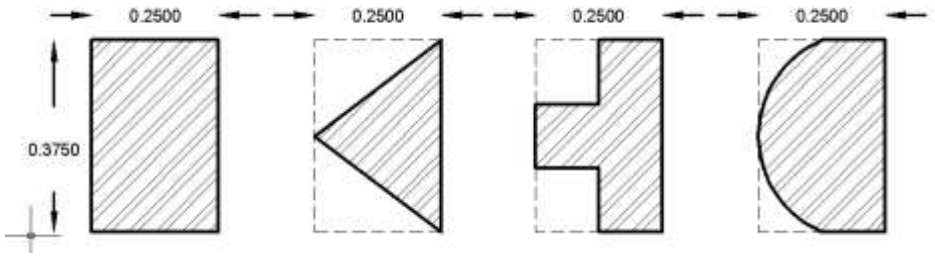

Figure 34:Schematic of structures with different cross-sections, (Dimensions in meters).

Figure 35 shows that the shape of a structure plays an important role for the magnitude and time history of the total base force exerted by a tsunami-like bore. As expected, based on the physical conservation laws, it can be argued that the more hydrodynamic the structure's shape, the lower the base shear force exerted on the structure. Hence, the total horizontal base shear force on a rectangular cross section column is larger than that exerted on the other structures investigated whose cross sections were equivalent. The reason for that is that, from a hydrodynamic point of view, the rectangular shape is the least efficient. The flat vertical upstream surface of the rectangular shape allows more water inflow to impact its exposed surface while the corners generates significant turbulence. Hence, this generates a base shear force with a larger magnitude comparing to the more hydrodynamic cross-sections of the other structures investigated.

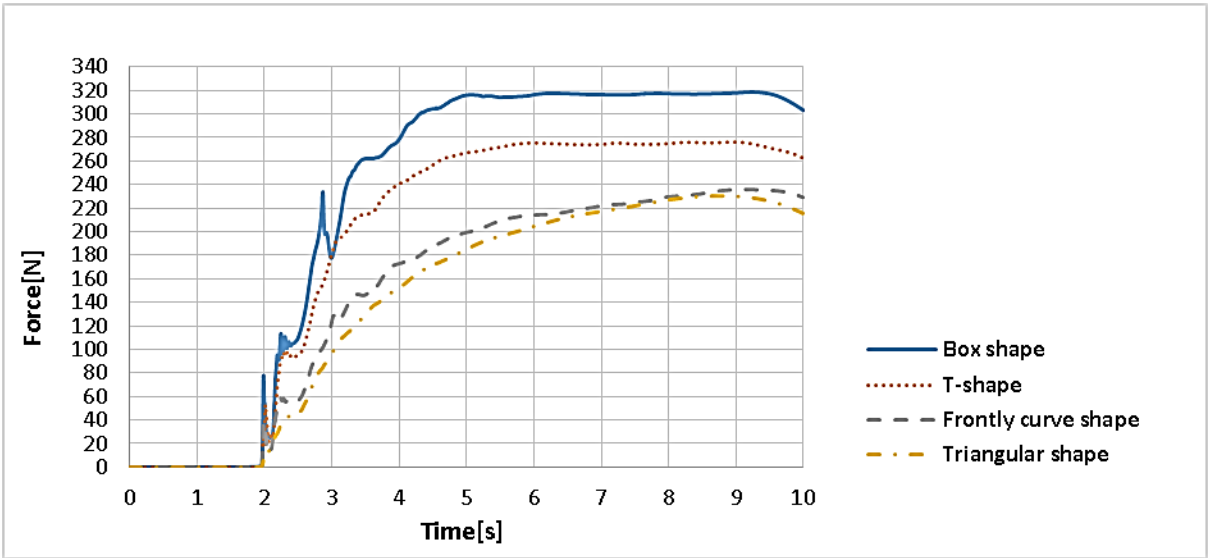

(a)

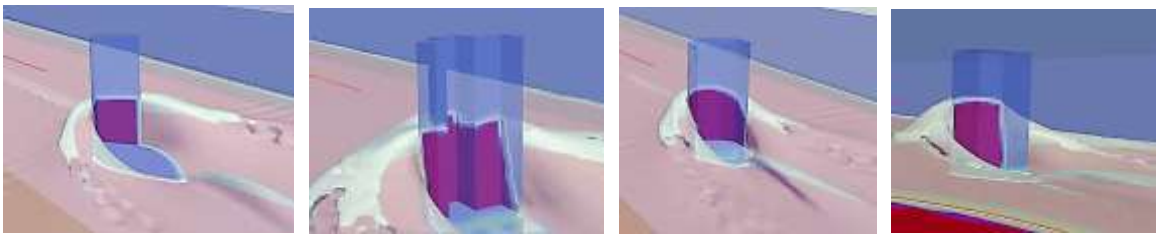

(b)

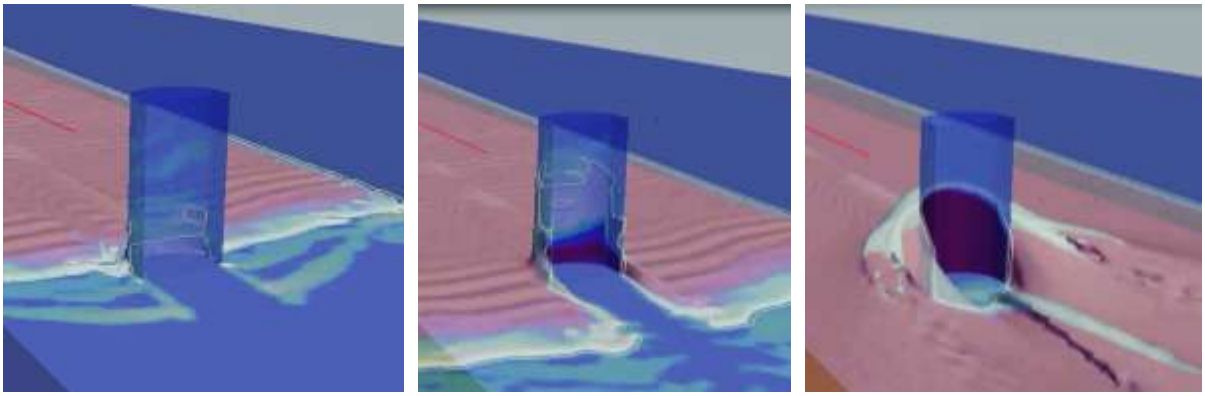

(c)

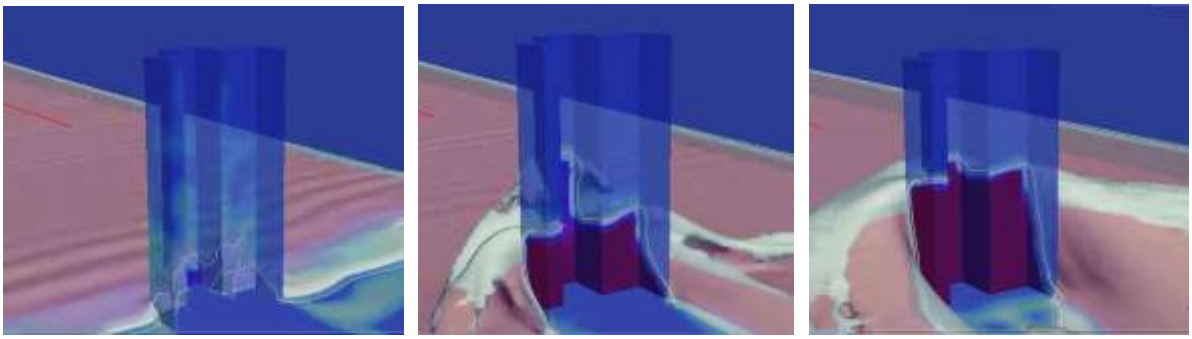

(d)

Figure 35:. (a) Time-histories of the base shear force for rectangular, frontally-curved, triangular, and T-shaped structures. (b) Visual of the interaction between the incoming flow and the triangular, T-shaped, frontally-curved and box-shaped structures. (c) Enlarged visual of the first interaction between the frontally-curved column and incoming flow (left), the moment of maximum impact force (middle), the moment of maximum hydrodynamic force (right). (d) Enlarged visual of the first interaction between the T-shape column and incoming flow (left), the moment of maximum impact force (middle), the moment of maximum hydrodynamic force (right).

Considering the resulting force on various cross shape structures, the magnitude of the first rise in the base shear force exerted on the rectangular cross section structure is considerably smaller than the maximum force exerted by the continuous turbulent flow afterwards. The first rise in the base shear force is usually called the impulse force.

The reduction in the base shear force after the initial bore impact is approximately 30 % of the first spike of the force exerted on the rectangular cross section case. This is significantly more than the reduction observed for other cases such as the T-shape and front curve structures, for which the reduction was found to be close to 50%. It worth noting that the initial impulse force is not observed for the case of the triangular cross

section case - this structure is oriented with one of its corners pointing in the direction of the flow - this deflects the flow to the sides rather than blocking it.

For all structures, following the initial spike, a sudden reduction in the base shear force was observed, followed by the second spike that is generated as a result of the hydrodynamic bore running up the columns. Following this, the exerted total force on the frontally-curved and triangular cross section structures increases gradually until it reaches the peak and then starts to decrease abruptly. This decrease is due to the limited size of the reservoir: for an infinitely long reservoir, the base shear force would remain constantly at this second peak magnitude. However, for a T-shaped cross section structure, this increase in force is steeper until it reaches the peak point. Following the second spike for a rectangular cross structure, a third sudden rise in the force is observed, something not observed in the other cases. The significant spikes in the base shear force observed in the case of this cross section is the result of a much larger blockage of the flow by the flat frontal surface. This spike is also observed in the other cross sections but is it larger for the rectangular cross shaped structure. However, the geometry of the frontally-curved, T-shape, and triangular structures directs the water towards the lateral sides of the structure and this significantly reduces the volume of water accumulated at the upstream side of these structures. Consequently, this reduces the magnitude of the maximum initial base shear force.

The guideline by Federal Emergency Management Agency (FEMA) in 2012, FEMA P646, provides useful instructions about the construction and design of vertical evacuation structures. The main reason for publishing this guideline was the lack of standards in designing tsunami resistance structures. This guideline provides a useful equation for estimating the hydrodynamic force of tsunami bores on a structure as

$$F_D = \frac{1}{2} C_d \, \rho \, B \, (h \, u^2)_{max} \tag{17}$$

where C_d is drag coefficient having the value of 2 for rectangular structures, u and h are bore velocity and depth, respectively at the location of the structure, B is the projected width of the structure that is perpendicular to the direction of the flow and $\rho(h \, u^2)_{max}$ estimates the momentum flux. Due to the fact that the terms h and u do not reach their maximum value at the same time, estimation of hydrodynamic force is dependent on measuring the temporal variations of $(h \, u^2)_{max}$.

One of the key factors required for calculating the hydrodynamic force is C_d which has the value of 2 recommended by FEMA. This recommendation is only limited to rectangular structures and it does not provide any value of drag coefficient for more complex geometries. It reveals that FEMA recommendation for the drag coefficient can be improved. One way to calculate drag coefficient is to go through a reverse

process of estimating a value for hydrodynamic force, bore depth and velocity numerically. (Yeh, 2007) proposed to estimate the bore depth and velocity by considering no obstruction condition. This means that a value for h and u can be taken from the location of the structure without considering any structure at that location.

In order to apply equation (17) for test case 1 we considered values of 3.2 m/s and 0.35 m for bore velocity and depth respectively. Those amounts correspond to an unobstructed condition (Fig.36) at time 3.5 second, which is the moment that the hydrodynamic force reaches its maximum magnitude being approximately 1050 N. Therefore, the value of drag coefficient is calculated to be equal to 2. This indicates that the FEMA suggested value of 2 for drag coefficient for rectangular column can be reasonable. However, based on results of Fig.23 and by considering bore depth of 0.35 meter and bore velocity of 3.2m/s at the location of the structure for the time of maximum force and B which is the same for all of the columns, the drag coefficient is dependent on force which depends on the geometry. As the more hydro-dynamically shape structure reduces the maximum force, one can conclude that drag coefficient can also be considered less than 2.

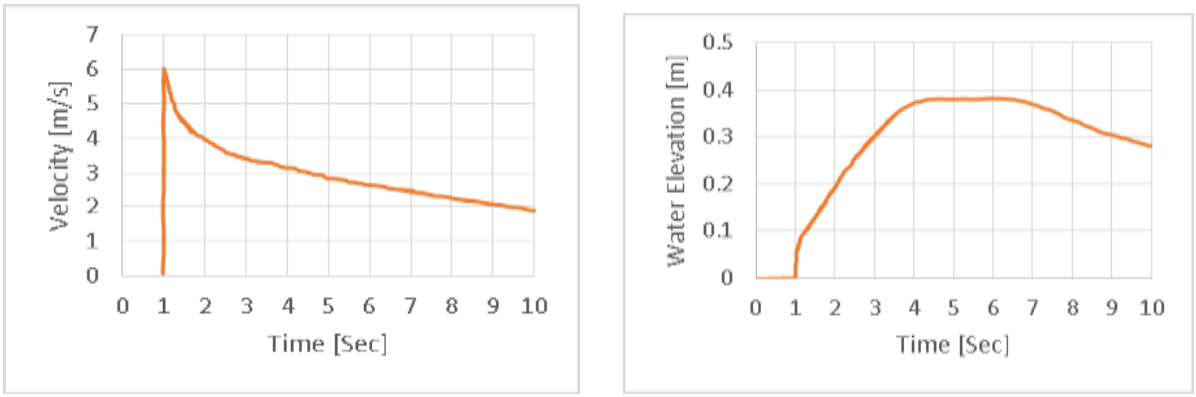

Figure 36:Time-history of the base shear-force for a 1.15m impoundment depth at the square column location without the presence of square column.

7. Conclusions

The interaction between tsunami-like bores propagating overland and impacting structural models of various cross-sections, including rectangular, frontally-curved, triangular, and T-shape, was studied by applying a newly developed three-dimensional hydrodynamic numerical model. The performance of the model is assessed by comparing the obtained numerical results with experimental data obtained from laboratory tests conducted at the OCRE-CHC in Ottawa, Canada, the Hydraulic Laboratory at the University of Ottawa,

Canada and in the Hydraulic Laboratory of the Université catholique de Louvain, Belgium. Good agreement was demonstrated between the numerical model results and the experimental data. Following a comparative study and validation, the numerical model was employed to investigate the impact of a tsunami on columns with various structural geometry (cross-sections). Results indicated that the more hydrodynamically-shaped structures allowed the bore to be deflected along the sides of the structure, reducing thus the maximum base shear force exerted on it. In addition, the proposed value of 2 for drag coefficient for rectangular structure by FEMA can be considered less than that for more hydrodynamically-shaped structure.

Comparing the results for various cross-sections of the structures, it can be argued that the magnitude of the hydrodynamic loads was the largest for the rectangular-shaped structure while it was smaller by approximately 12% in the case of the T-shapes and frontally-curved structures. The minimum value of total force was observed for the case of the triangular column.

The present study demonstrates that the shape of a structure has an important effect and plays an important role in the magnitude of the hydrodynamic loading. As such, the cross section of a nearshore structure should be considered when planning and designing it. A careful selection of the architectural plan of a building may significantly reduce tsunami-induced loading.

Chapter 5

Technical paper 2:

Large Eddy Simulation of Extreme Hydrodynamic Forces on Structures with Mitigation Walls Using OpenFOAM.

Samieh Sarjamee. Ioan Nistor. Abdolmajid Mohammadian.

Abstract

The objective of this study is to evaluate the performance of a Large Eddy Simulation (LES) numerical model to assess the influence of mitigation walls with various cross sections on the tsunami-induced loading exerted on a free-standing structure. The validation of the model was performed using laboratory experiment results previously conducted by the second author. The employed experiments simulated a tsunami-like bore at two different impoundment depths, including 55 and 85 cm. The results showed that the one-equation subgrid-scale energy transport Large Eddy Simulation approach performs better than RANS models such as *k-ε, k-ω, and LRR* and can accurately reproduce experimental data obtained for a wide range of experimental conditions.

Keywords: hydrodynamic loading, tsunami, extreme hydrodynamic forces, OpenFOAM, force-time histories, mitigation wall, Large Eddy Simulation, RANS

1. Introduction

The occurrence of natural disasters and associated coastal damage, such as floods and tsunamis is predicted to increase. Coastal community and infrastructure exposure to risks from coastal hazards such as tsunamis and storm surges is increasing because population density and volume in vulnerable coastal areas has grown significantly over the past decades.

Tsunamis are a threat to people's lives and coastal communities. One of the primary mitigation strategies is horizontal evacuation to uphill or inland locations, which requires significant warning time to execute effectively. This has led researchers to turn their attention to improving tsunami warning systems which are designed to increase aware of an impending tsunami danger and help evacuate the tsunami hazard areas in time. This strategy can be effective to save human lives. However, in case where the affected coastal regions are low-lying, horizontal evacuation does not lessen the huge social, economic, environmental, and political

losses. In this case, vertical evacuation using tsunami-resistant structures can be an ideal mitigation strategy and, hence, studies are required to fully understand tsunami loading and to determine the optimal structure capable of withstanding the tsunami impact and loading.

While experimental studies can be used to understand different aspects of the phenomena, they are typically expensive, time-consuming and prone to scale effects and measurement inaccuracies. Numerical modeling, on the other hand, is an alternative that, if demonstrated to be accurate enough, could be much less expensive, faster, as well as capable of assessing a wider range of scenarios and be also applicable to the actual scale of the problem. This motivates the present study where the objective is to examine various numerical modeling approaches and provide an insight into their performance in the context of tsunami bores and their impacts on costal structures.

Various coastal structures such as seawalls, bulkheads, and breakwaters have been proposed by researchers as protection methods for coastal regions. The main objective of the construction of these structures is to avoid the subsequent inundation and lessen the possibility of further damages by flooding and bores impacts. There are numerous papers on the subject of seawall and beach interaction. Kraus and Mcdougal (1996) reviewed 40 papers on this subject and found that there is controversy regarding the effectiveness and functionality of seawalls. Some people believe that seawalls are not only costly and intrusive on shoreline views, but that they also limit beach access and interrupt longshore sediment transport. In addition, seawalls have also failed to fulfill expectations of protection against tsunamis. In the past, seawalls have been toppled and tsunami-induced bores have displaced, overtopped, and destroyed many of the seawalls built to protect against such phenomena. For example, in 1993 at Okushiri (Shuto and Matsutomi 1993), Island, Japan, a tsunami caused 185 deaths in spite of a 4.5-meter-high seawall that was constructed to shield this area. An investigation conducted on the post-tsunami surviving buildings showed that there were some factors which played a major role in reducing the tsunami-induced force. These factors include the orientation and design of the buildings as well as the existence of low-height walls located upstream of the structures, which proved to be effective at reducing the exerted tsunami force by dissipating their energy (Lukkunaprasit and Ruangrassamee 2008). Nowadays, researchers are trying to understand the characteristics of tsunami-induced forces in order to design tsunami-resistant buildings or structures.

In order to validate the performance of different RANS and LES approaches, this paper compares the results of multiple numerical experiments performed to study the influence of mitigation walls with various shapes and locations on reducing the force exerted on a free standing square-shaped column. In this paper, a computational model of the laboratory experiments conducted by Al-Faesly et al. (2012) is developed, and the numerical results are analyzed in comparison with the physical test data in order to validate the model.

This paper is organized as follows. Section 2 provides a literature review on the subject investigated while the numerical model is described in Section 3. Section 4 deals with structural and walls geometry and location as well as the initial boundary conditions. In Section 5, comparisons of the numerical results with experimental data are presented for various cases and the performance of various numerical models is discussed and evaluated. Finally, some concluding remarks complete the study.

2. Literature Review

There have been several studies investigating the shear force exerted on structural elements such as vertical walls. However, few studies have directly focused on the efficiency and effectivity of mitigation walls in reducing the force generated by the impact of a tsunami bore on near-shore structures. To the best knowledge of the authors, LES modeling of tsunami bores using an equation for subgrid scale kinetic energy has not been performed prior to this study. Furthermore, numerical simulation of the effect of low-height mitigation walls on force reduction for tsunami bores has not been conducted before as well.

Investigations on tsunami loading began with the experimental tests conducted by Stoker (1957), aiming to investigate tsunami loading on a vertical wall. He concluded his study by proposing an equation for estimating tsunami loads. Cumberbatch (1960) attempted to estimate the force imposed on a rigid wall originating from a water wedge which was assumed to be 2-dimensional before impact. His two proposed solutions could not describe the flow on all regions located between the tip and the origin and was only valid for regions far from and close to the contact point. Hence, he proposed matching the solutions so that his formula could cover all the regions. Laboratory tests conducted by Fukui et al. (1963) focused on estimating the base-shear force exerted on dikes by applying two different tank sizes to determine how different scales could affect the results. Cross (1967) tried to refine Cumberbatch's (1960) proposed formula for the shock pressure of a small-scale tsunami wave on a vertical wall by adding a hydraulic term. Ramsden (1996) also focused on the interaction of a tsunami force and a structural element or a vertical column. Their findings revealed that the maximum run-up force was responsible for imposing the maximum force on the wall. A similar experiment was also performed by Arikawa (2008) on a vertical concrete wall.

As mentioned above, the earliest studies on hydraulic bore-induced forces focused on structural elements which later switched to 3-D structures. Extensive physical and numerical studies have been performed to date. Arnason's (2005) PhD dissertation objective was to determine how tsunami forces could affect onshore structures. Asakura et al. (2002), Fujima et al. (2009), and FEMA p-646 (2012) proposed formulae for estimating tsunami-induced forces on structures. These formulae were an improvement in comparison to the previous ones but were not however capable of covering all the effective parameters such as the

transitory characteristic buoyancy forces. Thusyanthan and Madabhushi (2008) and Wilson (2010) examined the tsunami loads on a model of a wood structure coastal house. In a similar experiment performed by Bandara (2012), a real 2 story school building similar to those that withstood the 2014 Indian Ocean Tsunami was used to study different aspects of tsunami loads. The results obtained in these types of studies are case dependent and they are hence limited playing a significant role in the design process yet.

Various studies have been performed to numerically examine the effect of tsunami-induced bores on structures. Lagrangian-based particle methods have been used by researchers to study the effect of tsunami waves on structures. Gotoh et al. (2004) applied a combination of SPH (smoothed particle hydrodynamics) and LES models to study the tsunami interaction with partially immersed breakwaters. Gotoh et al. (2005) simulated the overtopping process over vertical seawalls. St-Germain et al. (2014) studied numerically and experimentally the influence of tsunami bores on columns of square cross section by employing a three dimensional smoothed particle method numerical method. The item in which a significant difference was observed between the collected data and simulation results was the presence of an impulsive force predicted by the SPH model but not observed in the physical test. Liu et al. (2014) also applied a SPH model to study the propagation of tidal bores numerically and compared their results with the similar experimental data performed. The comparison showed a good agreement between numerical and physical results. Huang and Zhu (2015) proposed an MPS (Moving Particle Simulation) approach which is also a Lagrangian approached method. It does not need any computational mesh and is able to accurately simulate the interaction between tsunami waves and structures.

Nouri et al. (2010) conducted an experimental test program to study the influence of tsunami bores in laboratory in terms of the exerted force and pressure on the structure. They considered two free standing structures with circular and square cross sections located close to the downstream end of a flume with high-discharge. The forces on the structure were recorded as well as the pressure distribution exerted on them generated by the bore. A good agreement was observed with the results of similar experiments available in the literature at the time. However, some discrepancies with tests of Arnason (2005) were observed in the pressure-time histories on of the structure (the upstream side).

The recent experimental work of Al-Faesly et al. (2012) is most closely related to this study. The authors of this comprehensive experimental program investigated the use a low-height mitigation walls located upstream of the structure (Fig.37).

(a) **(b)**

Figure 37: Bore front impact and deflection by the 450 mitigation wall. (Al-Faesly et al., 2012)

Such walls are expected to have a damping effect on the base shear force and can lessen the effect of the tsunami driven debris field. The authors focused on the effect of flat and curved mitigation walls while varying their height and location on the exerted force on the square column. They found a relationship between the walls parameters and the force exerted by the tsunami-like bore on free-standing structures. The results revealed that, if located correctly, using protection walls with various cross sections can be a mitigation strategy to decrease the exerted overall shear force on the column. In terms of the flat mitigation wall with angles of 45 and 90 degree relative to the bottom of the flume and placed at the distance equal to the cross-sectional dimension of the square model (1D), the magnitude of the base shear force decreased considerably. Extending the location of the protection wall from 1D to 3D (at a distance three times the width of the column) was also effective but had a less pronounced effect in reducing the base shear force – this was valid only for the test with the vertical mitigation wall. For the test with an inclined wall, it was not only ineffective but also harmful. In terms of curved mitigation wall, the results showed the most effective location for this mitigation wall was 3D. The location 1D, which was closer to the structure, resulted in a higher magnitude of base shear force on the column.

Rahman (2014), conducted an experimental study to investigate the force reduction effects of seawalls on onshore structures. He focused on two parameters, including the location and height of the wall to determine their effect on the generated force. Based on his findings, he concluded that seawalls located close to the coastal structure with adequate height are capable of significantly reducing the exerted base shear force. The results also revealed that the efficiency of a porous wall is equal to the efficiency of a solid wall. A large scale experimental study of Oshnack (2009) using a large scale flume located at Oregon State University evaluated the effectiveness of a small seawall at reducing the exerted tsunami load. His results indicated that the small seawall is effective in reducing the wave force and due to the absence of spike in the force-

time histories. The author concluded that small seawalls can also be useful in decreasing the impulsive force. Thomas and Cox (2011) proposed an equation capable of estimating the tsunami force reduction due to a seawall.

A reconnaissance visit performed by a Japanese team of researchers from the Research Center for Disaster Reduction Systems (Bishop et al., 2005) and surveys on Phuket, Thailand after the 2004 Indian Ocean Tsunami revealed that coastal geomorphic features such as sand dune belts, associated forests (Mascarenhas and Jayakumar 2008) , mangroves (Dahdouh-Guebas et al., 2005), (Ismailet al., 2012) and low-height seawalls, played a significant role in reducing the destruction due to the tsunami waves by decreasing the bore velocity. For example, the Kata-Karon area of Phuket reported less damage due to the fact that some buildings were constructed behind a sand dune. It is interesting to note that the tsunami bore overtopped the sand dunes, such that while the damage due to direct flooding was inevitable, the damage due to the direct tsunami bore impact was omitted. Another example is Patong Beach, where no serious structural damage was reported. The low seawall acted as tsunami-bore deflector and, as a result, a considerable reduction in the magnitude of the exerted force on the impacted structures was noticed. The field survey indicated that seawalls made of sandbags or landward sloping seawalls are less effective as coastal protection structures.

3. Development of the Numerical Model

The software used to develop this newly proposed numerical model is OpenFOAM v2.3.0 which runs on the Linux operating system. OpenFOAM is a free, open source software package capable of solving problems of continuum mechanics such as CFD (Computational Fluid Dynamic) analysis. There are several models and solvers written in C++ language available in OpenFOAM which are applicable for various engineering and science problems. There are various tools for meshing, pre-processing and post-processing and one of the most interesting functional aspects of this software is its open source feature which enables the users to customize its existing functionality. Having access to the source code is a powerful feature which offers those who have a background in programming the possibility to assess and modify the codes. It is worth noting that the programming language of the available libraries in OpenFoam is object-oriented, which is provides programmers with a new approach to overcome the complexity of traditional programming languages. OpenFOAM has good extensibility qualities. For instance, users are able to create custom objects such as boundary conditions and incorporate turbulence models which existing solvers can respond to. Therefore, there is no need to change and recompile the source code. This software is capable of simulating a broad range of engineering problems by applying the Finite Volume Method (FVM) that is inherently mass conservative (OpenFOAM 2014).

The OpenFOAM solver applied for this case is InterFoam. It is capable of handling the problems with free-surface where two fluids are separated from each other through a sharp boundary. To describe the flow, the procedure of discretization is performed by using a finite volume technique, the applicable equations are incompressible RANS and the turbulence is modeled applying an LES model (Large Eddy Simulation) as well as the SGS are modeled by applying a one equation subgrid-scale energy model, which is explained later herein. Structured grids are applied to the simulation domain in this study (OpenFOAM 2014).

3.1. Governing Equations

The Navier-Stokes equations are the principal partial differential equations capable of predicting the motion of fluid by describing how flow parameters such as pressure, density, velocity and temperature are related and are derived from conservation laws. These parameters can be obtained directly (DNS), in temporal averaged form (Reynolds-Averaged Navier-Stokes, RANS) or by using the spatially-filtered form (LES) as described in the following section.

3.1.1. Reynolds-Averaged Equations

Using tensor notation, the differential form of the continuity equation for a three-dimensional system is written as (Chamani, 2013, p. 209):

$$\frac{\partial \bar{u}}{\partial x} + \frac{\partial \bar{v}}{\partial y} + \frac{\partial \bar{w}}{\partial z} = 0 \tag{1}$$

where $\bar{u}$, $\bar{v}$, and $\bar{w}$ are the mean velocity components in the *x*, *y*, and *z* directions respectively:

$$u(t) = \bar{u} + \acute{u} \qquad v(t) = \bar{v} + \acute{v}\, w(t) = \bar{w} + \acute{w} \qquad p(t) = \bar{p} + \acute{p} \tag{2}$$

The Reynolds-Averaged continuity equation is based on the average flow velocity.

Similarly, the differential form of the momentum equation for a three-dimensional system can be written as (Chamani, 2013):

$$\bar{u}\frac{\partial \bar{u}}{\partial x} + \bar{v}\frac{\partial \bar{u}}{\partial y} + \bar{w}\frac{\partial \bar{u}}{\partial z} = -\frac{1}{\rho}\frac{\partial \bar{p}}{\partial x} + g_x + v\left(\frac{\partial^2 \bar{u}}{\partial x^2} + \frac{\partial^2 \bar{u}}{\partial y^2} + \frac{\partial^2 \bar{u}}{\partial z^2}\right) - \left(\overline{\frac{\partial \acute{u}^2}{\partial x}} + \overline{\frac{\partial \acute{u}\acute{v}}{\partial y}} + \overline{\frac{\partial \acute{u}\acute{w}}{\partial z}}\right) \tag{3}$$

$$\bar{u}\frac{\partial \bar{v}}{\partial x} + \bar{v}\frac{\partial \bar{v}}{\partial y} + \bar{w}\frac{\partial \bar{v}}{\partial z} = -\frac{1}{\rho}\frac{\partial \bar{p}}{\partial y} + g_x + v\left(\frac{\partial^2 \bar{v}}{\partial x^2} + \frac{\partial^2 \bar{v}}{\partial y^2} + \frac{\partial^2 \bar{v}}{\partial z^2}\right) - \left(\overline{\frac{\partial \acute{v}^2}{\partial y}} + \overline{\frac{\partial \acute{u}\acute{v}}{\partial x}} + \overline{\frac{\partial \acute{u}\acute{w}}{\partial z}}\right) \tag{4}$$

$$\bar{u}\frac{\partial \bar{w}}{\partial x} + \bar{v}\frac{\partial \bar{w}}{\partial y} + \bar{w}\frac{\partial \bar{w}}{\partial z} = -\frac{1}{\rho}\frac{\partial \bar{p}}{\partial z} + g_x + v\left(\frac{\partial^2 \bar{w}}{\partial x^2} + \frac{\partial^2 \bar{w}}{\partial y^2} + \frac{\partial^2 \bar{w}}{\partial z^2}\right) - \left(\overline{\frac{\partial \acute{w}^2}{\partial z}} + \overline{\frac{\partial \acute{w}\acute{v}}{\partial y}} + \overline{\frac{\partial \acute{u}\acute{w}}{\partial x}}\right) \tag{5}$$

where, ρ is the fluid density, p is the fluid pressure, t is the time and g is the gravitational acceleration.

3.1.2. Large Eddy Simulation Model (LES)

There is a wide variety of turbulence models which can be used to simulate turbulence. Determining the most suitable model depends on the nature of the problem since no model provides a fully satisfactory solution. One modelling approach, initially proposed in 1963 by Joseph Smagorinsky, is LES, which is proven to be more accurate than RANS (Reynold Averaged Navier Stoke equations) and computationally less expensive than DNS (Direct Numerical Simulation). The main drawback of the RANS model is the fact that this model is responsible for representing a broad range of scales, which could ultimately affect the accuracy of the results. Small scales and large scales are dependent on viscosity and boundary conditions respectively, and, as a result, it does not seem to be possible to consider the same approach for modeling the effect of large scales for different flows. The principal shortcoming of DNS is the fact that the precise result is highly dependent on very fine grid points to capture all the scales of the motion, which is computationally very expensive. As a result, this model is more applicable to simple geometries at low Reynolds numbers. LES is an intermediate method between DNS and RANS and has become one of the most successful models for turbulence. This model's principal operation is based on resolving large scales while modeling the small subgrid scales. In comparison to RANS, LES is more precise because it does not cover the entire spectrum of length scales and it models only the small scales of the flow. As a result, it is an appropriate approach for turbulence at high Reynolds numbers. Furthermore, LES operates through applying a spatial filtering approach via dividing the large-eddies which are resolved from the small-eddies that are modeled. A proposed convolution for filtering process is Piomelli, (1999).

$$\bar{\emptyset}(\zeta) = \int_D \emptyset(\zeta')G(x,\zeta';\bar{\Delta})d\zeta' \tag{6}$$

where G is the spatial filter function, $\bar{\Delta}$ is the filter width and D is domain of integration. The role of the filter function is to determine the magnitude of the small scale.

LES models use the Navier-Stokes equations. Hence, the governing equations are filtered N-S system. The filtered governing equations are expressed as follows (Piomelli, 1999).

$$\frac{\partial \bar{u}_i}{\partial x_i} = 0 \tag{7}$$

$$\frac{\partial \bar{u}_i}{\partial t} + \frac{\partial}{\partial x_j}(\bar{u}_i\bar{u}_j) = -\frac{1}{\rho}\frac{\partial \bar{p}}{\partial x_i} - \frac{\partial \tau_{ij}}{\partial x_j} + \upsilon\frac{\partial^2 \bar{u}_i}{\partial x_j \partial x_j} \tag{8}$$

where $\bar{u}_i$ is the velocity component in the x_i direction, $\bar{u}_i$ is the resolved velocity component in the x_i direction, p is pressure, ρ is fluid density and τ_{ij} is subgrid scale stress tensor. The equations (7)-(8) are

widely used to model the large scale flow, while for the small scales of the flow, a subgrid-scale stress modeling term (SGS) is required because some scales of flow, namely the dissipative scales, are not resolved in LES. As a result, subgrid scale modeling is employed to dissipate energy:

$$\tau_{ij} = \overline{u_i u_j} - \overline{u_i}\,\overline{u_j} \tag{9}$$

There is a broad range of proposed SGS models in literature. A popular group is based on the eddy-viscosity hypothesis and equilibrium assumption, which states that equilibrium condition is dominant for small scales and their main role is dissipating the energy they receive from the resolved scales

$$\tau_{ij} - \frac{1}{3}\,\delta_{ij}\tau_{kk} = 2\mu_t\,\overline{s_{ij}} \tag{10}$$

where τ_{ij} is subgrid scale stress tensor, μ_t is turbulent viscosity, δ_{ij} is Kronecker tensor, s_{ij} is resolved strain-rate tensor. A one-equation model is employed in this study to account for the SGS energy dissipation. The role of this model is to estimate the velocity scale by solving an equation for the transport of subgrid-scale energy. This equation can expressed as follows:

$$\frac{\partial K_{sgs}}{\partial t} + \frac{\partial}{\partial x_j}\left(K_{sgs}\overline{u_j}\right) = +\frac{\partial}{\partial x_j}\left[\left(C_k K_{sgs}^{\frac{1}{2}}\bar{\Delta} + v\right)\frac{\partial K_{sgs}}{\partial x_j} + \tau_{ij}\overline{u_i}\right] - C_\varepsilon\frac{K_{sgs}^{\frac{3}{2}}}{\bar{\Delta}} - \tau_{ij}\bar{S}_{ij} \tag{11}$$

and

$$v_T = C_v K_{sgs}^{1/2}\Delta \tag{12}$$

where K_{sgs} is subgrid-scale energy that is equivalent to $\tau_{kk}/2$, C_k and C_ε are SGS stress model coefficients, $\bar{\Delta}$ is principal (grid) filter width, $\overline{u_j}$ is velocity component in the x_j direction, v is kinematic viscosity and $\bar{S}_{ij}$ is resolved strain-rate tensor (Piomelli, 1999).

3. 2. Treatment of the Free Surface

One proposed interface-capturing method capable of tracking the free surface is the volume of fluid (VOF) technique. This method calculates the flow occurring in a two-phase domain, such as air and water in this study, by considering each phase as a single fluid that experiences variation of physical properties through the interface. In order to determine the value for variables such as density ρ and the value of the volume fraction c (Andrillon and Alessandrini 2004) should be computed first because the value of ρ *and* μ are dependent on that parameter: c can take values of 0 or 1 for the air and water phase, respectively. For a system with two phases, the VOF method considers an advection process for the volume fraction. The role of advection term is to determine the location of the free surface and its main advantage is that it provides sharp boundaries for the free surface, which is sensitive to the grid size in most other methods.

The transport equation employed in the VOF method is written as follows (Heyns et al., 2013),

$$\rho = c\rho_1 + (1 - c)\rho_2 \tag{13}$$

$$\frac{\partial c}{\partial t} + \vec{\nabla}.(c\vec{u}_c) = 0 \tag{14}$$

where $\vec{u}_c$ can be defined as the estimated relative velocity between air phase and water phase.

3.3. Computational Time Step

Determining an appropriate time step is a key and challenging aspect of any computational simulation. While a shorter time step can lead to more accurate results, it inherently increases the simulation time. Adaptive time-stepping is a technique which allows varying the time step as the estimation proceeds, rather than defining a constant value for the step size for the entire calculation. This technique exists in the Finite Volume library of OpenFOAM and it is applied in some standard solvers such as InterFoam. It is based on keeping a certain max Courant number which is defined below (Berberović, 2010):

$$Co = \frac{|U_f|}{d}\Delta t \tag{15}$$

where Δt the time step and the vector d is the distance between the interfaces of two computational cells. The following formula can be used for estimating the value of the Courant number (Co_0) in order to estimate the time step.

$$\Delta t = min\,\{min\,[min\,(\frac{Co_{max}}{Co_0}\Delta t_0, (1 + \lambda_1\frac{Co_{max}}{Co_0})\Delta t_0)\,, \lambda_2\Delta t_0], \Delta t_{max}\,\} \tag{16}$$

where Co_{max} is the maximum courant number specified by the user. The role of the two variables $\lambda_1 = 0.1\ and\ \lambda_2 = 1.2$, applied in the above equation, is to prevent numerical oscillations by controlling the increase in the time step.

4. Domain Geometry and Initial and Boundary Conditions

The numerical experiments are designed to reproduce the laboratory experiments conducted in a flume with a reservoir containing impounding water at rest, located at the upstream side of a column which has a square cross section. The laboratory experiment where conducted at the National Research Council (NRC), Canada (Al Faesly et al, 2012). Due to the demonstrated resemblance between tsunami-induced bores and the generated bore in a dam break case (Chanson, 2006), the hydraulic bore generated in their study is produced by a sudden water release. Two different shapes of mitigation walls in the form of inclined and curved walls were placed at two locations upstream of the column. The objective of the experiments was to examine

whether the low-height wall could be effective in reducing the tsunami hydrodynamic force and the associated initial spike induced by the tsunami bore on the column. The tests were also repeated without any mitigation wall in the flume in order to compare the data with the condition where the mitigation wall are installed. The rapidly opening swing gate was opened and the impoundment water was released inside the flume in the form of a dambreak wave. The water impacted first the mitigation wall before impacting the column and, as a result, it produced a complicated flow pattern. At time = 0, the initial velocity, pressure, and phase fractions for all the domain computational cells except for the reservoir were set equal to zero as the experiments were conducted over dry bed (that is, the flume is initially dry before opening the gate of the reservoir). Phase fraction was set to 1 for the reservoir cells.

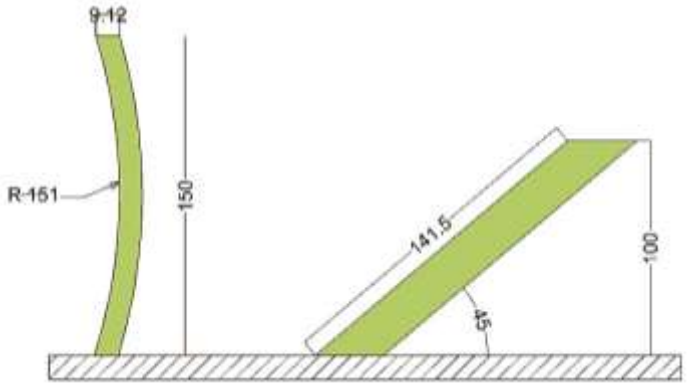

Figure 38:Schematic of the mitigation wall cross-sections (dimensions in mm): Left: Curved wall; Right: 45o –Inclined wall.

Flume geometry (Fig.39) is modeled to exactly reproduce the (National Research Council) NRC flume in order to allow for model validation and for an accurate comparison of the numerical and experimental

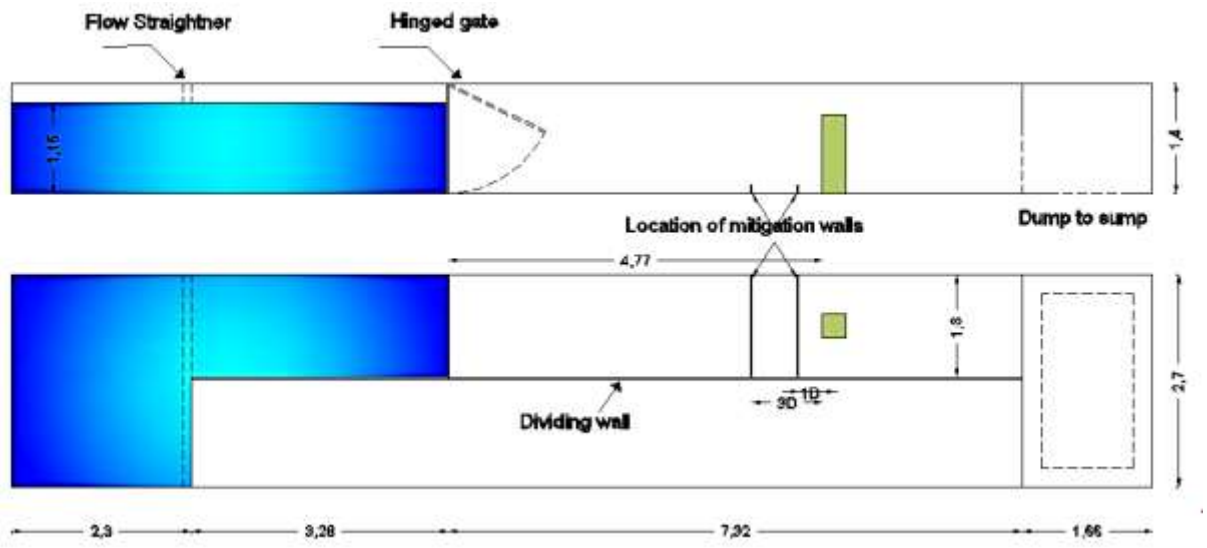

Figure 39: Side (top) and plan (bottom) views of the NRC flume with mitigation walls located at 1D and 3D (dimensions in m).

In the numerical model, the boundary condition of all of the vertical (lateral) and horizontal (bottom) faces of the L shape flume were defined as solid walls, except for the outlet at the downstream of the flume, which was considered as a zero gradient condition in order to directly evacuate flow out and thus avoid water accumulation at the outlet. Velocity at the computational cells of the wall was set to. Several structured grids with the cell dimension of 2x2x2 cm were generated for each case to numerically replicate the physical model.

In this numerical study, the wall function method was applied to account for viscous effects on the transport processes at the wall. In order to compute turbulent viscosity (v_T), boundary conditions for v_T had to be defined. OpenFOAM offers various v_T wall functions, including nutKWallFunction, which was used in this study as a generic wall function suitable for a high-Re turbulence models. This boundary condition provides a turbulent kinematic viscosity condition when applying wall functions, based on turbulence kinetic energy.

5. Model Validation

The validation of the proposed numerical model was performed by comparing experimental and simulated results for several case studies. It should be noted that, in order to ensure the model is independent of mesh resolution, a sensitivity analysis was performed to establish the suitable grid for the proposed model. This analysis was performed by running several simulations with different grid sizes starting at 3 cm, then 2 cm and, finally, 1 cm. The 2 cm grid size yielded the most accurate results while the 1 cm grid size did not significantly improve them. Thus, all the simulations are performed using the 2 cm grid size.

In order to develop an accurate model capable of simulating these cases accurately, various models such as RANS (*k-ε, k-ω, and LRR*) and LES were tested. The results shown in Fig. 40 revealed that RANS models were not able to simulate these cases accurately. However, the experimental data were accurately reproduced by applying the large eddy simulation approach described in Section 3.1.2. Due to the nature of the problems considered in this paper that correspond to turbulence with high Reynolds numbers, LES can be more efficient because it does not cover the entire spectrum of length scales; it directly simulates larger scales of the flow and models only the effect of smaller scale eddies. Therefore, LES is found to be a more appropriate approach for tsunami bores which are turbulent with high Reynolds numbers as can be observed in Fig. 40. Based on this conclusion, the LES approach is employed in the rest of the paper.

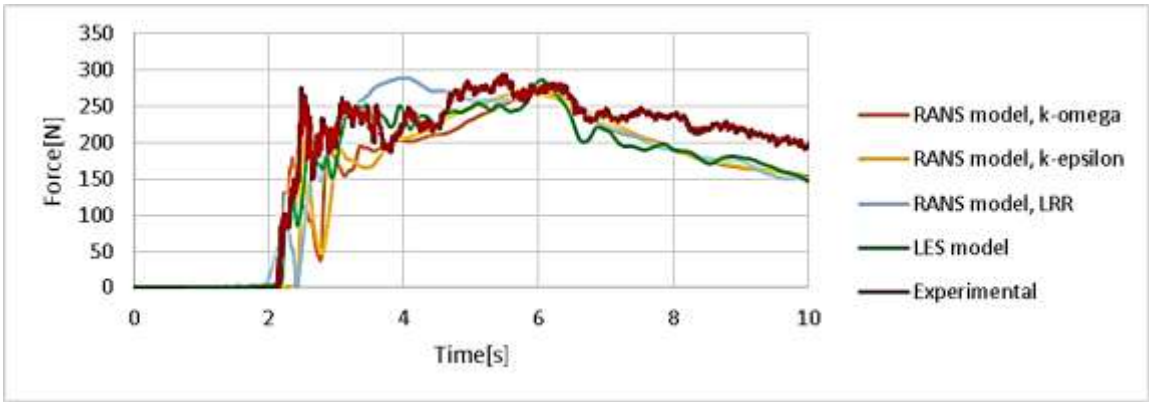

Figure 40:Examining the effect of various turbulence models.

The following five cases were investigated to obtain a better insight into the effects of the mitigation walls in reducing the tsunami-induced force and to examine the capability of RANS and LES models in simulating such cases. The first three cases include examining the influence of curved mitigation walls on the tsunami bore force on the column under the three conditions (1) without the mitigation wall, (2) with the mitigation wall placed at 1-D upstream of the column and (3) the wall placed at 3-D (where D is the side length of the square column cross section which is of 305 mm). The initial impoundment depth for all three cases was set to 55 cm and the effect of inclined mitigation wall was examined. The impoundment depth of 85 cm was applied for the last two cases.

5.1. Test Case 1 –Effect of bore-induced force on a square cross section column without mitigation walls

In this case, the total net force exerted on the square column without the presence of the mitigation wall was estimated. The base shear forces was calculated by integrating the estimated pressure over the entire surfaces of the structure at each time step. The results are shown in Figure 41.

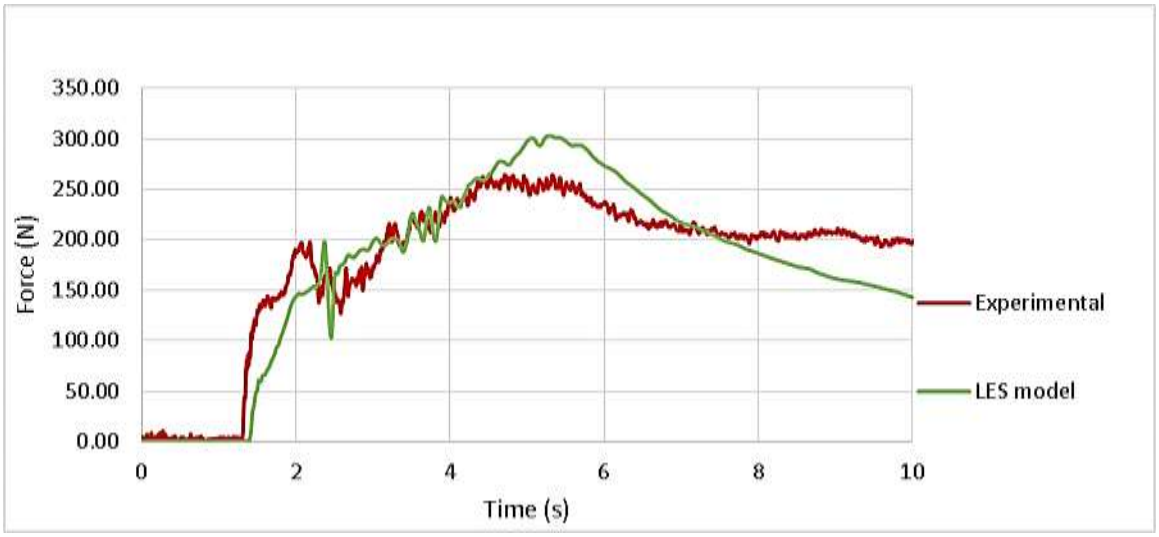

Figure 41:Test Case 1 –Total hydrodynamic force for dry bed conditions without mitigation wall. Initial impoundment water depth of 55 cm.

The initial force spike, which occurred at the beginning of the force-time history, indicates the initial impingement due to the impact of the dambreak wave on the structure. The force data recorded from the experimental test and which are also shown in Fig.5 revealed a peak occurring at t = 2 s. This was generated as a result of the initial impact of the rapidly advancing bore across the upstream side of the column. The magnitude of this force was accurately reproduced by the numerical model. However, a small time delay was observed and this could be attributed to the slight differences in the flume roughness of the flume (slightly rougher in the experiment comparing to the model).

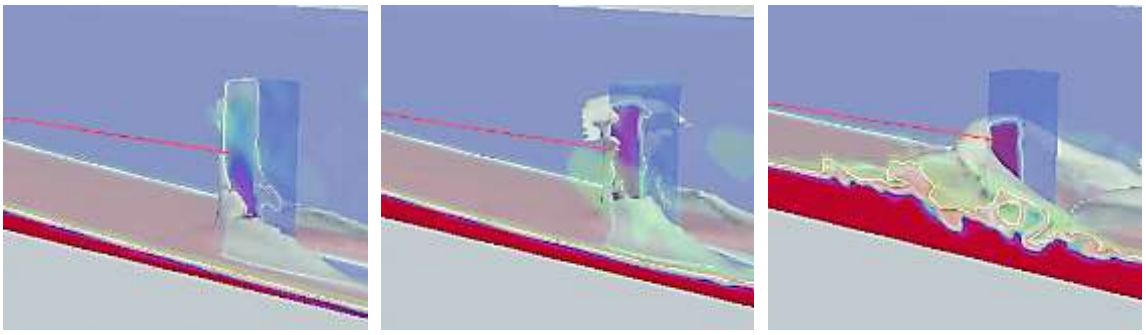

(a) **(b)** **(c)**

Figure 42:(a) Initial run up of the incoming flow onto the upstream side of the structure (b) Runup flow begins to return onto the incoming flow (c) Collapse of the rising runup of water onto the incoming flow.

Additionally, the gradient of the total force in the model was gradual comparing to its steeper variation observed in the experimental case. This could be attributed to the approximation of the eddy viscosity and wall shear stress. Following the initial force peak, a noticeable reduction in the total force was observed –

this stemmed from the collapse of the rising water back onto on the incoming flow, reducing the contact surface with the structure as shown in Fig. 42. Following this instant, this volume of water that joins the ongoing incoming flow causing a gradual increase in the calculated force up to its maximum magnitude peak point. The numerical results are similar to the experimental results up to the maximum run-up force: at this point, a noticeable difference is observed for the magnitude of this maximum force. A similar simulation performed by Douglas and Nistor (2015) using a RANS model, revealed divergence between numerical results and experimental data, with different force rise rates at this instant. The magnitude of the maximum force that is due to the run-up was overestimated by about 50 N and this overestimation was also identified in the study performed by Douglas and Nistor (2015). Finally, the decrease in the calculated net force did not occur at the same rate for the experimental data and numerical results. To the later decreased faster during the last seconds of the simulation due to the fact that the pump used to supply water to the flume continued to operate and, hence, some water continued to flow in the flume – this was neglected in the numerical simulation.

5.2. Test Case 2 – Effect of bore-induced force on a square cross section column with a curved mitigation wall located at 1D

The objective of this experimental test case was to examine the effectiveness and functionality of low-height walls in reducing the tsunami-induced force on a structure. In this test case, a 15 cm high curved mitigation wall with a width of 1 cm was located at 1D (305 mm from the upstream surface of the structure). More details about the experimental test can be found at Al-Faesly et al., (2012). Figure 43 shows that the LES model is capable to reproduce the experimental data, while the RANS model failed to predict accurately.

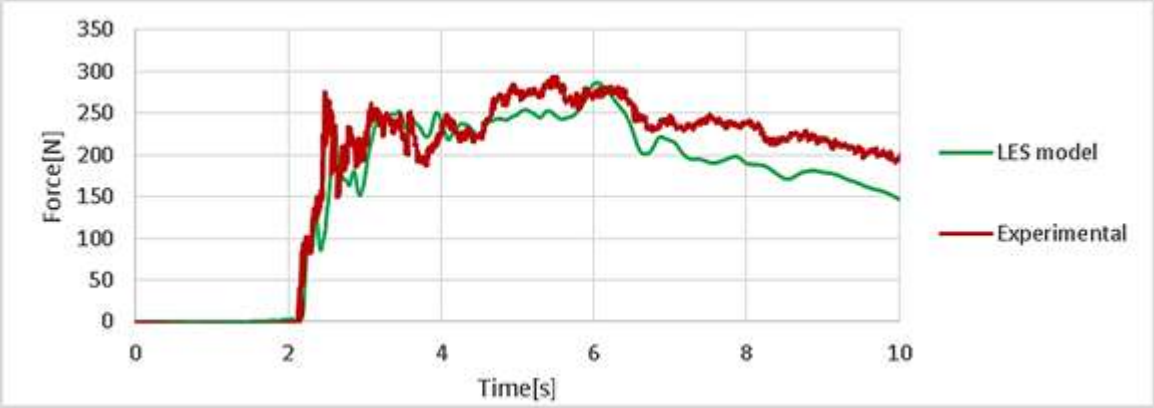

Figure 43:Test Case 2- Total hydrodynamic force for dry bed condition with curved mitigation wall located at 1D and an initial impoundment water depth of 55 c.

When comparing experimental data and numerical results, the greatest discrepancy was observed for the predicted magnitude of the impact force, which revealed an underestimation of the OpenFOAM model in capturing the precise experimental variation, which might be the result of approximations in calculation of

the shear stress in the wall and eddy viscosity. Comparing the experimental data and numerical results for Case 1 and 2 revealed that placing the mitigation wall at the 1D distance was not effective in reducing the exerted tsunami force on the model structure which could be the result of the fact that the curved mitigation wall blocked the flow of the water, resulting in water accumulation and higher water levels behind and very close to the upstream side of the column (Fig.44).

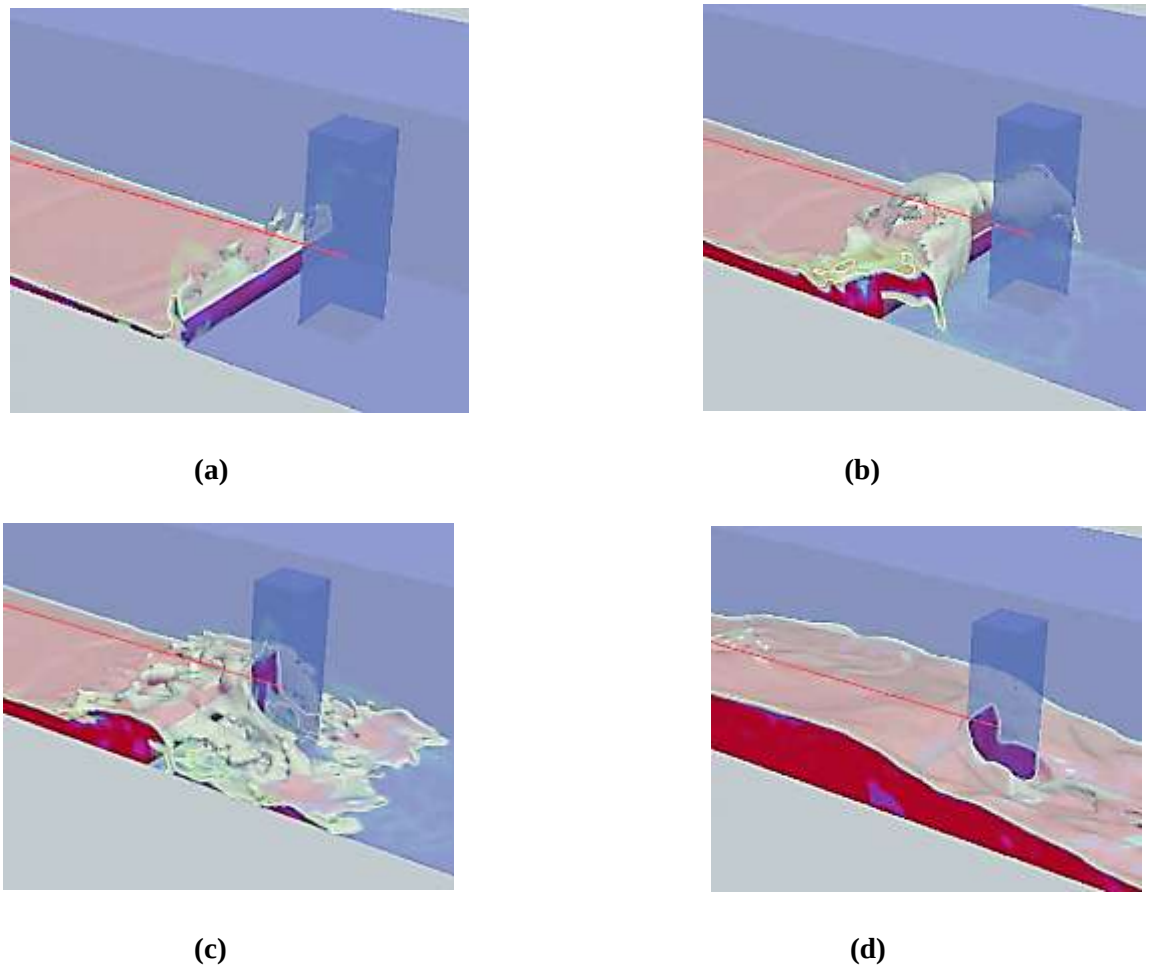

(a) **(b)**

(c) **(d)**

Figure 44: Water blockage due to the presence of curved mitigation wall; (a) Bore front impacts the mitigation wall (b) Incoming flow overtops the mitigation wall (c) Water begins to accumulate behind the mitigation wall and between the mitigation wall and the column (d) Water accumulates at the upstream side of the column.

This was followed by the collapse of the accumulated water column behind and very close to the model structure which led to a significant run-up force which lasted approximately 3 seconds. The peak force predicted on the column with mitigation wall at 1D was estimated to be higher in comparison to the case without mitigation wall for the physical test.

5.3. Test Case 3 –Effect of tsunami-induced force on a square cross section column with a curved mitigation wall located at 3D.

In this test case, the location of the curved mitigation wall was modified from 1D to 3D. The LES model predicted this case very well. Figure 45 shows the comparison between the numerical results and the experimental data.

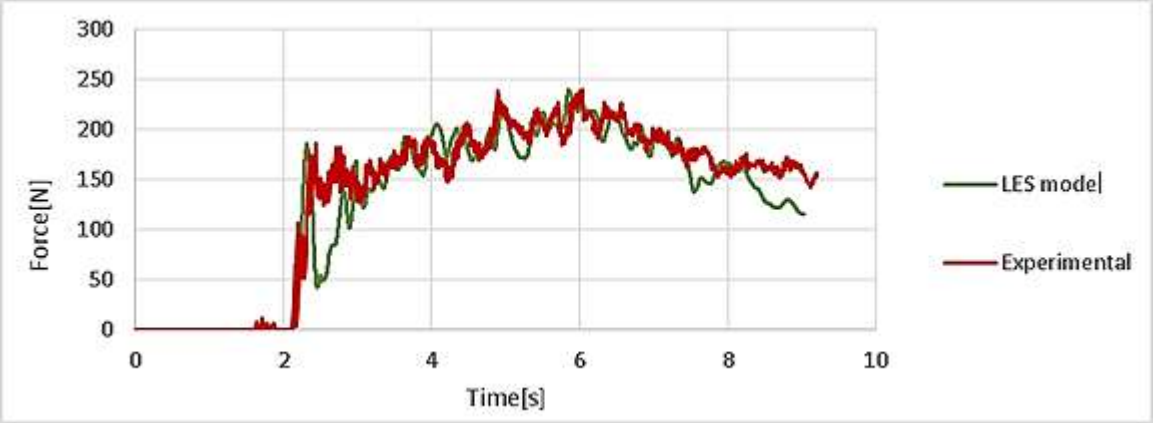

Figure 45:Test Case 3- Total hydrodynamic force for dry bed condition with curved mitigation wall located at 3D and an initial impoundment water depth of 55 cm.

The largest discrepancy between the experimental data and numerical results occurred at approximately 2.5 seconds after the initial impact force. At this instant, the predicted model results showed a significant decrease in total force due to the sudden reduction of water level after the initial run-up. Fig .46 revealed that placing the mitigation wall at 3D damped the peak force and impulsive base shear because the location of the impacted water on the column was lower in this case.

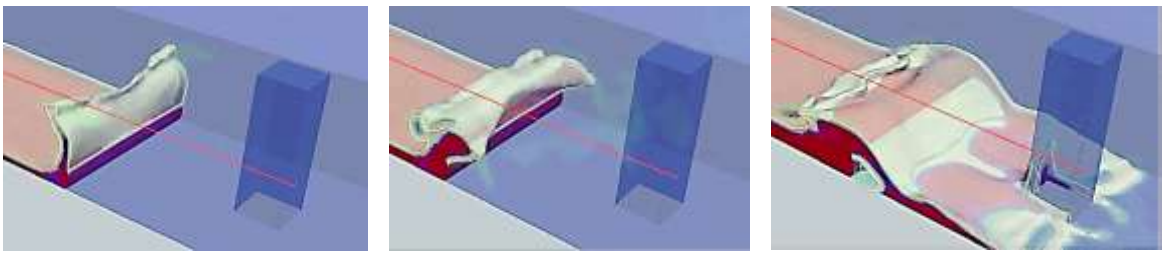

(a) **(b)** **(c)**

Figure 46: Water blockage due to the presence of curved mitigation wall; (a) Bore front impacts the mitigation wall (b) Incoming flow overtops the mitigation wall (c) Water accumulates behind the upstream side of the column and reduces the efficiency of the curved mitigation wall located at 3D.

In comparison to test case 2, the mitigation wall located at 1D is more effective in reducing the dambreak wave-induced force by reducing the speed of the incoming flow and reducing thus the impacted area of the column surface at initial impact.

5.4. Test Case 4 – Effect of tsunami-induced force on a square cross section column without considering mitigation wall.

The net force-time histories across the structure surfaces are shown in (Fig. 47).

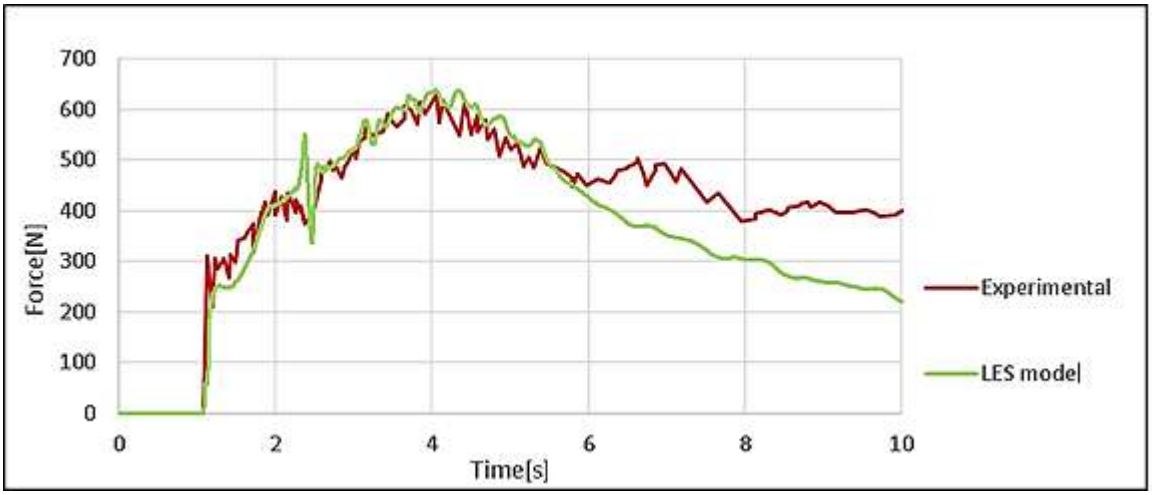

Figure 47: Test Case 4- Time-histories of the experimental data. The total hydrodynamic force exerted on a column with square cross-section by a dam break flow considering dry bed condition and without mitigation wall and an initial impoundment water depth of 85 cm.

A small spike observed at t = 1 s was the result of the initial interaction between the column and the incoming bore. The numerically-predicted value was slightly smaller than the experimental one. At approximately t = 2.5 s, a distinct rise and subsequent fall in the total force was observed in numerical data for a short period of time which is due to the collapse of the rising volume of water onto the incoming flow. The same trend was also observed in the experimental data but with a smaller magnitude and for a longer period of time. After this instant, numerical and experimental data revealed very good agreement with each other and the run-up force was captured very well by applying the LES model. Similar to the previously calculated force-time histories, the rate of decrease in the calculation of the net force was faster.

5.5. Test Case 5_ Effect of tsunami-induced force on a square cross section column with considering inclined (45º) mitigation wall located at 3D.

The calculated force imposed on the column (Fig. 48).

Figure 48:Test Case 5- Total hydrodynamic force by a dam break flow on a column considering dry bed condition and a mitigation wall located at 3D and an initial impoundment water depth of 85 cm.

Good agreement can be observed between the numerical model results and the laboratory data up to the instant of 5 sec. An abrupt initial spike is observed in the experimental data, while the numerical model is not able to capture this spike. The second noticeable rise and fall observed in the physical data is due to the collapse of the rising volume of water, which is less pronounced for the numerical data (Fig .49).

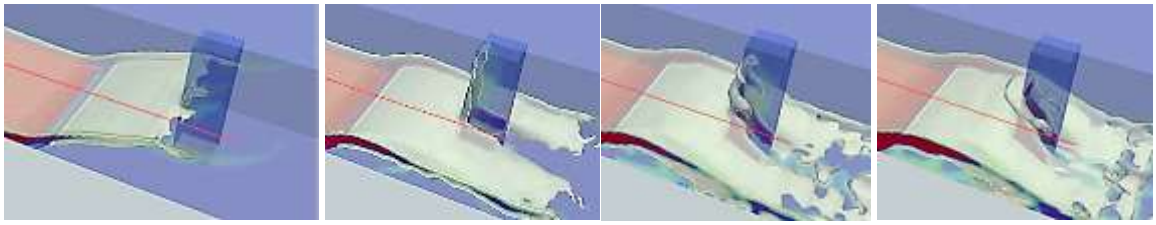

(a) **(b)** **(c)** **(d)**

Figure 49:(a) The first interaction of incoming flow and the column (b) Initial runup of the impacted bore onto the column (c) Runup water starts collapsing onto the incoming flow.

It can be concluded that positioning the mitigation wall at 3D upstream from the structure is not as effective in reducing the tsunami-induced force on the structure. The resultant peak force is also slightly larger in comparison to the case without wall. The incoming bore overtopped the 45°-inclination wall located at a distance of 3D and was projected into the air and caused the bore front to hit the structure at a higher elevation than in the case without a wall. This phenomenon led to a large impulsive overturning moment.

6. Conclusions

In this study, the interaction between the forces exerted by tsunami-like bores on free standing vertical structures in the presence of mitigation walls was simulated using a Large Eddy Simulation model. The configurations investigated included using curved and inclined walls (at 45^o), positioned at two different distances from the upstream side of the structure. The problem was studied via applying a 3-dimensional hydrodynamic computational model with free surface, RANS turbulence models and an LES model for simulating complex turbulent behavior of the hydrodynamic field. The capabilities of the applied RANS and LES models were compared. It was demonstrated that LES approach with one equation for subgrid scale kinetic energy performed better than the employed RANS models such as *k-ε, k-ω, and LRR*. The comparisons were performed using the data obtained from a comprehensive experimental program conducted at the NRC (National Research Council), in Ottawa, Canada. The functionality and effectiveness of the numerical model was validated by comparing the simulated data to experimental results in a wide range of experiments. The numerical model results using the LES model showed good agreement with the measured experimental data. Therefore, LES can be considered as a better choice in modeling the turbulence in such cases. To the best of the authors' knowledge, LES modeling of tsunami bores using an equation for subgrid scale kinetic energy has not been performed prior to this study. Furthermore, numerical simulation of the effect of low-height mitigation walls on force reduction for tsunami bores has not been conducted before. The numerical results confirmed that placing mitigation walls at an appropriate distance from the upstream side of the structure can be effective in decreasing the impulsive and run-up forces. The role of the mitigation walls of low height is to decrease the force but not necessarily to prevent overtopping. Numerical results confirmed the experimental findings which indicated that positioning a curved mitigation wall at 3D can lead to a noticeable reduction on exerted net force on the structure, while it is not as effective at 1D. Moreover, placing inclined 45^o mitigation wall at 3D was not effective in reducing the net force either due to the "launching" effect which results in the wave hitting the structure at a higher elevation impact point on the structure – this induced a significant increase in the moment of the hydrodynamic force exerted on the structure.

Concluding, the present study demonstrates that LES with one equation for subgrid scale kinetic energy is a good approach for simulating turbulence in modeling tsunami bores and confirms that mitigation walls could be effective in reducing the impulsive and run-up forces and can also damp the peak force if placed at an appropriate place.

Chapter 6

Conclusions and Recommendations for future work

6.1 Conclusions

In this thesis, a series of numerical models developed for a series of physical tests available in literature were performed to study the interaction of a propagating single bore, by applying the dam break approach. The main purpose of this study is subdivided into two different branches which is presented in the format of two technical papers. Technical paper one's focus is on assessing the tsunami net force on columns with various cross sections by applying RANS turbulence models along with evaluating the capabilities of various models such as k-e, k-w, LRR to close the system of equations. The highlighted conclusions drawn from this numerical study are summarized herein as follows:

6.1.1 Conclusions of technical paper 1:

1- The performance of the model was assessed by comparing the obtained numerical results with experimental data obtained from laboratory tests conducted at the OCRE-CHC in Ottawa, Canada, the Hydraulic Laboratory at the University of Ottawa, Canada and in the Hydraulic Laboratory of the Université Catholique de Louvain, Belgium. Good agreement was demonstrated between the numerical model results and the experimental data.

2- Following a comparative study and validation, the numerical model was employed to investigate the impact of a tsunami on columns with various structural geometries (cross-sections). Results indicated that the more hydrodynamically-shaped structures allowed the bore to be deflected along the sides of the structure, reducing thus the maximum base shear force exerted on it.

3- Comparing the results for various cross-sections of the structures, it can be argued that the magnitude of the hydrodynamic loads was the largest for the rectangular-shaped structure while it was smaller by approximately 12% in the case of the T-shapes and frontally-curved structures. The minimum value of total force was observed for the case of the triangular column.

4- The present study demonstrates that the shape of a structure has an important effect and plays an important role in the magnitude of the hydrodynamic loading. As such, the cross section of a nearshore structure should be considered when planning and designing it. A careful selection of the architectural plan of a building may significantly reduce tsunami-induced loading.

5- It appears that the model scale plays an important role on the magnitude of the run-up force for cases with 3D objects. The smaller the object is, the value of this force is more pronounced than the case of the 3D object dimensions approaching larger scales.

6- It was observed that interFoam estimation of the impulsive force for most cases was significantly close to the recorded impulsive force, which proves that entrained buckets of air did not play a role on this matter. However, the trapped air affected the value of the run-up force remarkably.

7- It was observed that the maximum force occurred when the water level reached approximately its maximum level on the upstream side of the structure. Maximum water profile was produced when the raised water at the upstream side of the column collapsed on to the incoming flow and accumulated behind it and joined the continuous flow of fluid until it reached its maximum level.

6.1.2 Conclusions of technical paper 2:

8- The interaction between the forces exerted by tsunami-like bores on free standing vertical structures in the presence of mitigation walls was simulated using a Large Eddy Simulation model. The configurations investigated included curved and inclined walls (at 45o), positioned at two different distances from the upstream side of the structure. The problem was studied via applying a 3-dimensional hydrodynamic computational model with free surface, RANS turbulence models and an LES model for simulating complex turbulent behavior of the hydrodynamic field. Good agreement was demonstrated between the numerical model results and the experimental data.

9- The capabilities of the applied RANS and LES models were compared. It was demonstrated that LES approach with one equation for subgrid scale kinetic energy performed better than the employed RANS models such as k-ε, k-ω, and LRR.

10- The functionality and effectiveness of the numerical model was validated by comparing the simulated data to experimental results in a wide range of experiments. The numerical model results using the LES model showed good agreement with the measured experimental data. Therefore, LES can be considered as a better choice in modeling the turbulence in such cases.

11- To the best of the author's knowledge, LES modeling of tsunami bores using an equation for subgrid scale kinetic energy has not been performed prior to this study. Furthermore, numerical simulation of the effect of low-height mitigation walls on force reduction for tsunami bores has not been conducted before.

12- The numerical results confirmed that placing mitigation walls at an appropriate distance from the upstream side of the structure can be effective in decreasing the impulsive and run-up forces.

13- Numerical results confirmed the experimental findings, which indicated that positioning a curved mitigation wall at 3D can lead to a noticeable reduction on exerted net force on the structure, while it is not as effective at 1D. Moreover, placing an inclined 45o mitigation wall at 3D was not effective in reducing the net force either due to the "launching" effect which results in the wave hitting the

structure at a higher elevation impact point on the structure. This induced a significant increase in the moment of the hydrodynamic force exerted on the structure.

14- The present study demonstrates that LES with one equation for subgrid scale kinetic energy is a good approach for simulating turbulence in modeling tsunami bores and confirms that mitigation walls could be effective in reducing the impulsive and run-up forces and can also damp the peak force if placed at an appropriate location.

6.2 Recommendations for future work:

- Numerical models need to be improved in order to better simulate the entrapped air to reduce its influence on forces, specifically run-up force.
- Examine and compare the influence of various turbulence models including RANS, LES and DNS.
- Study the effect of tsunami force on several structures

References:

Al-Faesly, T., Palermo, D., Nistor, I., & Cornett, A. (2012). Experimental modeling of extreme hydrodynamic forces on structural models. International Journal of Protective Structures, 3(4), 477-505.

Altomare, C., Crespo, A. J., Domínguez, J. M., Gómez-Gesteira, M., Suzuki, T., & Verwaest, T. (2015). Applicability of Smoothed Particle Hydrodynamics for estimation of sea wave impact on coastal structures. Coastal Engineering,96, 1-12.

Andrillon, Y., Alessandrini, B. (2004) A 2D+T VOF fully coupled formulation for calculation of breaking free surface flow Laboratoire de M´ecanique des Fluides, Ecole Centrale de Nantes, BP 92101, 1 rue de la No¨e, 44321 Nantes, France.

Arikawa, T. (2008, December). Behaviors of concrete walls under impulsive Tsunami load. In AGU Fall Meeting Abstracts (Vol. 1, p. 1331).

Arnason, H. (2005). Interactions between an incident bore and a free-standing coastal structure,[Ph.D. thesis] Seattle, Wash, USA: University of Washington; 200.

Asakura, R., Iwase, K., Ikeya, T., Takao, M., Kaneto, T., Fujii, N., & Ohmori, M. (2002, July). The tsunami wave force acting on land structures. InCOASTAL ENGINEERING CONFERENCE (Vol. 1, pp. 1191-1202). ASCE American Society of Civil Engineers.

Bandara, K. M. K., Dias, W. P. S. (2012). Tsunami wave loding on buildings: a simplified approach, J. Natn.Sci. Foundation Sri Lanka, 40 (3), 211-219.

Becker, K. (2003). Perspectives for CFD. DGLR-2002-013, DGLR Jahrbuch 2002, Band III, Germany.

Berberovic, E. (2010). Investigation of free-surface flow associated with drop impact: numerical simulations and theoretical modeling (Doctoral dissertation, TU Darmstadt/FG Strömungslehre und Aerodynamik).

Biscarini, C., Francesco, S. D., & Manciola, P. (2010). CFD modelling approach for dam break flow studies. Hydrology and Earth System Sciences,14(4), 705-718.

Bishop, P., Sanderson, D., Hansom, J., & Chaimanee, N. (2005). Age-dating of tsunami deposits: Lessons from the 26 december 2004 tsunami in thailand. The Geographical Journal, 171(4), 379-384.

Chamani, M.R., Dehghani, A.A., Beirami, M.K., and Gholipour, R. (2013). "Fluid mechanics.2ed Ed., IUT Publishing, p 613.

Chanson, H. (2006). Tsunami surges on dry coastal plains: Application of dam break wave equations. Coastal Engineering Journal, 48(04), 355-370.

Chinnarasri, C., Thanasisathit, N., Ruangrassamee, A., Weesakul, S., & Lukkunaprasit, P. (2013, March). The impact of tsunami-induced bores on buildings. In Proceedings of the Institution of Civil Engineers-Maritime Engineering (Vol. 166, No. 1, pp. 14-24). Thomas Telford Ltd.

Chock G., Robertson I., Kriebel D., Francis M., and Nistor I. (2012) , Tohoku Japan Tsunami of March 11, 2011 – Performance of Structures, Final Report, ASCE, 297 p.

Cross, R. H. (1967). Tsunami surge forces. Journal of the waterways and harbors division, 93(4), 201-234.

Cumberbatch, E. (1960). The impact of a water wedge on a wall. Journal of Fluid Mechanics, 7(03), 353-374.

Dahdouh-Guebas, F., Jayatissa, L. P., Di Nitto, D., Bosire, J. O., Lo Seen, D., & Koedam, N. (2005). How effective were mangroves as a defence against the recent tsunami? Current Biology, 15(12), R443-R447.

Douglas, S., & Nistor, I. (2015). On the effect of bed condition on the development of tsunami-induced loading on structures using OpenFOAM. Natural Hazards, 76(2), 1335-1356.

Federal Emergency Management Agency (FEMA) FEMA P646 Report. Redwood City, Calif, USA: The Applied Technology Council for the Federal Emergency Management Agency; 2008. Guidelines for Design of Structures for Vertical Evacuation from Tsunamis.

FEMA P646. (2012). Guidelines for Design of Structures for Vertical Evacuation from Tsunamis. Federal Emergency Management Agency, Washington, D.C.

Ferziger, J. H., & Peric, M. (2012). Computational methods for fluid dynamics. Springer Science & Business Media.

Fourie, J. G., & Du Plessis, J. P. (2003). A two-equation model for heat conduction in porous media (I: Theory). Transport in porous media, 53(2), 145-161.

Fukui I., Nakaraura M., Shiraishi H., and Sasaki Y. (1963), Hydraulic Study on Tsunami, Coastal Engineering in Japan, Vol. VI, pp. 68 - 82.

Fujima, K., Achmad, F., Shigihara, Y., & Mizutani, N. (2009). Estimation of tsunami force acting on rectangular structures. Journal of Disaster Research,4(6), 404-409.

Gotoh H, Ikari H, Memita T, Sakai T (2005) Lagrangian particle method for simulation of wave overtopping on a vertical seawall. Coast Eng J 47(2&3):157–181.

Gotoh H, Shao S, Memita T (2004) SPH-LES model for numerical investigation of wave interaction with partially immersed breakwater. Coast Eng J 46(1):39–63.

Harlow, F. H., & Nakayama, P. I. (1968). Transport of turbulence energy decay rate (No. LA--3854). Los Alamos Scientific Lab., N. Mex.

Hemida, H. (2008). OpenFOAM tutorial: Free surface tutorial using interFoam and rasInterFoam. Division of Fluid Dynamics, Department of Applied Mechanics Chalmers University of Technology, SE-412 96 G¨oteborg, Sweden.

Heyns, J. A., Malan, A. G., Harms, T. M., & Oxtoby, O. F. (2013). Development of a compressive surface capturing formulation for modelling free-surface flow by using the volume-of-fluid approach. International Journal for Numerical Methods in Fluids, 71(6), 788-804.

Hirsch, C. (2007). Numerical computation of internal and external flows: The fundamentals of computational fluid dynamics. Butterworth-Heinemann.

Huang, Y., & Zhu, C. (2015). Numerical analysis of tsunami–structure interaction using a modified MPS method. Natural Hazards, 75(3), 2847-2862.

Ismail, H., Abd Wahab, A. K., & Alias, N. E. (2012). Determination of mangrove forest performance in reducing tsunami run-up using physical models. Natural Hazards, 63(2), 939-963.

Jasak, H., Jemcov, A., & Tukovic, Z. (2007, September). OpenFOAM: A C++ library for complex physics simulations. In International workshop on coupled methods in numerical dynamics (Vol. 1000, pp. 1-20). IUC Dubrovnik, Croatia.

Kolmogorov, A. N. (1942). Equations of motion of an incompressible turbulent fluid. Izv Akad Nauk SSSR Ser Phys, 6, 56-58.

Kraus, N. C., McDougal, W. G. (1996). The effects of seawalls on the beach: Part I, an updated literature review. Journal of Coastal Research, 12(3), 691-701.

Lafore, R. (1997). Object-oriented programming in C++. Pearson Education.

Linton, D., Gupta, R., Cox, D., van de Lindt, J., Oshnack, M. E., & Clauson, M. (2012). Evaluation of tsunami loads on wood-frame walls at full scale.Journal of Structural Engineering, 139(8), 1318-1325.

Liu, H., Li, J., Shao, S., & Tan, S. K. (2015). SPH modeling of tidal bore scenarios. Natural Hazards, 75(2), 1247-1270.

Lukkunaprasit, P., Ruangrassamee, A., & Thanasisathit, N. (2009). Tsunami loading on buildings with openings. Science of Tsunami Hazards, 28(5), 303.

Mangani, L. (2008). Development and Validation of an Object Oriented CFD Solver for Heat Transfer and Combustion Modelling in Turbomachinery Aplications (Doctoral dissertation, Dipartmento di Energetica, Universita degli Studi di Firenze).

Mascarenhas, A., & Jayakumar, S. (2008). An environmental perspective of the post-tsunami scenario along the coast of tamil nadu, india: Role of sand dunes and forests. Journal of Environmental Management, 89(1), 24-34.

Matsutomi, H. (1991). An experimental study on pressure and total force due to bore. In Proceedings of Coastal Engineering, JSCE (Vol. 38, pp. 626-630).

Menter, F. R. (1993). Zonal two equation k-turbulence models for aerodynamic flows. AIAA paper, 2906, 1993.

Nistor, I., Palermo, D., Nouri, Y., Murty, T., & Saatcioglu, M. (2009). Tsunami-induced forces on structures. Handbook of coastal and ocean engineering, 261-286.

Nouri, Y., Nistor, I., Palermo, D., & Cornett, A. (2010). Experimental investigation of tsunami impact on free standing structures. Coastal Engineering Journal, 52(01), 43-70.

OpenFOAM (2014). "OpenFOAM: The open source CFD toolbox", < http://www.openfoam.com> OpenCFD Ltd, OpenFOAM, the Open Source CFD Toolbox, User Guide, OpenCFD Ltd., 2008, http://www.opencfd.co.uk/openfoam/

Oshnack ME, Aguiniga F, Cox D, Gupta R, van de Lindt J. Effectiveness of small onshore seawall in reducing forces induced by Tsunami bore: large scale experimental study. Journal of Disaster Research. 2009; 4(6):382–390.

Patankar, S. (1980). Numerical heat transfer and fluid flow. CRC press.

Piomelli, U. (1999). Large-eddy simulation: Achievements and challenges. Progress in Aerospace Sciences, 35(4), 335-362.

Rahman, S., Akib, S., Khan, M. T. R., & Shirazi, S. M. (2014). Experimental study on tsunami risk reduction on coastal building fronted by sea wall. The Scientific World Journal, 2014, 729357.

Ramsden, J. D. (1996). Forces on a vertical wall due to long waves, bores, and dry-bed surges. Journal of Waterway, Port, Coastal, and Ocean Engineering, 122(3), 134-141.

Ramsden, J. D., & Raichlen, F. (1990). Forces on vertical wall caused by incident bores. Journal of Waterway, Port, Coastal, and Ocean Engineering, 116(5), 592-613.

Ramsden, J. D. (1993). Tsunamis: forces on a vertical wall caused by long waves, bores, and surges on a dry bed (Doctoral dissertation, California Institute of Technology).

Ritter, A. (1892). Die fortpflanzung de wasserwellen. Zeitschrift Verein Deutscher Ingenieure, 36(33), 947-954.

Rodi, W. (1993). Turbulence models and their application in hydraulics. CRC Press.

Shuto, N., & Matsutomi, H. (1995). Field survey of the 1993 Hokkaido Nansei-Oki earthquake tsunami. Pure and applied geophysics, 144(3-4), 649-663.

Soares Frazão, S. (2002). Dam-break induced flows in complex topographies. Theoretical, numerical and experimental approaches. Louvain-la-Neuve,, Belgium: Université catholique de Louvain. PhD Thesis.

Sodja, J. (2007). Turbulence models in CFD. University of Ljubljana, 1-18.

St-Germain, P., Nistor, I., & Townsend, R. (2012). Numerical modeling of the impact with structures of tsunami bores propagating on dry and wet beds using the SPH method. International Journal of Protective Structures, 3(2), 221-256.

St-Germain, P., Nistor, I., Shibayama, T., & Townsend, R. (2014). Smoothed-particle hydrodynamics numerical modeling of structures impacted by tsunami bores. Journal of Waterway, Port, Coastal, and Ocean Engineering, 140(1), 66-81.

Stoker, J. J. (1957). Waler Waves: The Mathematical Theory with Applications. Intersciences.

Street, R. L., Watters, G. Z., & Vennard, J. K. (1996). Elementary fluid mechanics (p. 757). J. Wiley.

The 2011 Tohoku Earthquake Tsunami Joint Survey Group (2011), Field survey of 2011 Tohoku earthquake tsunami by the Nationwide Tsunami Survey, Jpn. Soc. of Civ. Eng., Tokyo.

Thomas, S., & Cox, D. (2012). Influence of finite-length seawalls for tsunami loading on coastal structures. Journal of Waterway, Port, Coastal, and Ocean Engineering, 138(3), 203-214.

Thusyanthan, N. I., & Gopal Madabhushi, S. P. (2008, May). Tsunami wave loading on coastal houses: a model approach. In Proceedings of the Institution of Civil Engineers-Civil Engineering (Vol. 161, No. 2, pp. 77-86). Thomas Telford Ltd.

Weller, H. G. (2008). A new approach to VOF-based interface capturing methods for incompressible and compressible flow. OpenCFD Ltd., Report TR/HGW/04.

Wilson, J. S., Van de Lindt, John. W., Cox, D. T. (2010). Surge wave loading on wood structures, Proceedngs of the international convection of society of wood science and technology and United Nations economic commission for Europe.

Xing, T., Shao, J., & Stern, F. (2007, August). BKW-RS-DES of unsteady vortical flow for KVLCC2 at large drift angles. In Proceedings of the 9th International Conference on Numerical Ship Hydrodynamics (pp. 5-8).

Yeh, H. (2007). Design tsunami forces for onshore structures. Journal of Disaster Research, 2(6), 531-536.

Appendix

1.1 Introduction

The prediction of fluid-flow can be obtained by two main methods including experimental investigation and theoretical calculation. It is clear and obvious that the most acceptable data about the physical processes can be obtained by real measurement. However, identical copies of full-scale equipment that are needed for prediction are expensive and impossible in most cases. Performing experiments on small-scale models and extrapolation of the outcomes to the full scale can be considered as an alternative. However, this approach may not be reliable because, due to the unavailability of the general principles, the phenomena is not scalable or not all the components can be simulated (Patankar, 1980).

Application of mathematical models is an alternative for describing the actual physical process and avoiding the above-mentioned problems. The theoretical calculations have enabled solving the mathematical models, consisting of differential equations, which otherwise would stay unsolved with classical mathematical techniques.

A look at a classical text on fluid mechanics can reveal that there are only a very limited number of practical problems for which closed form solution are available. Furthermore, the solutions are very limited. As a result, solving the equations numerically appears to be a very important option. Fortunately, because of the development of numerical methods and the technological advances in the world of computers, numerical models can provide a reasonable solution for most fluid mechanic problems (Patankar, 1980).

There are pros and cons with numerical calculations. On the positive side, the cost of computational prediction is low or lower than the experimental investigation, in most cases. What is more, computational prediction can be done with noticeable speed in comparison with experimental investigation. Another important advantage is providing complete information because it can provide the user with most of the relevant properties such as velocity, pressure and turbulence throughout the studied area. However, it is clear and obvious that experimental tests cannot provide values for all variables over the entire domain. Another important factor that is worth noticing is the ability of idealization for the specific situation which enables the researchers to focus on specific aspects of the problem and to eliminate the irrelevant aspects e.g. two dimensionality, consistent density. On the negative side, some aspects of numerical methods are based on simplification, which make it hard to prove accurate (Mangani, 2010). Numerical results are always based on approximation. For most phenomena, such as multiphase flow and turbulence, precise equations are either not achievable or available. Hence, there are differences between the results that are obtained from the computer and reality. In many cases, we cannot obtain acceptable solutions for all flows because of approximations or idealizations that is applied to close the differential equations. Approximations

are also essential in the discretization process and iterative methods to find a solution to the discretized equations. However, one needs to be careful with the produced results and the way that the results are judged and analyzed. (Patankar, 1980).

Considering everything, it can be concluded that in the process of model validation one important way to ensure the accuracy of the data is comparing the results of experimental investigations and mathematical models. In this thesis, the numerical results are compared with experimental data that are available in literature.

Numerical methods describe the motion of fluid by applying partial differential equations. These equations are derived from conservation laws, which govern the movement of all flows regardless of the type of flow. Target application needs to be taken into consideration when deciding on a numerical model, which may contain simplification of the conservation laws. It is important to note that it could be useless, if not impossible, to produce general solution methods. A solution usually corresponds to a particular set of equations (Ferziger, 2002).

In summary, partial differential equations can be applied in order to describe the characteristics of flows and setting up a mathematical model in fluid dynamic problems. However, due to the absence of available analytical solutions, applying approximations are required in a numerical form for calculating the differential equations by applying a system of algebraic equations. Because the computer language is only numbers, this requires translation of mathematical and geometrical models into numbers. Hence, in order to analyze the motion of the fluid and enable the computer to provide numerical solutions for the fluid dynamics problems, it is essential to translate the problems for the computers. In this procedure, the approximations are needed to be considered for small domains in terms of space or time, which can enable the model to extrapolate the results for the variables at some desirable discrete locations in time and space. There are a series of methodologies available for this purpose, which are known as Computational Fluid Dynamics (CFD). The CFD procedure can be described as follows (Hirsch, 1988):

The first step of this process is deciding about the mathematical model, which will in turn specify the degree of approximation that is needed to be considered related to reality. Next step, that is also the major processes of a simulation, is the discretization process. There are various approaches, but the most important ones are: finite volume (FV), finite difference (FD), and finite element (FE) methods (Ferziger, 2002). The remarkable point is the fact that the discretization should become exact as the grid spacing becomes smaller and finally tends to zero. Numerical solutions of partial differential equations (PDEs) require definition of numerical grid of nodal points in space and time. Determining the grid depends strongly on the kind of equations to be solved. The role of the numerical grid is to define the discrete locations where the results of

the variables are required. In other words, the geometric domain of the problem needs to be presented in a finite number of subdomains (elements, control volumes etc.). Finite approximation technique is the next step, which in turn requires establishing the numerical scheme and its properties. In this phase, a relationship should be established among the neighboring grid points, which can be a set of algebraic relations or numerical schemes (Baker, 2003).

Following discretization, the next step is applying an appropriate time step and a method in order to accelerate the rate of convergence. These techniques apply iterative methods in order to solve the linear system, that in turn originates as a result of applying linearization of the equations. Usually there are two levels of iteration, namely inner and outer. The first one is associated with linearity where the linear equations are solved, and the second one is related to non-linearity. Obtaining accurate results depends on choosing a proper convergence criteria and setting appropriate stopping conditions for both of the mentioned cycles at this step. The last step is graphic post-processing of the numerical data, which enables a better understanding of the obtained results and is possible by the availability of powerful visualization software (Baker, 2003).

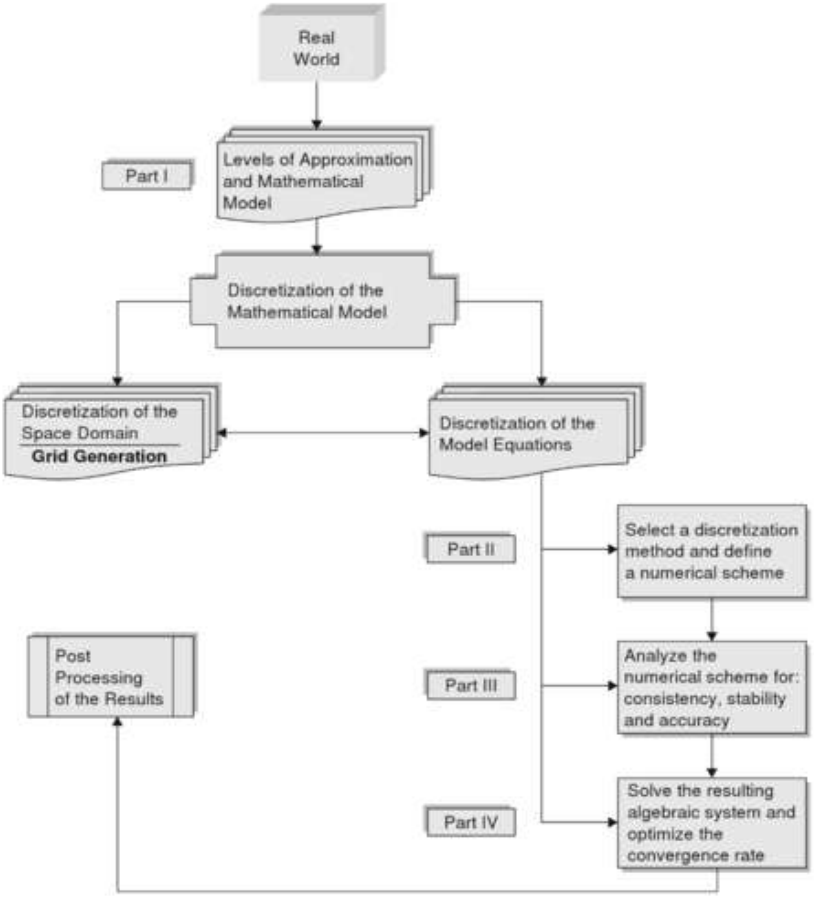

Figure 50:Structure of a CFD simulation system (Hirsch, 1988).

1.2 Mathematical model

In this section, the mathematical model for incompressible flow is described. Equations are presented in the most general form.

1.2.1 Laminar and turbulent flow

Two types of fluid motion are observed in studying the behavior of the fluid motion. The first is a well ordered, even motion in which elements or particles of the fluid seems to slide over each other in layers. Although there is diffusion and agitation at molecular level in the fluid, there is effectively no mixing that occurs in a large scale between the layers, and this motion is called laminar flow. The second distinct motion is characterized by unsystematic or chaotic motion of individual fluid particles and by macroscopic mixing of these particles through the flow that occurs rapidly leading to the formation of eddies of various scales. This motion is called turbulent flow (Street, 1996).

Computational prediction of flow separation from turbulent flows is a process of primary concern. Turbulent flows fluctuate on a broad range of scales in terms of time and length. This makes the simulation of such flows difficult and it is often necessary to model the turbulence in some way (Street, 1996). RANS (Reynolds-average Navier-Stokes), and LES (Large Eddy Simulation) are those model equations and can be used to describe such flows.

1.2.2 OpenFoam

1.2.2.1 Introduction

The recent development of Computational Continuum Mechanics (CCM) in engineering has led to the maturity of simulation tools. The challenges that dominate the current simulations are associated with automation and integration of the available tools in the software in a Computer Aided Engineering (CAE) environment such as surface and volume meshing, sensitivity and optimization studies. However, because of existing noticeable complexity, the current trend in terms of software development is toward producing monolithic general-purpose tools, which is likely to be able to overcome most physical problems for all users. In spite of efforts of the scientists so far, there is no software capable of covering all the aspects of the CFD problems (Lafore, 1997).

One of the recent programming languages that has been proposed so far and has received much attention is the object oriented programming.

As programming tasks became more expansive and more confusing, it revealed that the approach of writing code did not work, which motivated the programmers to turn their attention to other alternatives to cope with the problem of complexity of the traditional programs. Three major innovations have been devised including (Lafore, 1997):

1-Object-oriented programming (OOP)

2-The unified modeling language (UML)

3-Improved software development processes

The main reason that the programmer's tendency has shifted to object-oriented programming is the fact that OOP offers a new approach toward complexity. It views a program as a gathering of items with certain attributes capable of performing certain actions as opposed to viewing a program as a series of steps that needs to be performed systematically(Lafore, 1997).

The structure of the traditional program consists of a list of guidelines, which implies that for each statement in the language, the PC performs an undertaking: get some data, divide, add or multiply by a number and post processing the outcome. Even the idea of breaking down the program into smaller units as a way of making the program more understandable failed to work and fulfil the expectations. Hence, this caused the structured programming approach to present signs of strain.

There are two main limitations with procedural programming languages, namely unrestricted access and real world modeling. Two kinds of data are available, namely local data and global data. The first data is in a hidden condition to avoid any unintentional modifications. The characteristic of the second data is that it should provide accessibility by any function available in the program. In case of a complex program, this feature leads to a large number of connections among the data and functions leading to a complex structure for the program, which makes it difficult to modify when needed. Because this modification also needs to be extended on all functions that are operated on those data, it would result in the inability of the function, which in turn will result in inaccuracy of the results (Lafore, 1997).

The second drawback of procedural programming is that in the real world, we deal with objects such as cars and people which have attributes and behavior and are not like data and functions hence, data and functions cannot model real-world objects effectively.

The main idea behind object-oriented languages is based on the combination of data and the functions into a single unit, which is called the 'object'. Hence, the problem will be divided into objects instead of functions so the program can be easily designed because of the close match between the objects in the real and

programming world. The hidden data is one of the advantages of this language program because direct accessibility to data is impossible. This characteristic makes it safe from accidental alteration (Lafore, 1997).

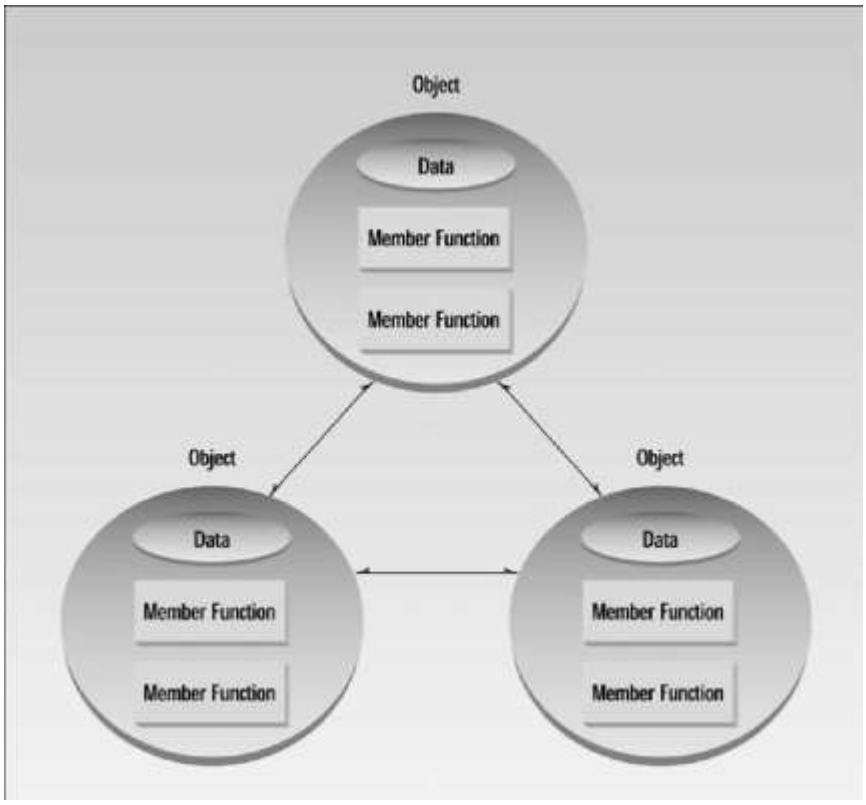

Figure 51:The object oriented paradigm (Lafore, 2002).

The impact of modern programming techniques on the state-of-the-art software, namely OpenFoam, is remarkable. In this thesis, all the numerical estimations are performed using OpenFOAM (Open Field Operation And Manipulation). The OpenFoam code is an object-oriented toolbox for simulating the CFD problems numerically. This software, via applying the form of partial differential equations, can execute complex physical models in Continuum Mechanics. The open-source software employed to develop the proposed computational model is OpenFOAM v2.3.0, which runs on Linux. The OpenFOAM code is a numerical simulation package which offers customized numerical solvers written in C++ language and is provided by Open CFD Ltd. The open-source aspect of OpenFOAM enables users to customize and extend its existing functionality and make it more efficient based on their own projects. For example, the extensibility aspect enables users to create typical modeling components such as boundary conditions or turbulence models or boundary and initial conditions without the need to change the existing source code. The most attractive feature of this software is its object-oriented library for CFD, which is an alternative for programmers to cope with the problem of the complexity of traditional programs. A wide range of engineering problems can be simulated using this software by solving the form of partial differential

equations. The model uses Finite Volume Method (FVM) with polyhedral grid and it can also be used for massively parallel computing (Jasak et al., 2007). The main advantage of OpenFOAM is that its source code is publicly available, so, if needed, users can assess the code and modify. If the model requires additional functionality, this can be added by the user. One of the notable aspects of OpenFOAM is equation representation, which provides close resemblance to the equations being solved and enables model users to develop various custom solvers (OpenFOAM, 2014).

Beside the significant favorable circumstances, there are likewise a few downsides. The fundamental one is presumably the way that OpenFOAM requires the users to perform a few plans; however, it would provide control over it. Along these lines, it would permit the users to run their own particular models for which the released package of the organization do not offer the right catches. Furthermore, the users can get support for OpenFOAM in several ways (OpenFOAM 2014).

1.2.2.2 Equation representation in OpenFOAM

The fundamental thoughts behind the design of OpenFoam is presenting the differential equations, which are the natural language of continuum mechanics in an object-oriented framework.

One of the most practical features of OpenFoam is its syntax language, which means that the codes are very similar to the partial differential equations. This valuable feature allow the users to perceive the equations and produce custom solvers easily (OpenFOAM, 2014).

Herein are two examples showing how to represent an equation in OpenFoam. The first equation is a representation of a turbulence kinetic energy equation in Reynolds averaged Navier-Stokes (RANS) models. As can be seen below, it does not need knowledge of programming to understand (OpenFOAM, 2014).

$$\frac{\partial k}{\partial t} + \nabla \cdot (u\,k) - \nabla \cdot [(\nu + \nu_t)\nabla k] = \nu_t \left[\frac{1}{2}(\nabla u + \nabla u^T)\right]^2 - \frac{\epsilon_0}{k_0}\,k$$

```
"solve
(
fvm::ddt(k(
+ fvm::div(phi, k)
- fvm::laplacian(nu() + nut, k(
== nut*magSqr(symm(fvc::grad(U(((
- fvm::Sp(epsilon/k, k(
);
```

Representation of continuity, momentum and pressure equations in OpenFoam.

```
// continuity equation
Solve
(
Fvm: :ddt (rho)
+fvm: :div (phiv, rho)
);
//Momentum equation
fvVectorMatrix UEqn
(
Fvm: :ddt (rho, U)
+fvm: :div (phi, U)
_fvm: :laplacian(mu, U)
);
Solve (UEqn = = -fvc: :grad (p));
// Pressure equation
Solve
(psi/sqr (rho) * (fvm: :ddt (rho, p)
+fvm: :div(phi, p))
+fvc: :div(phivStar)
-fvm: :laplacian (rUA, p)
+ MSave + fvm: :SuSp (dMdP, p)
-dMdp*pSave
); " (Jasak, 2009).
```

"OpenFOAM has its own programming language for writing solution algorithms for complex physics. It includes set of functions that describe standard differential operators (∇^2 , $\nabla_.$, ∇ , ∇x , $\frac{\partial}{\partial t}, \frac{\partial^2}{\partial t^2}$) which perform the discretization to create matrix equations" (OpenFOAM userguid).

"Differential operators within OpenFOAM are defined as follows:

Fvm::ddt=$\frac{\partial}{\partial t}$

Fvm::d2dt2=$\frac{\partial^2}{\partial t^2}$

Fvm::div::=$\sum \frac{\partial}{\partial x_i}$

Fvm::laplacian=$\sum_i \quad \frac{\partial}{\partial x_i}$" (OpenFOAM userguid)

1.2.2.3 Five main objects in OpenFOAM

1-Space and Time

Capturing space and time can be considered as the first point of order in field-based discretization. In order to translate the time for the computer, the temporal dimension needs to be divided into limited number of time steps for tracking. The technique of capturing space is via applying computational mesh. OpenFOAM defines a cell by the faces that cover it as well as the vertices that are labelled in order to define the faces. The useful aspect of OpenFOAM is considering the time as an object database capable of handling useful functions to control and update the solver, which would give users the opportunity of gaining the output of simulation every x time-steps, or y seconds of computational time (Jasak, 2007).

2-Field Variable

Continuum mechanics executes on various fields elements and their value can be calculated at predefined points of the mesh (Jasak et al., 2007).

3-Matrix and Linear System

"Code organization allows the FVM and FEM to share sparse matrix implementation and solver technology, resulting in considerable code reuse which is extremely useful" (Jasak et al., 2007).

4-Discretization Method

One of the practical aspects of OpenFoam for CFD users is the numerical tools, which offer methods to solve problems that can be described by discrete particles. A discretization method can be divided into two different functions, including interpolation and differentiation. The first one allows the estimation of a value of a field based on pre-defined spatial and temporal variations and the second one creates a new field via applying calculus operations on the existing fields. For example, a finite volume method pressure field volscalarfield p, can create a new vector field of the gradient of pressure (Jasak et al., 2007).

Volvectorfield g = fvc :: grad (p)

It can be said that the similar operations are applied in all CFD codes but the advantage of OpenFOAM is its flexibility and clarity of its programming execution.

5-Physical Modelling Libraries

Physical modelling capabilities of OpenFOAM incorporate an extensive variety of fluid and structural analysis models, with emphasis on nonlinear and coupled equation sets. In all cases, base mesh handling, field algebra, matrix and linear solver support and discretization are shared (Jasak et al., 2007).

1.2.2.4 Implementation of the solver interFoam

Nearly all of the modeling of physical phenomena is based on the simple statement "you cannot get something for nothing" i.e. there are certain important physical properties that must be conserved (Ghil and Childress 1987). Applying a system of conservation laws is a way of expressing most of the partial differential equations that are present in fluid dynamics. In physics, the Navier–Stokes equations describe the movement of flow particles. These equations can be expressed by linking the Newton's second law and the movement of flow, together with assuming that the stress in the fluid can be stated by the summation of a diffusing viscous term and a normal stress force term and as a result, is capable of describing viscous flow. These equations describe conservation of mass and momentum.